ISTANBUL TECHNICAL UNIVERSITY ★ GRADUATE SCHOOL OF SCIENCE ENGINEERING AND TECHNOLOGY

NVH EVALUATION OF A HIGH PRESSURE FUEL PUMP MBD MODELWITH THE CONSIDERATION OF INTERNAL HYDRAULIC EFFECTS AND VALVE TRAIN SYSTEM EXCITATION PARAMETERS

M.Sc. THESIS

Yahya SAHIP

Department of Mechanical Engineering

Mechanical Design Programme

Thesis Advisor: Prof. Dr. Ata MUGAN

JANUARY 2012

ISTANBUL TECHNICAL UNIVERSITY ★ GRADUATE SCHOOL OF SCIENCE ENGINEERING AND TECHNOLOGY

NVH EVALUATION OF A HIGH PRESSURE FUEL PUMP MBD MODELWITH THE CONSIDERATION OF INTERNAL HYDRAULIC EFFECTS AND VALVE TRAIN SYSTEM EXCITATION PARAMETERS

M.Sc. THESIS

Yahya SAHIP
(503081220)

Department of Mechanical Engineering

Mechanical Design Programme

Thesis Advisor: Prof. Dr. Ata MUGAN

JANUARY 2012

İSTANBUL TEKNİK ÜNİVERSİTESİ ★ FEN BİLİMLERİ ENSTİTÜSÜ

YÜKSEK BASINÇ YAKIT POMPASININ ÇALIŞMASINDAN KAYNAKLI HİDROLİK ETKİLERİ VE SUBAP TAHRİK SİSTEMİ PARAMETRELERİ DİKKATE ALINARAK DİNAMİK MODELİNİN TİTREŞİM ANALİZİ

YÜKSEK LİSANS TEZİ

Yahya SAHİP
(503081220)

Makina Mühendisliği Anabilim Dalı

Konstrüksiyon Programı

Tez Danışmanı: Prof. Dr. Ata MUĞAN

OCAK 2012

Yahya Sahip, a M.Sc. student of ITU GRADUATE SCHOOL OF SCIENCE ENGINEERING AND TECHNOLOGY, student ID 503081220, successfully defended the thesis entitled “NVH EVALUATION OF A HIGH PRESSURE FUEL PUMP MBD MODELWITH THE CONSIDERATION OF INTERNAL HYDRAULIC EFFECTS AND VALVE TRAIN SYSTEM EXCITATION PARAMETERS” which he prepared after fulfilling the requirements specified in the associated legislations, before the jury whose signatures are below.

Thesis Advisor : **Prof. Dr. Ata MUGAN** ....
İstanbul Technical University

Jury Members : **Prof. Dr. Ata MUGAN** ....
İstanbul Technical University

Assist. Prof. Vedat TEMIZ ....
İstanbul Technical University

Assoc. Prof. Dr. Vedat Ziya DOĞAN ....
İstanbul Technical University

Date of Submission : 19 December 2011
Date of Defense : 26 January 2012

FOREWORD

I would like to express my deep appreciation and thank my advisor Prof. Dr. Ata MUGAN who made this thesis possible. This work could not have been completed without his support and invaluable advice.

I would like to thank my friends Ebru ORHAN, Yavuz ÇAĞIR and Fehmi SERINOL for their patience and support during my study.

Also, I would like to thank colleagues in Ford Otosan for their technical support and advices during the testing and modeling of this study.

Last but not least, I would like to thank my family for their encouragement and assistance over my life.

January 2012

Yahya SAHIP
(Mechanical Engineer)

TABLE OF CONTENTS

Page

FOREWORD .... **vii**
TABLE OF CONTENTS .... **ix**
ABBREVIATIONS .... **xi**
LIST OF TABLES .... **xiii**
LIST OF FIGURES .... **xv**
LIST OF SYMBOLS .... **xix**
SUMMARY .... **xxi**
ÖZET .... **xxiii**
1. INTRODUCTION **1**
2. METHODOLOGY **5**
  2.1 Objectives and Scope 5
  2.2 Methodology Details 5
3. FUEL INJECTION SYSTEMS **11**
  3.1 Introduction 11
  3.2 Types of Modern Injection Systems 12
    3.2.1 Unit injector system 12
    3.2.2 Unit pump 15
    3.2.3 Common rail system 18
      3.2.3.1 Advantages 22
4. TIMING DRIVE SYSTEMS IN INTERNAL COMBUSTION ENGINES ... **25**
  4.1 Types of Timing Drive System 25
    4.1.1 Belt drive system 25
    4.1.2 Gear drive system 26
    4.1.3 Chain drive system 27
      4.1.3.1 Timing chain 28
      4.1.3.2 Guides 29
      4.1.3.3 Tensioners 30
      4.1.3.4 Sprockets 30
  4.2 Modeling and Simulation Theory 30
    4.2.1 Part modeling 32
      4.2.1.1 Chain link modeling 32
      4.2.1.2 Sprocket modeling 33
      4.2.1.3 Guide and tensioner modeling 34
      4.2.1.4 Chain contact kinematics 34
      4.2.1.5 Tensioner guide contact kinematics 39
      4.2.1.6 Chain contact dynamics 40
      4.2.1.7 Chain initialization 42
  4.3 Engine Specification and Components 42
    4.3.1 Chain drive simulation 44

- 4.4 Model Confirmation And Measurements 46
  - 4.4.1 Measuring equipment 48
  - 4.4.2 LH instrumented chain tensioner 49
  - 4.4.3 Instrumented sprocket 50
  - 4.4.4 RH Instrumented chain tensioner 50
  - 4.4.5 Measurement results 50

5. FIE SYSTEM SIMULATION 55

- 5.1 Pump Elements 59
  - 5.1.2 Plunger and subcomponents 59
- 5.2 General Plunger Equations 59
  - 5.2.1 Annular leak connection 61
  - 5.2.2 Flow splits 62
  - 5.2.3 Fluid piston 64
  - 5.2.4 Spring - massless spring connection 65
  - 5.2.5 Ball valves 65
  - 5.2.6 Delivery valve 67
- 5.3 Cam Lobe and Cam Shaft 67
  - 5.3.1 Hertz stress at camroller contact 69
  - 5.3.2 Journal 71
- 5.4 Simulation Results and Modeling Details 73
- 5.5 Measurement Equipment 79
- 5.6 Measurement Results and Model Confirmation Discussion 81

6. MULTI BODY DYNAMIC PUMP MODEL 85

- 6.1 Construction of Adams Model 87
  - 6.1.1 High pressure plunger 87
  - 6.1.2 Joints 90
  - 6.1.3 Cam shaft 91
    - 6.1.3.1 Mechanism of common-rail pumps 91
  - 6.1.4 Cam profile and shaft 91
  - 6.1.5 Bushings 93
- 6.2 Model Excitation 95
- 6.3 Rigid Model Results 96

7. NVH MEASUREMENTS ON ENGINE 99

8. MODAL ANALYSIS AND NVH EVALUATION 107

9. MULTI BODY DYNAMIC FLEXIBLE MODEL 111

10. CONCLUSIONS AND RECOMMENDATIONS 117

REFERENCES 123

APPENDICES 125

CURRICULUM VITAE 131

ABBREVIATIONS

MBD : Multi Body Dynamic
CAE : Computer-Aided Engineering
CR : Common Rail
NVH : Noise, Vibration and Harshness
HP : High Pressure
DoE : Design of Experiment
NOx : Nitrogen Oxides
CO2 : Carbon DiOxide
ECU : Electronical Control Unit
EGR : Exhaust Gas Recirculation
UPS : Unit Pump system
UIS : Unit Injector System
VGT : Variable Geometry Turbocharger
FIP : Fuel Injection Pump
LH : Left Hand
RH : Right Hand
CW : Clock Wise
CNC : Computer Numeric Control
FRP : Final Rail Pressure
FEA : Finite Element Analysis
MBS : Multi Body System
RBE2 : Rigid Body Element to
DOF : Degree of Freedom

LIST OF TABLES

Page

Table 4.1 : Specification of modelled engine. 44
Table 4.2 : Timing drive sub-component type and dimensions. 44
Table 7.1 : Vertical metering unit measurement results in table. 101
Table 7.2 : Long. metering unit measurement results in table 102
Table 7.3 : Lateral metering unit measurement results in table. 103
Table 7.4 : Lateral pump bottom-left measurement results in table. 104
Table 7.5 : Vertical pump bottom-left measurement results in table. 105
Table 7.6 : Long pump bottom-left measurement results in table. 106

LIST OF FIGURES

Page

Figure 1.1 : Drive by noise percentages [1]. 1
Figure 1.2 : Noise sources in an engine and accesories [1]. 2
Figure 1.3 : Power unit related noise sources [2]. 4
Figure 2.1 : Simulation methodology overview. 6
Figure 2.2 : Components in a simulation package [3]. 8
Figure 2.3 : Requirements of simulation tools [3]. 9
Figure 3.1 : Overview of a unit injector and sub-components [4]. 13
Figure 3.2 : Schematic of a modern unit injector commonly used in the field [5]. 14
Figure 3.3 : Unit pump fuel injection system schematic [4]. 16
Figure 3.4 : Modern unit pump system commonly used in the field [6]. 17
Figure 3.5 : History of European emissions standards [7]. 18
Figure 3.6 : Development of injection pressure of HD Engines [7]. 19
Figure 3.7 : Fuel injection system trend on highway application [7]. 20
Figure 3.8 : Key factors for diesel fuel injection system development [7]. 21
Figure 3.9 : Modern common rail system schematic [6]. 21
Figure 3.10 : Breakdown of modern injection systems for vehicles [9]. 23
Figure 3.11 : Comparison of different injection systems [10]. 24
Figure 3.12 : Schematic of a modern common rail system [6]. 24
Figure 4.1 : Typical belt drive system and sub-components [9]. 26
Figure 4.2 : Components of gear drive systems [9]. 26
Figure 4.3 : Components of chain drive system [9]. 27
Figure 4.4 : Sub-components of timing chain [11]. 28
Figure 4.5 : Sub-components of bushing chain [11]. 29
Figure 4.6 : Sub-components of silent chain [12]. 29
Figure 4.7 : Contact and connection forces in the chain simulation [13]. 31
Figure 4.8 : Representation of chain link [14]. 32
Figure 4.9 : Chain link connectivity [14]. 33
Figure 4.10 : Sprocket geometry. 33
Figure 4.11 : Guide and tensioning devices [11]. 34
Figure 4.12 : Generalized contact kinematics [14]. 35
Figure 4.13 : Roller and sprocket contact kinematics [14]. 37
Figure 4.14 : Illustrated roller and guide contact [14]. 39
Figure 4.15 : Tensioner and guide contact kinematics [14]. 40
Figure 4.16 : Chain link forces and link extension [15]. 40
Figure 4.17 : Contact forces - Chain bush and sprocket or guide [15]. 41
Figure 4.18 : Chain drive layout [11]. 43
Figure 4.19 : Valve train system schematic with respect to engine package. 43
Figure 4.20 : Valve train system of a 4.4L V8 engine with auxilary gears. 46
Figure 4.21 : Timing system layout. 47

Figure 4.22 : Instrumentation of adapter plate and tensioner around FIP. 48
Figure 4.23 : The CAD model of the instrumentation. 49
Figure 4.24 : Instrumentation of tensioner. 49
Figure 4.25 : Snapshot of an instrumented tensioner. 50
Figure 4.26 : Valve train system according to engine orientation. 51
Figure 4.27 : Comparison of different results from simulation and tests. 52
Figure 4.28 : Load distribution according to CW teeth orientation. 52
Figure 4.29 : FIP gear orientation according to key. 53
Figure 4.30 : Chain load distribution according to FIP drive torque. 54
Figure 5.1 : Cross section of a FIP including cam shaft and plungers. 57
Figure 5.2 : Cross Section of a plunger mechanism and position in FIP. 59
Figure 5.3 : Mechanical model of a plunger [18]. 60
Figure 5.4 : Sub components of a plunger mechanism. 60
Figure 5.5 : Geometry of user defined variable gap [18]. 61
Figure 5.6 : Schematic of a throttle with respect to angular connection [19]. 63
Figure 5.7 : Spring behaviour with respect to force. 65
Figure 5.8 : Ball valve schematic and explanation of equation [18]. 66
Figure 5.9 : Mechanical representation of a cam profile [19]. 68
Figure 5.10 : Geometry of cam profile [19]. 68
Figure 5.11 : Amplitude of cam center and torsional cam distortion [18, 19]. 69
Figure 5.12 : Cam profile with connections to shaft [18, 19]. 70
Figure 5.13 : Journal dimensional basics [19]. 71
Figure 5.14 : Journal bore eccentricity [19]. 72
Figure 5.15 : Journal eccentricitiy with rotation [19]. 72
Figure 5.16 : Plunger model snapshot from GT fuel. 74
Figure 5.17 : Plunger forces acting on pistons respectively. 74
Figure 5.18 : Cam profile lifting characteristics of plunger. 75
Figure 5.19 : Cam contact force distribution drived by plungers. 75
Figure 5.20 : Damping force variation with respect to cam angle. 76
Figure 5.21 : Total flow rate with respect to cam angle. 76
Figure 5.22 : Metering unit function for total fuel delivery [10]. 77
Figure 5.23 : Input and output drive torque required for pump excitation. 78
Figure 5.24 : Cam shaft and dynamical journals representation from model. 78
Figure 5.25 : Dynamical journal force distribution. 78
Figure 5.26 : Bearing load magnitude with respect to both directions. 79
Figure 5.27 : Bench Ttest of a fuel injection pump [5]. 80
Figure 5.28 : Fuel injection pump rig test [10]. 80
Figure 5.29 : Excitation torque required respect to different FRP profiles. 81
Figure 5.30 : Back to back comparison of rig tests and simulation results. 81
Figure 5.31 : Real world plunger force measurements. 82
Figure 5.32 : Testing of lifting profile measurement results. 83
Figure 6.1 : Generic flow chart of Adams simulation [21]. 86
Figure 6.2 : Fuel injection pump sub-components in general. 87
Figure 6.3 : Function diagram of a high pressure pump [10]. 88
Figure 6.4 : Sub-components of a plunger and basic components. 88
Figure 6.5 : Screenshot from Adams including plunger sub-components. 89
Figure 6.6 : Snapshot from Adams including spring element. 89
Figure 6.7 : Translational joint representation. 90
Figure 6.8 : Translational element mechanism details [23]. 90
Figure 6.9 : Representation of cam contact with plunger roller. 92

Figure 6.10 : High pressure fuel pump section showing sub-components. 93
Figure 6.11 : Cylindirical joint details [23]. 94
Figure 6.12 : Lifting profile with respect to cam profile. 96
Figure 6.13 : Both of the plunger forces in one graph. 97
Figure 6.14 : Drive torque for the sufficient excitation of FIP. 97
Figure 6.15 : Velocity and force on the plunger roller element. 98
Figure 7.1 : Snapshots of accelerometers from real engine test. 99
Figure 7.2 : Pump metering unit vertical direction vibration measurement. 100
Figure 7.3 : Pump metering unit long. direction vibration measurement. 101
Figure 7.4 : Pump metering unit lateral direction vibration measurement. 102
Figure 7.5 : Pump bottom- left lateral direction vibration measurement. 103
Figure 7.6 : Pump bottom- left vertical direction vibration measurement. 104
Figure 7.7 : Pump bottom- left Long. direction vibration measurement. 105
Figure 8.1 : 1st mode modal analysis results. 107
Figure 8.2 : 2nd mode modal analysis results. 108
Figure 8.3 : 3rd mode modal analysis results. 108
Figure 8.4 : 5th mode modal analysis results. 109
Figure 9.1 : Flexible modal analysis steps. 111
Figure 9.2 : Conversion method of modal neutral file. 112
Figure 9.3 : Representation of different RBE2 conversion capabilites. 112
Figure 9.4 : RBE2 points located on pum shaft. 113
Figure 9.5 : RBE2 points located on pump cover. 114
Figure 9.6 : RBE2 points located on system model. 114
Figure 9.7 : Different NVH modes including flexible bodies. 115
Figure 9.8 : Flexible model initial analysis results. 115
Figure 10.1 : Comparison of NVH response with different drive ratios. 117
Figure 10.2 : Comparison of NVH response with different final rail pressure. 118
Figure 10.3 : Thesis methodology for each phase including analysis outline. 119
Figure A.1 : 2 Teeth CW valve train measurement 126
Figure A.2 : 3 Teeth CW valve train measurement 126
Figure A.3 : 4Teeth CW valve train measurement 127
Figure A.4 : 5 Teeth CW valve train measurement 127
Figure A.5 : 5 Teeth CW valve train measurement 128
Figure A.6 : 11 Teeth CW valve train measurement 128
Figure A.7 : 2 Teeth CW valve train measurement 129
Figure A.8 : 5 Teeth CW valve train measurement 129
Figure A.9 : 10 Teeth CW valve train measurement 130
Figure A.10 : 11 Teeth CW valve train measurement 130

LIST OF SYMBOLS

k_{link} : Chain link stiffness coefficient
c_{link} : Chain link damping coefficient
F_{link} : Chain link force
Δ : Chain link relative displacement
R_{pitch} : Pitch radius
R_{roller} : Roller radius
R_{tooth} : Tooth radius
R_{out} : Tip radius
R_{guide} : Guide arc radius
R_{link} : Chain link roller radius
$\Theta_{contact}$: Roller contact angle
F_x, F_y : Sprocket contact force
k : Camshaft stiffness coefficient
c : Camshaft damping coefficient
x, y : Relative displacement of sprocket geometric center
$\underline{P}^k$: Position vector of body k
$\underline{t}$: Tangent vector
$\underline{n}$: Normal vector
q : Relative minimum distance between bodies
a : Interference between profiles
V_t : Tangential relative velocity
V_c : Tangential relative velocity between centers
δ : Distance between centers
s : Position of candidate contact points
L : Chain link length
D : Chain link clearance
d_{ij} : Distance between two adjacent bush
e : Link extension
A : Non-linear stiffness term
r_e : Tooth flank radius
r_i : Tooth root radius
α : Roller sitting angle
da : Tip diameter
Fhyd : Hydraulic resistance force
Ffrict : Coulomb friction force
Fshear : Viscous friction force due to leakage (if any)
m : Plunger mass
x local : x-coordinate of plunger
xi : local x-coordinate of i-th connected element on input end
yi : local y-coordinate of i-th connected element on input end
xj : local x-coordinate of the j-th connected element on output end

yj : local y-coordinate of j-th connected element on output end
α : Angle between element motion of direction (x-coordinate) and global x
αi : Angle between x-coordinate of i-th connected element and global xcoordinate
αj : Angle between x-coordinate of j-th connected element and global xcoordinate
αmc_i : Angle between i-th mechanical connection and global x-coordinate
αmc_j : Angle between j-th mechanical connection and global x-coordinate
ci ,ki : Damping and stiffness coefficients (functions) of the i-th mechanical connection on input end
cj , kj : Damping and stiffness coefficients (functions) of the j-th mechanical connection on output end
F0i ,F0j : Preload forces of the i-th input and j-th output mechanical connections, respectively.
pin and pout : Input and output pressures
pcam : Pressure in cam chamber (on input end)
dplung : Plunger diameter
D : Diameter of the annulus
Q : Volume flow rate
δ : Thickness of annular passage
Δp : Pressure differential
M : Dynamic viscosity evaluated at upstream pressure
L : Length of annular passage
Uwall : Relative velocity between piston and bore
M : Flow Rate Multiplier
eδ : Equivalent thickness for eccentric annular passage
δ : Thickness of annular passage
f : Correction factor
Q : Flow rate
ρ : Flow density
P : Pressure in the attached flow volume
Dp : Piston Diameter
Dr : Rod Diameter
Fext : External forces from components attached to the mechanical port.
x1 : Position of body 1 (defined by link; link from body 1 to body 2)
x2 : The position of body 2 (defined by link; link from body 1 to body 2)
Fp : The Pretension Force
F0 : Is the preload force of the valve spring
Fhyd : Is the hydraulic force,
Fin_stFout_st : Are additional forces from input and output stops
Fdamp : Is the damping force of squeezing fluid at valve closing.
T0i : Preload torque of the i-th input mechanical connection in w direction
TFx : Resistance torque of the reaction force normal to cam profile
nx and lx : Number of mechanical connections on input and output ends in x direction
ny and nw : Number of mechanical connections on input end in y and w directions,

NVH EVALUATION OF A HIGH PRESSURE FUEL PUMP MBD MODELWITH THE CONSIDERATION OF INTERNAL HYDRAULIC EFFECTS AND VALVE TRAIN SYSTEM EXCITATION PARAMETERS

SUMMARY

The main purpose of this thesis is to develop a reliable multi body dynamic (MBD) model of a high pressure common rail pump in order to understand the dynamic behavior of reciprocating pumps under the actions of the mechanical and hydraulic forces. The development and the use of a numerical model to predict vibrational response from reciprocating high pressure pumps with camshafts due to dynamic and hydraulic effect using Computer-Aided Engineering (CAE) technologies. This CAE methodology process, as outlined in this thesis study, includes measured data, computational flexible multibody dynamics and 1D and 2D analytic tools to evaluate internal effects.

The development of a complete new engine without extensive CAE support is no longer done. Beginning stages in the design and validation process decisions are based on preliminary assumptions and calculation. Calculations accompany revisions throughout. Requirements and recommendations vary from application to application and it is the reason, demand depends in engine design and calibration.

Generally called 'the heart of the engine', the high pressure fuel injection system is without any doubt one of the most important engine systems which takes a role for diesel engine working principle. High pressure fuel injection system meters the required fuel delivery according to engine requirements; meanwhile it generates the high pressure profiles on injector required for atomization of the fuel, for sufficient fuel air mixing and for diesel combustion event.

As the system working principle of conventional systes for instance; unit pump injection system, general load profiles and dynamic effects are expected with low profiles. The influence of high pressure mechanical systems of Common Rail (CR) on Noise, Vibration and Harshness (NVH) is typically inconsiderable and neglected, although there are excessive loads due to high pressure oscillation inside the rail, which is sufficient enough to excite cylinder head and combustion chamber area. In general, high pressure common rail pump working mechanism generates high range of force frequency which result in valuable contribution to overall engine NVH behavior.

The measured test data is used to identify and reproduce the input excitation which is primarily generated from engine and high pressure pump dynamic and hydraulic. The dynamic interaction of the high pressure pump components, including excitation camshaft, contacting gears, dynamic joints, and flexible housing is modeled using flexible multibody techniques. The vibrational response to the vibration of the high pressure pump housing is then predicted using simulation techniques.

For the multi body dynamic model, the operating engine speed defined at the high pressure fuel pump and the resistance load defined at the output of high pressure plungers are considered to be the boundary conditions. Both of these mentioned two boundary conditions, especially the engine speed, are very important to the model to reproduce the excessive vibrational characteristics. It has to be emphasized that the engine speed must contain both the frequency and amplitude of the problematic load cases of the engine’s operating conditions which are also reviewed.

YÜKSEK BASINÇ YAKIT POMPASININ ÇALIŞMASINDAN KAYNAKLI HİDROLİK ETKİLERİ VE SUBAP TAHRİK SİSTEMİ PARAMETRELERİ DİKKATE ALINARAK DİNAMİK MODELİNİN TİTREŞİM ANALİZİ

ÖZET

Bu tezin amacı, modern bir yüksek basınç yakıt enjeksiyon pompasının, dinamik hareketini yaparken, çalışmasından dolayı meydana gelen mekanik ve hidrolik etkilerin gerçekçi bir şekilde modellenmesi. Bilgisayar destekli mühendislik teknolojileri kullanılarak kam mili ve hareket eden parçaların titreşim, gürültü ve sertlik yönünden incelenmesi hidrolik ve mekanik etkiler göz önünde bulundurularak numerik modeller ve geliştirmeler kullanılmıştır. Bu bilgisayar destekli mühendislik metodolojisi, 1-boyutlu ve 2–boyutlu analitik araçlar kullanarak içten gelen etkilerin modellenmesi ve bilgisayar destekli esneyebilen bir dinamik modelinin oluşturulmasını içeriyor.

Emisyon normlarının gelişimi incelendiğinde egzoz gazlarındaki zararlı atık miktarlarının sürekli olarak sınırlandığı ve izin verilen üst Iimitlerin sürekli düşürüldüğü gözlenmektedir. Yeni emisyon normlarının ekipman üreticileri tarafından sağlanabilmesi için devreye yeni motorlar ve yeni teknolojiye sahip geliştirilmiş tasarımlar girmektedir. Gelişmiş yanma kontrolleri gecikmeli enjeksiyon, yüksek enjeksiyon ve silindir basıncı gibi bazı sonuçların doğmasına sebep olmuştur. Gecikmeli enjeksiyon ile yüksek kurum oluşumu riski artmakta bu da yağda kurum oluşumu olasılığını ve buna bağlı olarak daha fazla aşınma olasılığını arttırmaktadır. Yüksek enjeksiyon ve silindir basınçları ise yüzey yüklerini arttırmakta bu da segman silindir, duvarları ve yataklarında aşınma riskini arttırmaktadır.

Motor geliştirme projeleri genelde sıfırdan bir geliştirme projesinden ziyade, projelerin devamında yapılan dizayn ve doğrulama prosesi önce yapılmış hesaplara ve varsayımlara dayanır. Hesaplamalar, gerçekleşecek değişiklikleri içerirler. Bu yüzdendir ki, dizayn gereksinimleri uygulamadan uygulamaya ve kalibrasyon tipine göre değişkenlik gösterebilir. Kalibrasyon, genelde motorun kullanım koşullarını önceden tahmin ederek, arazide kullanılacak aracın olabilecek en kötü senaryolara göre modellenip, sistemlerin üstüne eklenmiş sensör paketlerininin yardımıyla, önceden hazırlanan modele göre motorun çalışma performansını iyileştirmek ve optimize etmek amacıyla yapılan operasyondur. İşte tüm bu kontrol, sistemde bulunan mekanik komponentlerin ‘’Elektronik Kontrol Ünitesi’’ sayesinde olur.

Otomobillerde emisyonlarla ilgili kanunlar çıkmadan önce bir araba motoru mikroişlemcilere gerek kalmadan üretilebilirdi. Fakat günümüzde katalitik konverter kullanmayan bir araç kullanamayız. Dolayısıyla hava/yakıt karışımını ayarlayacak bilgisayar kontrolcüsüne ihtiyaç vardır.

Bir otomobilin en çok işlem yapan bilgisayar birimi motor kontrol ünitesidir bahsi edilen elektronik kontrol unitesidir. Bahsedildiği gibi bu ünite sensörlerden aldığı verileri işleyerek optimum işletimin yapılmasını sağlar. Örneğin, motorun sıcaklık seviyesi ve soğutma miktarını, aracın anlık hızı, motor devri, egsozdan atılan oksijen miktarı gibi detay bilgileri toplar ve saniyede milyonlarca işlem yaparak ateşlemenin nasıl ve ne şekil bir karışımda yapılacağına karar verir. Modern enjeksiyonlu benzin motorlarında vuruntu olmaması için ateşlemenin ne zaman yapılacağı ve enjektörün hangi salisede ne kadar yakıt püskürteceğini de yine bu modül ayarlar. Bir anlamda motorun çalışmasını ve işletimi için herşeyi kontrol edip karar veren ve bunları komut vererek uygulatan en önemli ünitedir. Tabi bunu kendine has yazılımı ve özelleştirilmiş yapısıyla gerçekleştirir. Yani sadece bu iş için optimize edilmiştir.

Genelde, ‘’motorun kalbi’’ denilen yakıt enjeksiyon sistemi, motor çalışma sisteminde şüphesiz en önemli rollerden birine sahiptir. Yakıt enjeksiyon sistemi, motor ihtiyacına göre gerekli yakıt miktarını motora ulaştırmaya çalışır, aynı zamanda dizel patlama prosesinin temelini oluşturan yeterli yakıt-hava karışımını sağlamak için yüksek basınçlı yakıtın atomizasyon olmasını sağlar. Geleceğin dizel püskürtme sistemi olarak tanımlanan ‘’Common Rail’’ yakıt enjeksiyon sistemi, özellikle Avrupa'da gün geçtikçe yaygınlaşmaktadır. ‘’Common Rail’’ teknolojisinde basınç üretimi ve enjeksiyon birbirinden ayrı. Ayrı bir yüksek basınç pompası yakıt hattını sürekli olarak yakıtla besliyor. Diğer dizel doğrudan sistemleri her püskürtme işlemi için yüksek yakıt basıncını her defasında yeniden biriktirmek zorunda kalırken, ‘’Common Rail’’ Sistemi düşük motor devirlerinde bile uygun basınçlı yakıtı daima hazır bulunduruyor. Üstelik, ‘’Common Rail’’ teknolojisi her çalışma döngüsü başına çoklu püskürtme sağlıyor olmasından ötürü de klasik sistemlerden ayrılır. Bu döngü, sessiz çalışma için ön püskürtme (pilot enjeksiyon), ideal güç konuşlandırması için ana püskürtme, düşük emisyonlar için ise ikincil püskürtme şeklinde üçe ayrılır. Yakıt enjeksiyon memelerine basınçlı kısa hatlar aracılığıyla ulaşır. Püskürtme basıncı ne kadar yüksekse, enjeksiyon sistemi de yakıtı o kadar ince bir şekilde püskürtebilir ve böylelikle daha da verimli bir yanma sağlayabilir.

Genel olarak konvansiyonel çalışma sistemine sahip olan enjeksiyon sistemlerine örnek olarak, tek pompa enjeksiyon sisteminde, yük profilleri ve dinamki etkiler yüksek beklenmez.Fakat, yüksek basınçlı modern enjeksiyon sistemlerinin titreşim, gürültü ve sertlik üstüne etkisi genelde ihmal edilmesine rağmen, yüksek basınç rayında bulunan basınç ki, yanma için gerekli basıncı sağlamak adına, basınç dalgalanmalarının titreşimleri nedeniyle çok büyük etkisi vardır. Genele olarak, modern enjeksiyon pompalarının çalışma sistemlerinden meydana gelen etki, yüksek bir aralıkta hareket ettiği için motor gürültüsüne ciddi bir şekilde etki eder.

İvme ölçerlerle kritik noktalardan alınmış veri, hassas bir şekilde motordan ve yüksek basınç pompasından, öncelikli olarak pompanın dinamik ve hidrolik etkilerini analiz etmeye uygun bir şekilde alındı. Bunun yanısıra silindir kafası üzerinde duran kam mili, valfler, emme manifoldu, egzos manifoldu, valf tahrik sistemi ve yüksek basınç rayı gibi komponentlerin hepsinden de yine titreşim karakterlerini açıklayabilecek şekilde titreşim ölçümü alındı.Yüksek basınç pompası içinde çalışan komponentlerin dinamik etkileşimi, özellikle kam mili, kontak halinde bulunan dişliler, dinamik yataklar ve dış gövde bilgisayar destekli esneyebilen bir modelin oluşturulmasıyla incelendi. Böylece pompanın titreşim varsayımı, bu model üzerinden hesaplandı.

Dinamik bir modelin oluşturulmasında, motorun kullanılan devri ve yüksek basınç pompasının basma sistemi komponentlerinin yük profilleri sınır şartlar olarak nitelendirilebilir. Bu iki sınır şartının, özellikle motor devri, titreşim etklierinin gözlenmesinde önemli bir role sahiptir. Bu nedenle, dikkate alınan motor devri, tüm frekans ve genlik dağılımının motor titreşimi yönünden sorunlu olabilecek kullanım şartlarını göstermesi gerekir.

Tezin ilk aşamasında projenin metodolojisi anlatıldı. Metodolojide, basamak basamak hangi komponent ve sistemlerin ne şekilde modelleneceği anlatıldı. Bu modelleme detayları ise ilerleyen bölümlerde detaylandırıldı. Metodoloji kısmında, hangi test verilerinin kullanılacağı, hangi komponentlerden hangi çıktılar alacağını anlatan bir kısım hazırlandı. Tezin en önemli kısmı, tezin metodolojisi olduğu için modellerin birbirleriyle olan etkileşimi çok önemli. Bu etkileşimin verimli bir şekilde oluşturulması ve farklı dinamik ve sınır şartlarında birbirlerine olan etkileşimi her zaman daim çalışabilmesi için kararlılığı iyi bir sistem oluşturulması gerekiyordu. Modellenmiş sistemlerim matematiksel denklemleri ilgili bölümlerde anlatıldı. Genel olarak modellerin mekanik etkileşimleri kısmen daha çok önemsendi.

Takip eden bölümlerde modellenecek sistemlerin zaman içerisinde gelişim prosesleri anlatıldı. Dizel sistemlerin yakıt enjeksiyon sistemleri ve dizel sistemlerin valf sistemi tahrik sistemlerinin tipik özellikleri ayrı ayrı anlatıldı.

Dizel motorlarda yakıt enjeksiyon sisteminin tipinden bağımsız olarak başlıca amaçları genel olarak, püskürtülecek yakıt miktarını ayarlayarak silindirlere göndermek, motorun tüm devirlerinde ve çalışma yüklerinde yakıtı istenilen zamanda ve miktarda silindirlere püskürtmek, püskürtmenin hızlı bir şekilde başlamasını ve bitmesini sağlamak, yakıtı çok küçük parça ve zerreler halinde (atomize halde) püskürterek, yanma odasının her tarafına ve düzgün bir şekilde dağılmasını sağlamaktır. İşte tüm bu operasyon detaylarının sağlanması için dizel motor enjeksiyon pompası en önemli rollerden birine sahiptir.

Yüksek basınç yakıt enjeksiyon pompası, içinde bulunan yakıt pompa pistonu sayesinde düşük basınç tarafından içeriye dolan yakıt, kam profiline sahip yakıt enjeksiyon poması şaftı sayesinde basma hareketini yapar. İşte bu dinamik hareket sayesinde yakıt basıncı yaklaşık 2 bar mertebesinden 2000 bar mertebesine kadar ulaşır. Bu dinamik hareket esnasında, emiş ve basış kısmında sıralanmış çekvalfler sayesinde basınç kontrolü yapılabilmektedir.Bu dinamik hareket yüzünden, yüksek basınç yakıt enjeksiyon pompasının şaftına yüksek miktarda kuvvet biner. Bu kuvvet yüzünden, dinamik etkiler altında beklenenden değişik titreşim cevabı verebilir.

Valf tahrik sistemi ise zincir, kayış veya dişli olmak üzere değişik tipte güç aktarma sistemleri kullanılabilir. Yüksek basınç pompasının çekmiş olduğu tork değeri yüksek mertebelerde olduğu için, bu yukarıda sayılan valf tahrik sistemlerinden herhangi birinin etkileşimi yine önemli olacaktır. Bu çalışmada, zincir tipli valf tahrik sistemi dikkate alınmıştır. Zincir tipi valf tahrik sisteminde, zincir lokmalarının birbirlerine göre dinamik hareketleri incelenmiş, matematiksel denklemleri gösterilmiştir.

Günümüz dizel motorlarında, Elektronik Kontrol Ünitesi valf tahrik sisteminin hızını ve pozisyonunu anlık olarak takip eder, ona göre motorun yakıt enjeksiyon sisteminin püskürteceği yakıt miktarını, motor sistemine giren hava miktarına göre kontrol eder. Tüm bu karışık algoritma içerisinde, püskürtülecek yakıt miktarına bağlı kontrolden sorumlu sensörler, aynı zamanda yakıt enjeksiyon pompasının titreşim karakteristiklerine etki eder.

Bunun yanısıra, krank milinin çevrim oranına bağlı olarak, yakıt enjeksiyon pompasının deviri belirlenir. Bu çevrim oranı, hem motorun basacağı yakıt miktarının kalibrasyonuna ve bu bağlamda titreşim karakterlerine etki eder.

Bu tez çalışmasının sonucunda, krank şaftının çevrim oranının optimizasyonu bunun yanısıra kalibrasyon optimizasyonu ve fazlama sayesinde titreşim karakteri değiştirilebilir. Böylece, tüm bu optimizasyon parametrelerinin değiştirilmesi için motor testi yapmak yerine, daha hızlı ve maliyetsiz bir şekilde bu tez metodolojisini kullanarak yapmak mümkün.

1. INTRODUCTION

This study presents NVH optimization procedure for the 4.4L V8 common rail diesel engine High Pressure (HP) Fuel Pump. For the high speed diesel engines, common rail high pressure fuel injection is the key system components which control engine torque, level of emissions and combustion noise. The principle of diesel engines have to be actually overseen in view of an early detection of unexpected problems which may have bad effect on fuel consumption, safe engine operation, emissions, noise, and vibrations.

With the growing industrialization and motorization, the usage of diesel engines has been increased up inevitably. Because of this increasing demand, noise has become an environmental problem. That is why; the regulations with respect to the NVH emission have become stricter with the years passing. As you can see in figure1.1below**,** the noise sharing of several noise sources in a passenger car and in a light duty truck are demonstrated for rated speed levels. For light duties as well as for passenger cars, the main source of noise for low speeds is the engine as can be seen in Figure 1.1 as mentioned.

As it is figured out apparently from the reference Figure 1.1 below, engine and exhausting system which are the three main sources of noise shows parallelism with both passenger car and light duty.

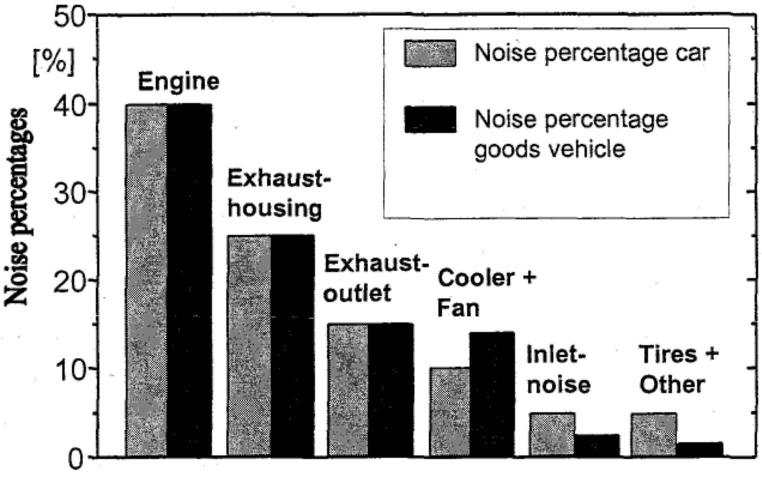

Figure 1.1 : Drive by noise percentages [1].

Taking into consideration that engine is the main source of noise; the focusing points and emphasis in noise reduction are often placed on engine noise. These sharing of noises are relied on exterior noise during accelerating operation measurements. As presented in Figure 1.2 below, mentioned noise sources are indicated.

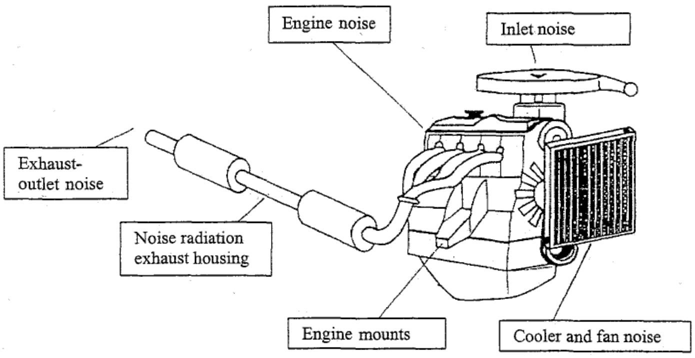

Figure 1.2 : Noise sources in an engine and accesories [1].

With the additional insulation and sound inhibitors, there is an opportunity for the reduction of the emitted noise. When the source of noise is acoustically identified and also a consequent optimization is done, it is found much more effective.

The engine noise can be subdivided into several noise sources.

- Noise of combustion coming from pressure at combustion area
- Valve train, camshafts, valves motion etc.
- Power conversion system noise varying loads, accessories etc.

By the recent stricter regulations demand highly reduction of required system resources and emissions with regards to fuel consumptions, CO2 as well as noise. Consideration of these demands in order to have light and compact design and low costs, there is an increasing complexity of power units, which extends the importance of simulation in the engine design process. There are factors such as excessive system complexity, dependency with environment and interaction with the surrounding systems of different effects with the combination of the requirement in understanding the contribution of even minor changes to the overall vibrational behavior, results in more extended simulated systems to predict the influence of a specific component in system integrity [2]. Furthermore, methodology has been going in details with targeted sub-systems and components. Assuming NVH analysis of power units closer to reality is very challenging to evaluate. The challenging part is to simulate and consider all excitation sources, transfer paths and radiating structures, contributing to the target frequency range. It is very important to particularly establish the investigation of indirect noise generation via interaction of moving mechanical components and the direct noise generation via intake and exhaust systems. Power conversion system; valve and timing train and dependent sub components (high pressure fuel pump) are focused as an indirect noise generation in some years.

In spite of improvement taken a step within fuel economy and thus the emission of less CO2 in diesel engines, reduction of nitrogen oxides (NOx) and particular matters emissions is hard from the point of environmental challenge. Because of this on-going demand in markets has resulted in development of high-performance fuel-injection system with higher pressure profiles on final rail pressure, enables higher injections that better atomize fuel. Correspondingly, this supports precise control of injection timing and quantity.

However especially in diesel motors, high pressure fuel injection system may be source of noise that plays a significant role. As a result, it has been become a challenge for valve train design with the consideration of excitation of these high pressure mechanical components. Achieve the new limits these high pressure mechanical components are subject to large varying load and speed profiles, which result in noise.

As you can clearly figure out from the Figure 1.3, it gives an opportunity to go improvement with fan, auxiliary parts as for instance pumps, turbo charging system, timing drives, power conversion (Piston, connecting rod. etc.) and fuel injection system as stated again in the figure1. From the mechanical side of the injection system, there is a general assumption which is considered as additional forces and mechanical dynamics on cam shafts in the case of unit pumps. As the system working principle of unit pump injection system, the mentioned loads and dynamic effects are expected with low profiles. The influence of high pressure mechanical systems of Common Rail on NVH is typically neglected, although there are excessive loads due to high pressure oscillation inside the rail, which is sufficient enough to excite cylinder head and combustion area. In general, high pressure common rail pump working mechanism contents high range of force frequency which result in valuable contribution to overall engine NVH behavior.

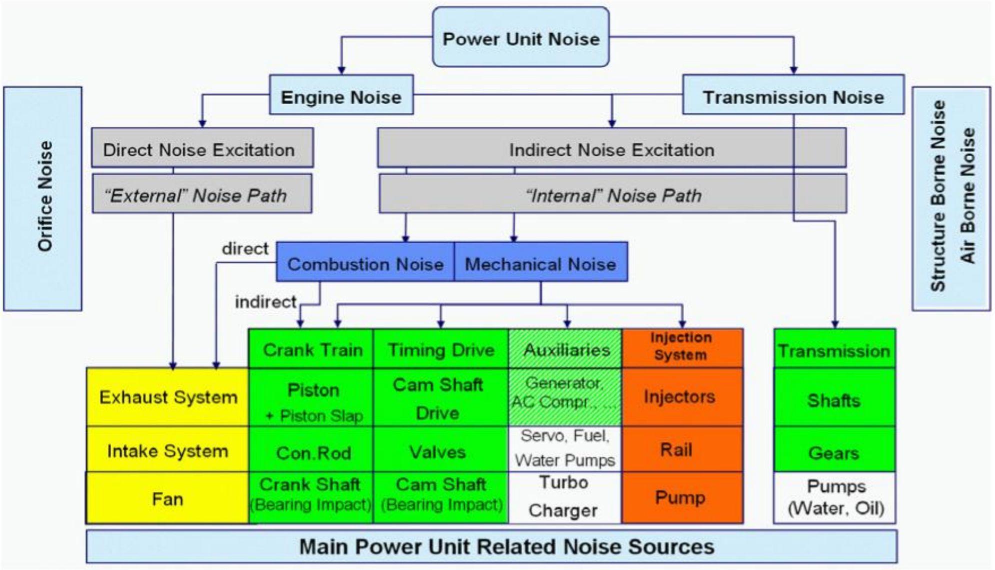
Power Unit Noise
Engine Noise
Transmission Noise
Orifice Noise
Structure Borne Noise
Air Borne Noise
Direct Noise Excitation
"External" Noise Path
Indirect Noise Excitation
"Internal" Noise Path
direct
indirect
Combustion Noise
Mechanical Noise
Crank Train
Timing Drive
Auxiliaries
Injection System
Transmission
Exhaust System
Piston + Piston Slap
Cam Shaft Drive
Generator, AC Compr.
Injectors
Shafts
Intake System
Con.Rod
Valves
Servo, Fuel, Water Pumps
Rail
Gears
Fan
Crank Shaft (Bearing Impact)
Cam Shaft (Bearing Impact)
Turbo Charger
Pump
Pumps (Water, Oil)
Main Power Unit Related Noise Sources

Figure 1.3 : Power unit related noise sources [2].

The latest high pressure common rail systems in use by modern diesel engines, the high pressure fuel injection pump governs the overall performance of the fuel system required. Under the condition of such a high pressure profiles, the conventional high pressure fuel injection pumps may not perform satisfactorily for heavy-duty diesel engine applications required due the large input drive torque, low efficiency and excessive bearing load.

In scope of work takes a V8 4.4 L engine model which is operated with 2000 bar final rail pressure profiles at common rail. There are also required validation is performed with recommended measurements taken from different engine load/speed cases. Performance of the radial plunger pump used in the V8 4.4L diesel engine common rail fuel systems for rail-pressure supply is questioned. On the ground of the pump mechanism, hydraulic characteristics, drive torque and mechanical efficiency of the pump are evaluated with various load/speed conditions. The analysis shows that changeable characteristics of a high pressure common rail pump enables a better NVH response and Design of Experiment (DoE) study.

While required time and cost effect plays a crucial role in the development of power train industry, the importance and efficiency of simulations has increased. With the support of dynamical and hydraulic models can be evaluated and optimized before a prototype is built. By this way, CAE studies can be a projection at the beginning of development work and this kind of methodologies can improve engineers' control on engine system unpredictable failure modes.

2. METHODOLOGY

2.1 Objectives and Scope

The main purpose of this thesis is to develop a reliable MBD model of a high pressure common rail pump in order to understand the dynamic behavior of reciprocating pumps under the actions of the mechanical and hydraulic forces. The effects of any design changes to the dynamics of the high pressure pump can be easily observed with such numerical models. Consequently, reliable numerical models of high pressure pumps can be used to for designing better integration with engine valve train system and can help to reduce the number of prototypes during the development stage. In this context, the works that need to be carried out in this thesis are summarized below as;

1) To build 1D analytic simulations of high pressure pump in order to collect load data coming from reciprocating movement and hydraulic effects and validate these with the provided test rig data.
2) To build finite element models of individual parts of a high pressure pump and validate these finite element models by means of real data.
3) To engage these models by using appropriate software and obtain dynamic model by adding the effects of dynamic forces.
4) To simulate operating conditions of high pressure pump and determine the vibration characteristics.
5) To validate the forced response model.
6) To investigate key parameters which affect the vibration characteristics of high-pressure pump.

2.2 Methodology Details

As stated at the beginning of the thesis, the development and the use of a numerical model to predict vibrational response from reciprocating high pressure pumps with camshafts due to dynamic and hydraulic effect using Computer-Aided Engineering (CAE) technologies. This CAE methodology process, as outlined in this thesis study, includes measured data, computational flexible multibody dynamics and 1D and 2D analytic tools to evaluate internal effects. The measured test data is used to identify and reproduce the input excitation which is primarily generated from engine and high pressure pump dynamic and hydraulic. The dynamic interaction of the high pressure pump components, including excitation camshaft, contacting gears, dynamic joints, and flexible housing is modeled using flexible multibody techniques. High pressure pump model is simultaneously connected with these mentioned CAE tools to produce a real environment simulation which can be used in noise, vibration and harshness(NVH) performance evaluations. The developed CAE multibody model has a potential of key benefits of using it in the analysis and performance improvements of high pressure pumps. Another major advantage of using such a multibody model is its promising capability in reducing physical prototypes by virtually testing different design modifications. Such reduction in testing necessity and physical prototypes will result as efficiency in cost and time saving.

As you can see the illustration of the methodology Figure 2.1, each step is validated with either a real world engine testing or component rig data.

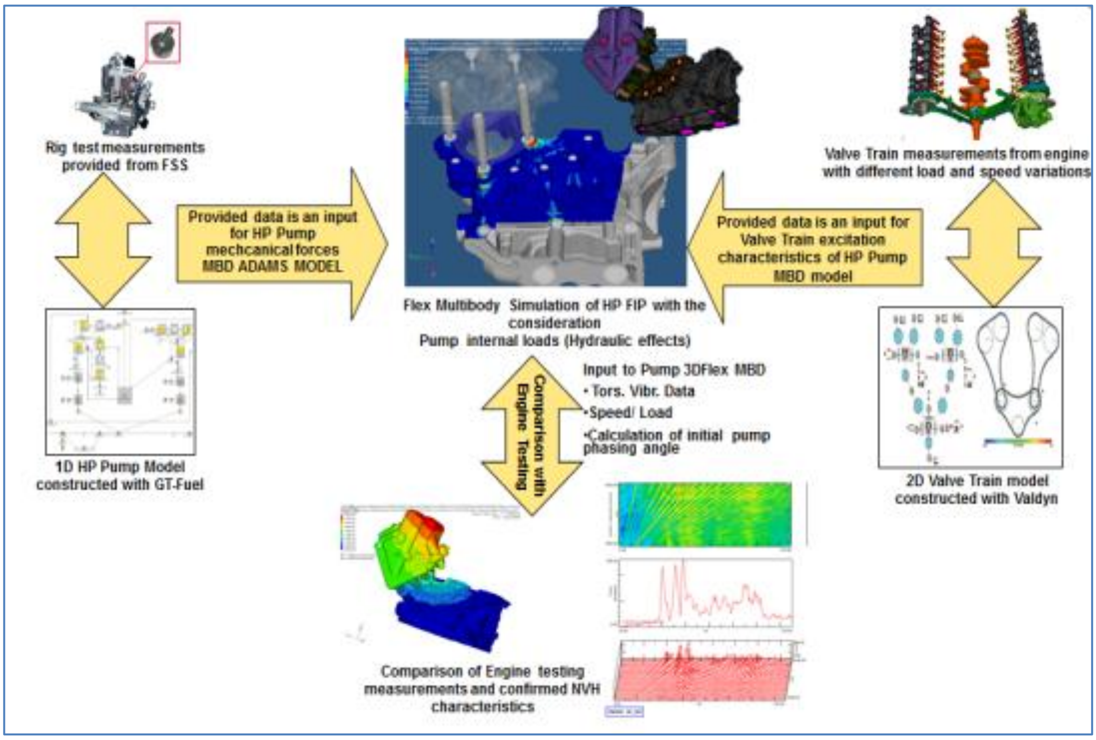
Rig test measurements provided from FSS
Provided data is an input for HP Pump mechcanical forces MBD ADAMS MODEL
Flex Multibody Simulation of HP FIP with the consideration Pump internal loads (Hydraulic effects)
Valve Train measurements from engine with different load and speed variations
Provided data is an input for Valve Train excitation characteristics of HP Pump MBD model
1D HP Pump Model constructed with GT-Fuel
Comparison with Engine Testing
Input to Pump 3DFlex MBD
• Tors. Vibr. Data
•Speed/ Load
•Calculation of initial pump phasing angle
2D Valve Train model constructed with Valdyn
Comparison of Engine testing measurements and confirmed NVH characteristics

Figure 2.1 : Simulation methodology overview.

The Valdyn® package was used to build a kinematic simulation model of a complete primary drive for a V8 Diesel engine used as case study. The responses of particular interest from the dynamic model are the gear-pair, tooth and train loads. The model was validated against real world load data measurements collected from a prototype engine. Also, the confirmation of the model will be explained in the following content of the thesis in detail. The constructed valve train model consists of support of camshaft stiffness, roller physical properties, detailed geometry definitions for the cam lobes (including rotational inertia), valve seat stiffness and valve spring definition.

The GT-Fuel® package was used to build a hydraulic and kinematic 1-D model of high pressure fuel injection pump. The hydraulic internal parts of the high pressure fuel pump are calculated separately with a 1-D hydraulic simulation approach. During the calculation of mechanical elements which are sub-components of the high pressure fuel pump, the methodology considered cover the interaction and the effect on resultant excitation loads correctly. Dynamic analyses of hydraulic and hydro-mechanical systems are simulated based on the theory of kinematic of multi body systems and fluid dynamics. This simulation technology is applied in a variety of opportunities concerned with dynamic analysis of hydraulic and mechanical systems. Basically, the modeling program has been focused for the simulation of diesel injection system. Constant and fixed set of input parameters are associated with each element in the content of high pressure pump which are geometrical properties, flow characteristics, fluid properties. With this simulation method, it gives us an opportunity to evaluate velocity and/or acceleration for mechanical elements pressure and rate for hydraulic elements and coordinate. As a boundary condition input, crankshaft angular velocity with the interaction of drive ratio excites the high pressure pump hydraulic model. Hydraulic, frictional and mechanical forces are transferred to the pump housing corresponding to the plunger and cams body to the pump shaft.

The Adams® package was used to build a multibody dynamic 3D model of high pressure fuel injection pump. To obtain a more realistic model, which will include additional hydraulic effects and mechanical excitation, a representative fuel pump model is build up within an existing Valdyn® timing drive model. With the support of using this model, also dynamical effects coming from valve excitation and internal effects are considered. Furthermore, pressure in pump piston is applied as load boundary condition acting on the pump plungers. Moveable mechanical components of the high pressure fuel pump are considered as internal multi-body components and integrated with the coming effect from valve train model. Fuel pump housing is modeled as flexible structures and fixed to the engine model. Resulting transient loads are torsional vibration effect coming from valve train and pressure oscillation in high pressure pistons of the plungers in pump body.

The development of a complete new engine without extensive CAE support is no longer done. Early in the design process decisions are based on preliminary calculation. Calculations accompany revisions throughout Also the trend to use the same engine in various cars, and therefore different application, generates a further need for use of computer codes. Requirements vary from application to application and therefore demand slight changes in engine design and calibration [3]. Some of the various tasks for simulation tools within the engine development process are summarized in the Figure 2.2 as represented below.

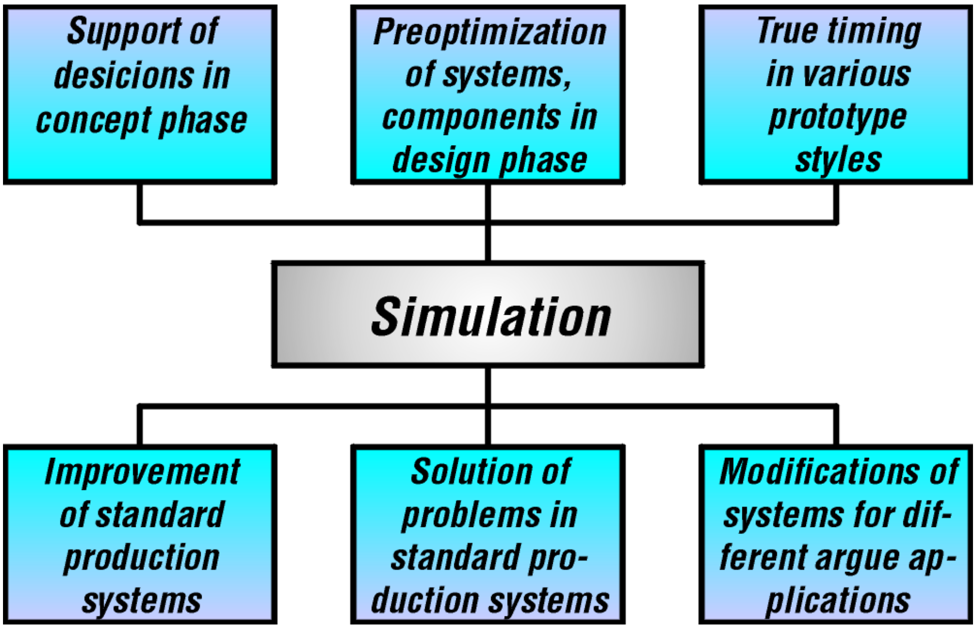
Support of desicions in concept phase
Preoptimization of systems, components in design phase
True timing in various prototype styles
Simulation
Improvement of standard production systems
Solution of problems in standard production systems
Modifications of systems for different argue applications

Figure 2.2 : Components in a simulation package [3].

Figure 2.3 illustrates the requirements of simulation codes, in above. A potential benefit in the use of commercial codes lies in the possibility of exchanging models between multiple parties within a common project. Nowadays projects are characterized by simultaneous efforts between manufacturer, engineering partner and system supplier [3].

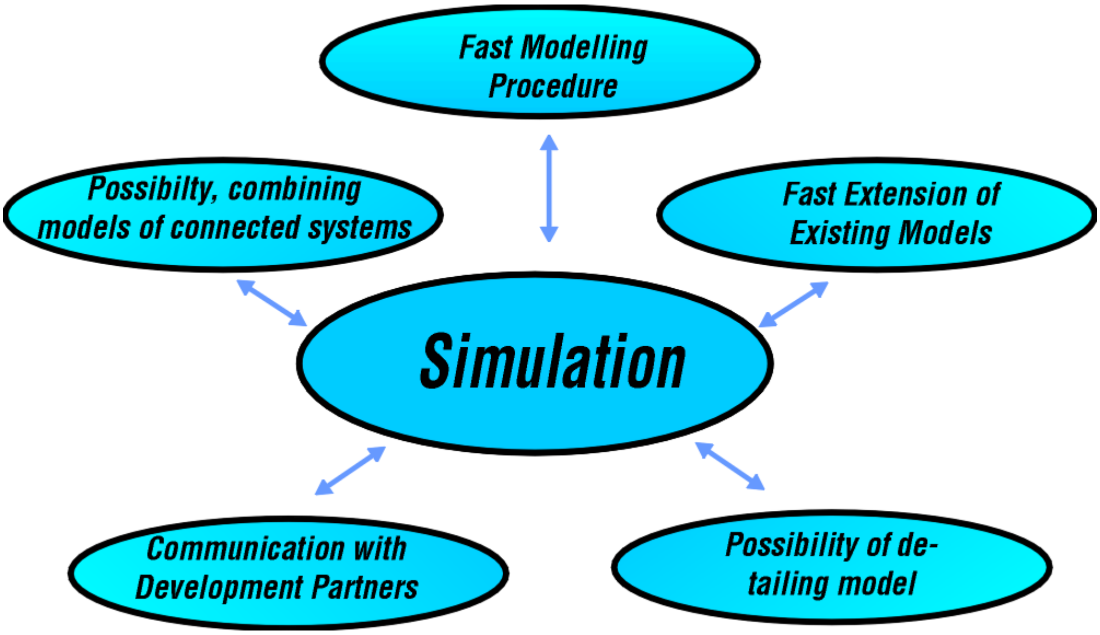
Fast Modelling Procedure
Possibilty, combining models of connected systems
Fast Extension of Existing Models
Simulation
Communication with Development Partners
Possibility of de-tailing model

Figure 2.3 : Requirements of simulation tools [3].

Each of the parties is concentrating on different components or tasks within the system. To avoid repetitious or redundant efforts it is necessary to decide which partner will create the basic model of the valve train and its drive. Usually the model is built by basic elements representing different components or parts of them. The intended extensions of the model can either be realized with the elements being implemented in the main program or by user defined subroutines. The ability to exchange models also offers opportunities for modification of production engines. If modifications are necessary, a calibrated simulation model is necessary to evaluate a specific change, e.g. of a cam contour or a modified valve spring [3].

3. FUEL INJECTION SYSTEMS

3.1 Introduction

Generally called 'the heart of the engine', the high pressure fuel injection system is without any doubt one of the most important engine systems which takes a role for diesel engine working principle. High pressure fuel injection system meters the required fuel delivery according to engine requirements; meanwhile it generates the high pressure profiles on injector required for atomization of the fuel, for sufficient fuel air mixing and for diesel combustion event. High pressure fuel injection system controls to the fuel distribution in the combustion system-hence it highly contributes to engine noise, performance and emissions.

The mechanical components of the high pressure fuel injection system require the key items listed in below;

- Proper selection of materials
- High precision manufacturing processes
- Accurate design standards.

That is the reason, these components lend themselves to serial production techniques and correspondingly, they become complex and higher level of costs [4].

As known, the applications of diesel engines diversified so did the fuel injection systems. As stated, along with the conventional from pump line to nozzle systems concepts evolved such as distributor pumps, common-rail systems, accumulated injection systems, unit pump injection systems and unit injector injection etc. Furthermore, the 'intelligence' of electronic control system enhanced the capability of the 'extreme power' of hydraulics making the efficiency of combustion system much more flexible and meanwhile responsive to new physical parameters: pressure, temperature, engine speed, etc.

Combustion can be thus optimized for best performance, emissions, smooth operation etc., according to the needs of the application. Through electronics, the fuel injection system can interface with other systems; automatic transmissions, cruise control, turbocharger operation, traction control, exhaust after treatment, etc. in an integrated system approach. The net result of this integration is an advanced diesel engine with high power density, very low emissions, low noise and superior drivability. Probably the most dynamic application of advances in fuel injection and electronic management is in the area of light-duty vehicles (passenger cars, light trucks, sport utilities) where constraints of high performance, low emissions, low noise, low cost, etc., render optimization very challenging. The research and development in fuel injection systems continues at a very sustained pace [4].

3.2 Types of Modern Injection Systems

3.2.1 Unit injector system

Lots of spectacular high pressure fuel injection systems have been produced by several manufacturers, usually in the form of a 'unit injector'. These unit injectors are driven from the diesel engine rotating camshaft for exhaust/intake systems and the pumping element and the nozzle are integrated in the same content of assembly.

Fuel control in usually by rotation of the pumping element, as in the basic jerk pump, but other ingenious mechanical means have been introduced to control fuel delivery. The engine camshaft needs to be somewhat stiffer in torsional deflection in order to maintain accurate injection timings despite variations in loading due to valve and injection events. The juxtaposition of nozzle and pumping element reduces the hydraulic wave travel time, however, the mechanism of operation still generates waves in the drillings within the unit injector, which are difficult to eradicate when high pressures are generated [4].

As you can see from the Figure 3.1 below, the subcomponents are explained by given numbers as;1 Cam, 2 Pump plunger, 3 Engine, 4 Return, 5 Injection nozzle, 6 Solenoid valve, 7 Inlet

As illustrated in the Figure 3.1 below again, basically concept is screwing the injector to the cylinder head, means the unit injector is mounted directly into the engine's cylinder head [4].

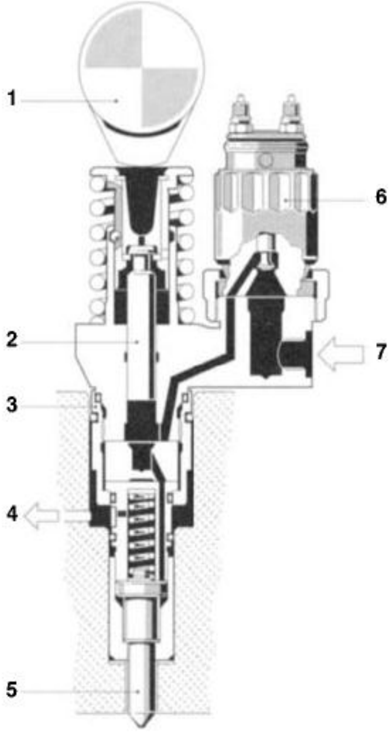

Figure 3.1 : Overview of a unit injector and sub-components [4].

As mentioned, high pressure injection pump and the injection nozzle are combined in a single unit which is directly excited by engine camshaft. Each high pressure unit injector has its own high-speed solenoid valve which enables controlling the timing of injection start and finish. By the activation of solenoid valve(opens), the unit injector forces fuel into the return line, and by the deactivation of the solenoid valve (closes), into the engine cylinder. The solenoid closing point defines the timing of injection start and also controls the injected fuel quantity by the closing time (the duration of the solenoid remains closed). With the usage of an ECU with map-based control triggers and adjusts the activation of the solenoid valve, which means the timing of start and finish of injection are programmable and controllable and therefore independent of piston to position (cylinder to cylinder variation) in the engine cylinder [4].

In comparison of the injection valve/injector in electronically controlled gasoline injection systems, the solenoid valve in use by diesel engines must be able to control the pressure profiles which are 300-500 times higher and must also be capable to switch their activation and deactivation mode 10-20 times faster. In today's conventional high pressure fuel injection systems, the physical characteristics of the high pressure pipes and lines between high pressure injection pump and injection nozzle limits the maximum injection profiles. As you can see Figure 3.2**,** the high pressure unit injector designs and makes such lines superfluous which up to 1500 bar pressure profiles on injector nozzle are possible and with this way highly atomization of the diesel fuel can be achieved. These magnitude of pressure levels with the contribution of map-based control of start of injection and duration of injection (injected fuel quantity), support to a considerable reduction in the diesel engine's emissions and directly effects pollutants emission.

Additionally, with the introduction of improved electronic control strategies, special models, functions and algorithms such as temperature-controlled start of injection, engine smooth-running control, anti-buck damping and also pilot fuel injection foreven further reductions in noise, become feasible. In addition, the use of unit injectors makes it possible to switch off individual engine.

As you can see the Figure 3.2 in above, this technology with higher injection pressure profiles enables diesel engines operated without any problem to achieve exhaust-gas values better than those prescribed by the strictly released regulations. Because of their high injection pressures, high pressure unit injection systems which are in use by diesel engines also shows a performance which are highly good degree of efficiency and provide a high torque with low brake specific fuel consumption even at low engine load and speed variations [5].

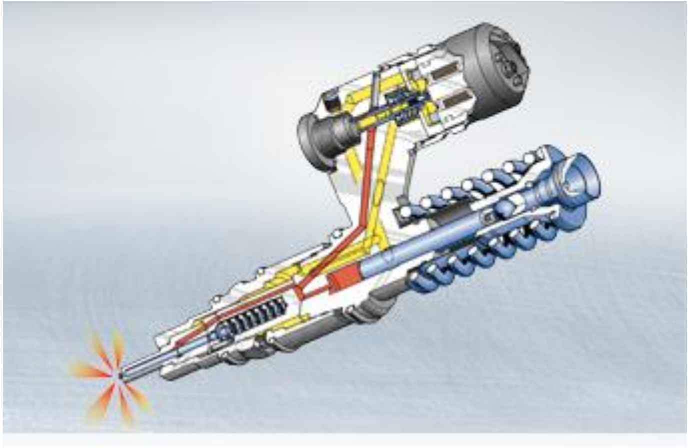

Figure 3.2 : Schematic of a modern unit injector commonly used in the field [5].

The recent system generation precisely permits injection with variable duration of injection throughout the entire engine map. So, improved combustion is produced by the resulting discharge rate and higher pressure profiles combustion. By this way, inevitably diesel engines can have more performance, lower fuel consumption and reduced exhaust and noise emissions [5].

- With the dual valve operation, sensitive for accurate control of injection events
- With the high pressure injection profiles, it can be easily to have more optimized combustion and reduced after treatment
- Lightweight, enhanced efficiency is got with compact design.
- Appropriate to be fit with a wide range of high pressure nozzle options
- Programmable shot-to-shot injection control is enabled with multiple injection
- Energizing time of the injectors may be programmable with the choice of variable nozzle concepts.
- Can be applicable with on board diagnostic tools
- Cost effective technology in comparison to common rail systems
- Surrogated data for durability indication of proven reliability and durability

3.2.2 Unit pump

The unit pump system is a modular high-pressure injection system. From the point of control engineering, the design concept is closely related to the unit injector injection system. As mentioned in the previous section, both systems use an individual injection pumps for each engine cylinder which is excited and driven by either an extra cam (injection cam) on the engine's camshaft or existed camshaft in use for inlet and exhaust valve system. The moment and accuracy of injection and the injected fuel quantity are precisely adjusted for each cylinder.

As shown in Figure 3.3; the typical sub-components of unit pump system is given which are; 1 Nozzle holder, 2 Engine, 3 Injection nozzle, 4 Solenoid valve, 5 Inlet, 6 High-pressure pump, 7 Cam

Furthermore, with the usage of this unit pump system permits:

- Fuel delivery to the injection nozzle
- Interruption of fuel delivery
- Return of excess fuel to the fuel tank.

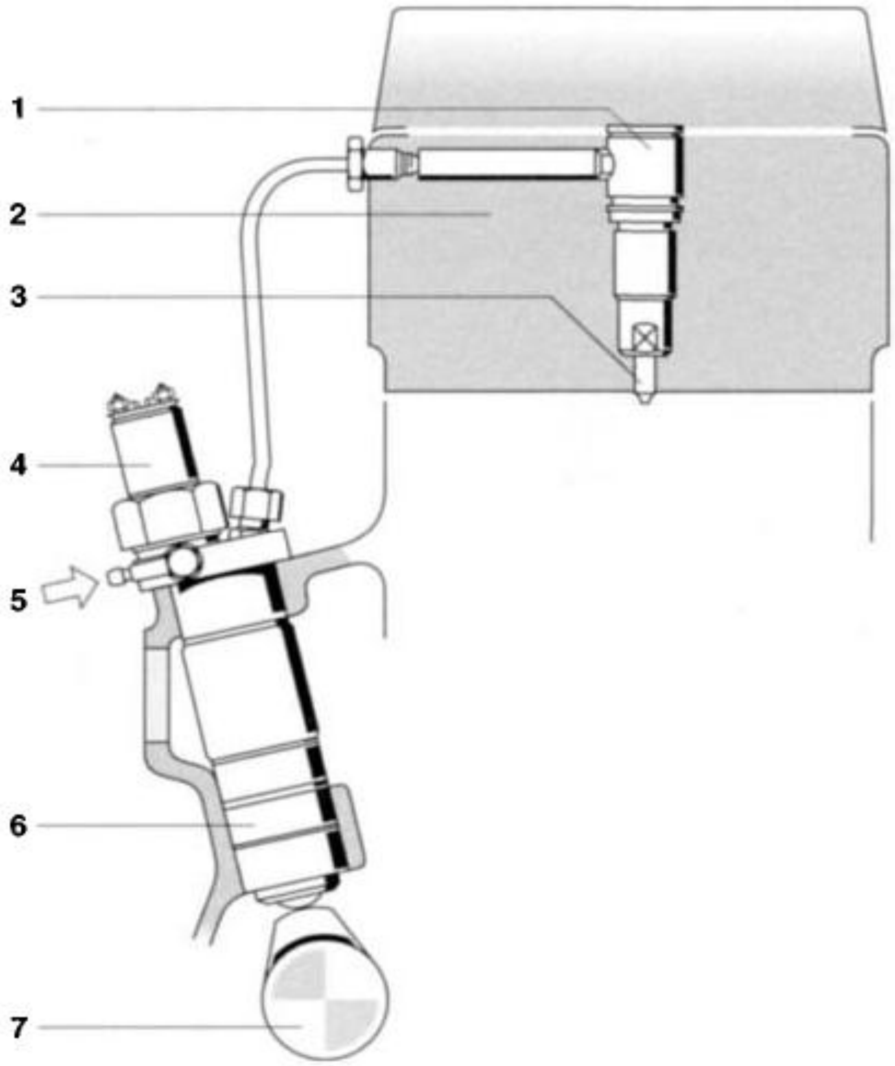

Figure 3.3 : Unit pump fuel injection system schematic [4].

Similar to the unit injector system, the unit-pump system registers the most important engine and environmental parameters, and converts them into the optimal start of injection and optimal injected fuel quantity for the given operating conditions. The system comprises the following modules:

- high-pressure pump with attached solenoid valve;
- short high-pressure delivery line; and
- nozzle-and-holder assembly.

With these advantages which are listed in above, coming with modular design. In comparison to the compact design of the unit injection system, the unit-pump system represents a directly controlled high-pressure injection system which is suitable for a wide range of different installation requirements [4].

This system is further characterized by a fault-recognition facility, the possibility of emergency operation and self-diagnosis, as well as the option of communicating with other control systems via already existing interfaces [4].

As shown in the Figure 3.4 below, working mechanism based on the required pressure which is accumulated with a directly driven and excited camshaft. In general, this mechanical system lies beneath a commercial engine; the cam pitch located on the excitation shaft is transferred to the small piston in the unit pump injection unit via a roller tappet. The shape of the cam profile is designed in such a way that the required and desired high pressure profiles are generated as quickly as possible in the section of the below of piston called plunger. There is an electronically-controlled fast-switching solenoid valve enables determination of injection start and finish. The activation duration determines the amount of fuel injected quantity directly related with energizing time.

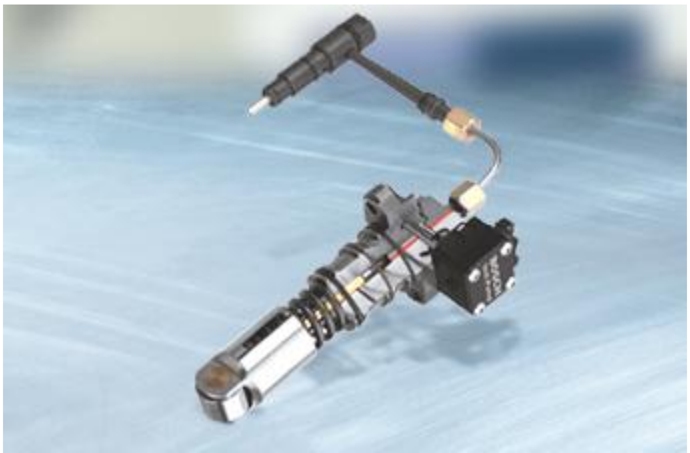

Figure 3.4 : Modern unit pump system commonly used in the field [6].

- With the dual valve operation, sensitive for accurate control of injection events
- With the high pressure injection profiles, it can be easily to have more optimized combustion and reduced after treatment
- Lightweight, enhanced efficiency is got with compact design.
- Appropriate to be fit with a wide range of high pressure nozzle options
- Programmable shot-to-shot injection control is enabled with multiple injection

- Energizing time of the injectors may be programmable with the choice of variable nozzle concepts.
- Can be applicable with on board diagnostic tools
- Cost effective technology in comparison to common rail systems
- Surrogated data for durability indication of proven reliability and durability

3.2.3 Common rail system

Heavy duty diesel engines are in conflict between the goals of emission reduction and optimization of fuel consumption. To fulfill future more stringent exhaust gas limits further developments on diesel engine technology are necessary. The diesel injection system assists this development and becomes the decisive factor to reach the emission targets. In the last 30 years a trend to high pressure fuel injection systems with an increase of maximum injection pressure from 800 up to 2000 bar is visible, as shown in Figure 3.5. In future very flexible high pressure fuel injection systems are necessary with multiple injection and rate shaping capabilities and a maximum injection pressure beyond 2000 bar.

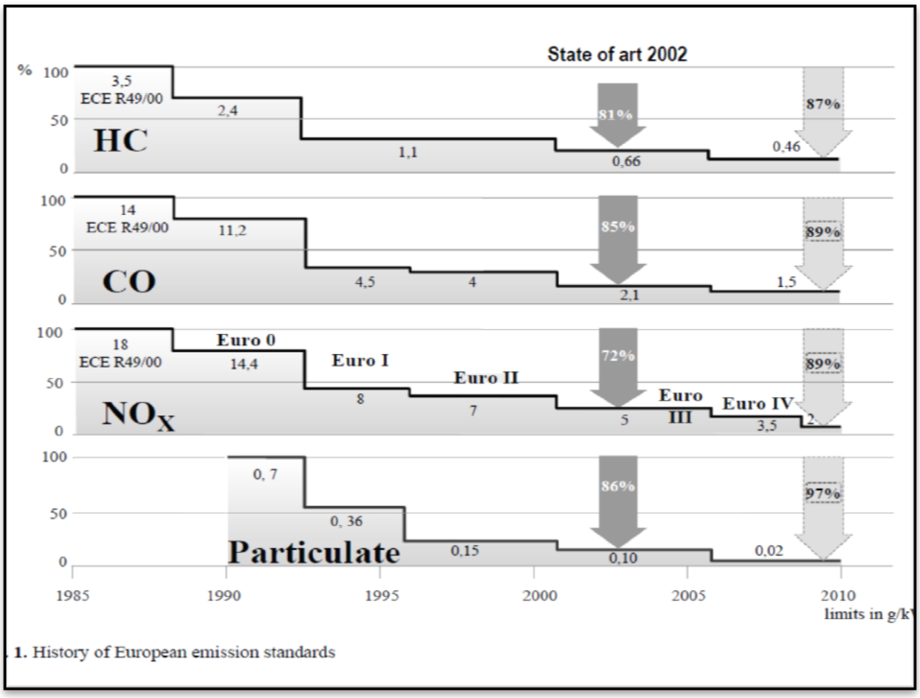

Figure 3.5 : History of European emissions standards [7].

Another very important point is the high efficiency of the fuel injection system itself to reach low fuel consumption. New product engineering like new nozzle design (k-factor, vario nozzle,..) or new developed actuators are key factors for the fuel injection development.

With the introduction of new systems shown in Figure 3.6, the late post injection is assisting the exhaust gas after treatment systems. Especially for the engine map the optimum rate shaping, injection timing and multiple injection is possible to get the best compromise between emission trade off and fuel consumption. The regeneration of the diesel particulate filter is for example because of too low exhaust gas temperature without the support of the injection system not under all circumstances possible. The exhaust gas temperature management by late post injection is a measure to improve the efficiency of catalyst systems at low exhaust gas temperatures [7].

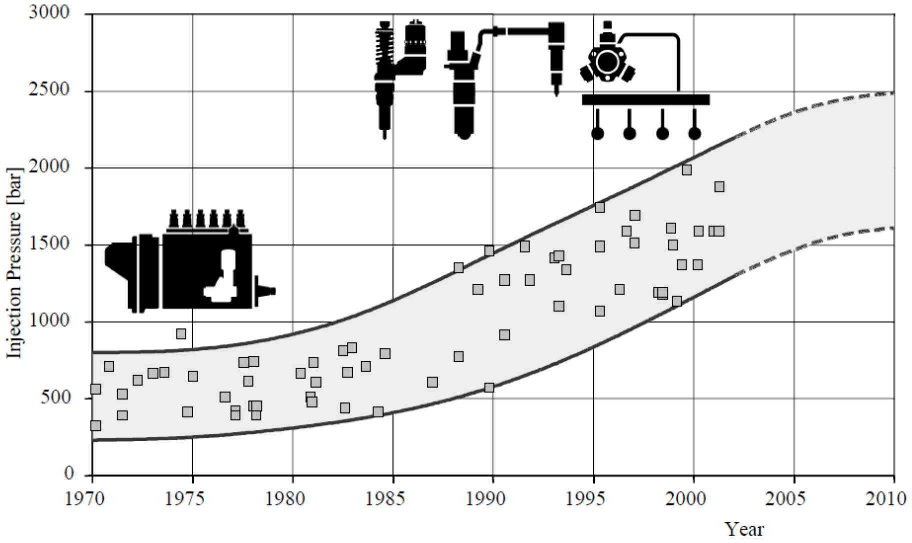

Figure 3.6 : Development of injection pressure of HD Engines [7].

For example with exhaust gas recirculation (EGR) a rectangular type main injection with high injection pressures at full load is recommended. On the other hand without EGR in this point of the engine map a boot or ramp shape injection leads to the best emission results at constant or improved fuel consumption. With a coupled post injection the soot emission could be reduced. Very important in future is the capability of the electronic control unit (ECU) of the diesel injection system to control air management, exhaust gas emission management, tolerance reduction, diagnosis, vehicle functions and combustion process by the fuel injection system. Diesel engines are in a conflict between emission reduction and optimized fuel consumption. Especially the fuel consumption of heavy duty diesel engines has a big impact on the overall costs of the haulage business. Since end of the 80's we have a dramatic reduction of HC, CO, NOx and particulate mass emissions to fulfill the exhaust gas legislation, Figure 3.5, NOx-emission was reduced about 72 percent from 1985 up to now. In the same period of time the CO-emission was reduced about 85 percent and the HC-emission about 81 percent. Additionally the diesel engine manufacturers reached a 86 percent reduction in the particulate mass emission since 1990. This was only possible with consequent optimization of the diesel engine technology. Examples of improvements are turbocharging, intercooling, four valve technology, EGR, combustion chamber design and high injection pressures [7].

In future furthermore exhaust gas after treatment systems, low sulphur diesel fuel and further improvements on diesel engine technology are necessary to fulfill future stringent exhaust gas legislation. The change in the on-highway market from inline pump systems to high pressure fuel injection systems (VP44, UIS, UPS, CRS) is in Figure 3.7 presented.

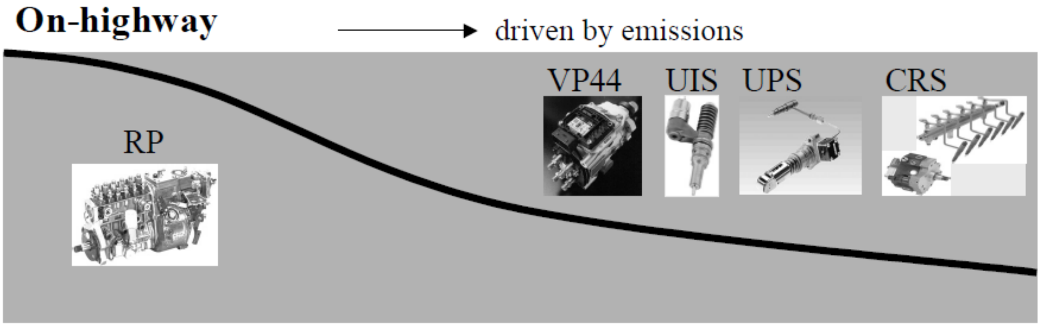

Figure 3.7 : Fuel injection system trend on highway application [7].

This market is mainly driven by emissions. In the off-highway diesel engine market this injectionsystem is also gradually replaced by the high pressure fuel injection systems [7].

With the introduction of variable geometry turbochargers (VGTs), the air charging role is much denser at the top dead center of the compression stroke at low and midrange speed profiles of engine rotation. As mentioned in previous paragraph, higher injection pressures are recommended to exploit the potential improvement in partial torque area and hence vehicle performance and drivability. As shown in Figure 3.8 below, these characteristics can be met in part by advanced cam-operated systems, such as recent developments. of unit injectors for passenger cars as emphasized in the previous sections, especially introduction of solenoid actuated injectors in unit injector systems.

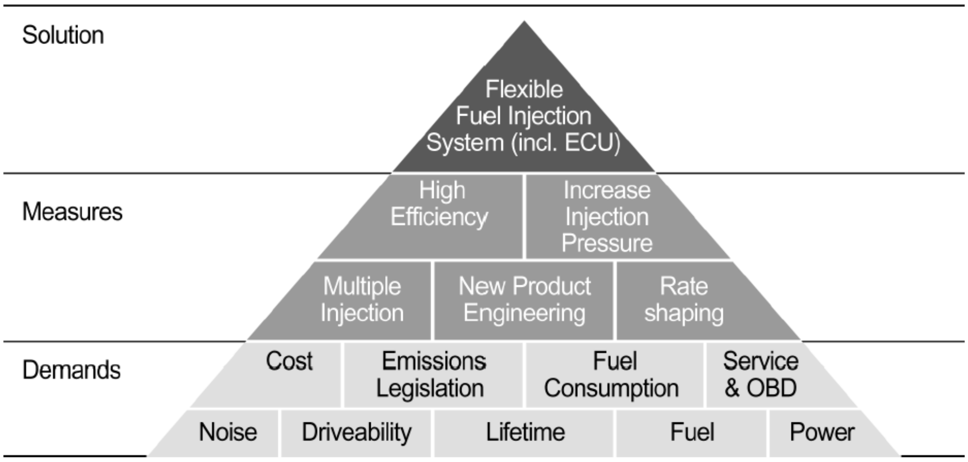
Solution
Flexible Fuel Injection System (incl. ECU)
Measures
High Efficiency
Increase Injection Pressure
Multiple Injection
New Product Engineering
Rate shaping
Demands
Cost
Emissions Legislation
Fuel Consumption
Service & OBD
Noise
Driveability
Lifetime
Fuel
Power

Figure 3.8 : Key factors for diesel fuel injection system development [7].

Nevertheless, the drive torque required poses some challenges in terms of mechanical noise and torque oscillations and fluctuations, due to the high rate profiles of cam required.

An alternative scheme as shown in Figure 3.9 below, which offers added flexibility, is to supply the requirements from each cylinder from a common high pressure supply (a common rail) via a valve in each injector.

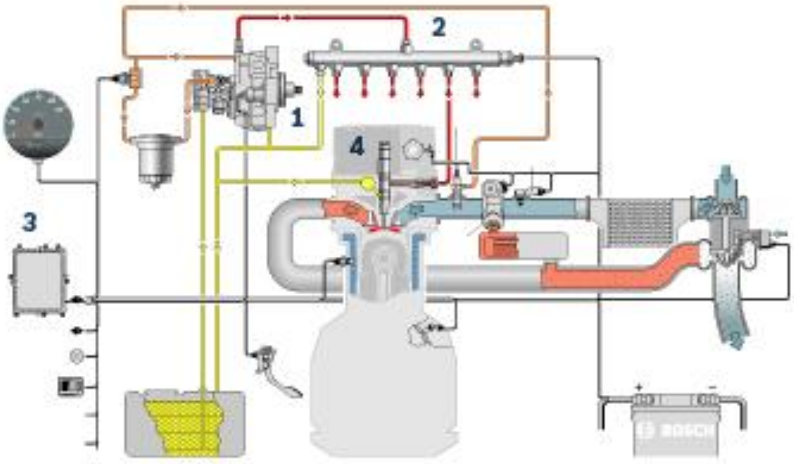

Figure 3.9 : Modern common rail system schematic [6].

Here are the working mechanism briefly explained in this section, the schematic of a modern common rail system is represented in Figure 3.9; The primary pump (1) supplies fuel to a high-pressure reservoir, the fuel rail (2), here the fuel is stored at the optimal pressure for the engine's instantaneous operating conditions in preparation for subsequent injection. Each of the engine's cylinders is equipped with an injector (4) featuring an integral solenoid valve. This solenoid valve opens and closes to define the starting point and mass of the injection process. The driver's demand is defined by the accelerator pedal. The ECU (3) registers driver demand and current vehicle operating conditions as the basis for calculating the required fuel pressure, injection duration (= fuel mass) and injection timing according to the parameters defined in the program map. High-pressure fuel from the supply pump is distributed to an injector mounted on each cylinder by means of the common rail, with fuel injection quantity and timing determined by controlling the injectors [5,6].

3.2.3.1 Advantages

In comparison with conventional injection system characteristics, a common rail system has the following benefits briefly:

--Injected fuel quantity and corresponding to that injection pressure are independent of each other, and are definable and controllable for each and every engine operating condition, allowing optimum air/fuel mix formation which means best-fit optimization.

-- At the beginning of the injection process at combustion area (during the ignition lag between the start of injection and the start of combustion), injected fuel quantities are very low means better brake specific fuel consumption.

In general, the common rail system gives a distinct opening and closing of the solenoid actuated injection valve. This actuation (closing and opening of the valve) operation secures rapid atomization, better penetration and mixing between fuel and air ratio in the initial phase and minimizes the end-phase of the injection period with the consideration of rapidly dropping pressure. There is a pressurized fuel reservoir at the inside of the injector nozzle end which is called sac volume is fairly constant throughout the injection. With the consideration of conventional systems, the pressure in the sac volume rises more slowly in the early stages of injection.

On the other hand, throughout the injection the pressure in the sac volume continues to increase due to the cam profile and is exceeding the pressure obtained by the common rail system. But in the final stage, the pressure in the sac volume decreases slower as the pressure is relieved at the pump side of the system. Now, what does this mean? A constant or slightly decreasing pressure in the sac volume gives a too intensive rate of injection at the start causing a steep combustion pressure rate, limited by the maximum firing pressure. The next phase of combustion, the rate of energy conversion is mixing controlled meaning that the injection pressure should be as high as possible. The injection pressure supplied by the common rail system is at its highest during the initial stages of the combustion, and may even decrease throughout the injection. All together this means that the rate of injection is not optimal for a medium speed combustion process.

There is a comparison given in below with the Figure 3.10 for the traditional cam driven system the rate of injection is progressive which is beneficial for the diesel process. The start of the injection is depending upon the spring force of the injector and the injection process is load dependent. The end of the injection is also a weak part of a mechanical system. Thus, the ideal system should be a combination of the two [8].

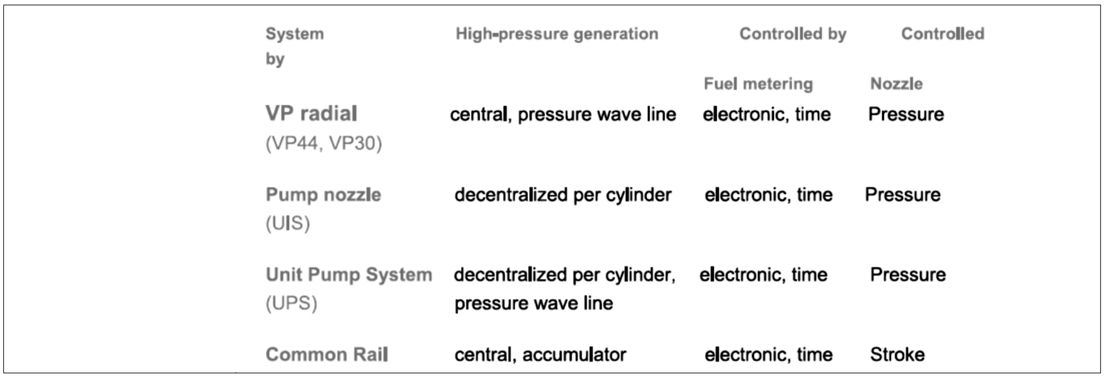

System by	High-pressure generation	Controlled by	Controlled
		Fuel metering	Nozzle
VP radial (VP44, VP30)	central, pressure wave line	electronic, time	Pressure
Pump nozzle (UIS)	decentralized per cylinder	electronic, time	Pressure
Unit Pump System (UPS)	decentralized per cylinder, pressure wave line	electronic, time	Pressure
Common Rail	central, accumulator	electronic, time	Stroke

Figure 3.10 : Breakdown of modern injection systems for vehicles [9].

Before the introduction of common rail fuel system, two common types include the unit pump/injection systems and the distributor/inline pump injection systems.

As shown in the Figure 3.11 below, both of the unit injector and distributed inline pump systems were cam driven and injection pressure was directly proportional to engine speed profiles. This means, the highest injection pressure profiles can only be achieved at the higher engine speed profiles and when engine speed decreases, the maximum achievable injection pressure decreases. Besides, It becomes clear that the injection pressure increases as the engine speed increases in camshaft-driven systems.

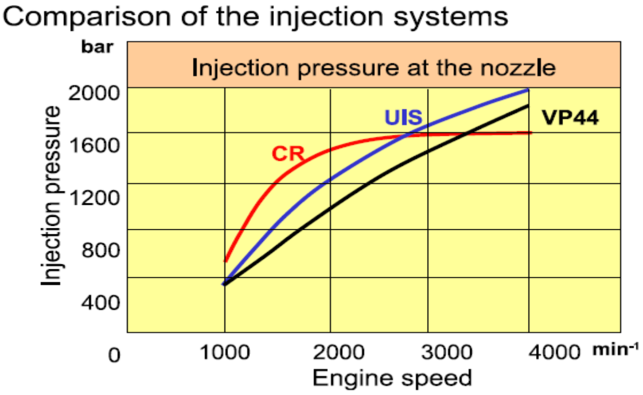

Figure 3.11 : Comparison of different injection systems [10].

In common rail systems, a higher pressure is available at lower engine speeds due to the decoupling of pressure generation and injection. This pressure is then held at a maximum pressure which is suitable for the system, whereas it increases linearly in camshaft-driven systems This working mechanism is true with all high pressure pumps, even those used on common rail systems; with the unit or inline systems, nevertheless, the instantaneous pressure of a single pumping event with no accumulator tries the injection pressure profile and thus the interaction and operation is more prominent and troublesome [10].

As shown in the Figure 3.12, they system architecutre and schematic of a typicalcommon rail system is given;

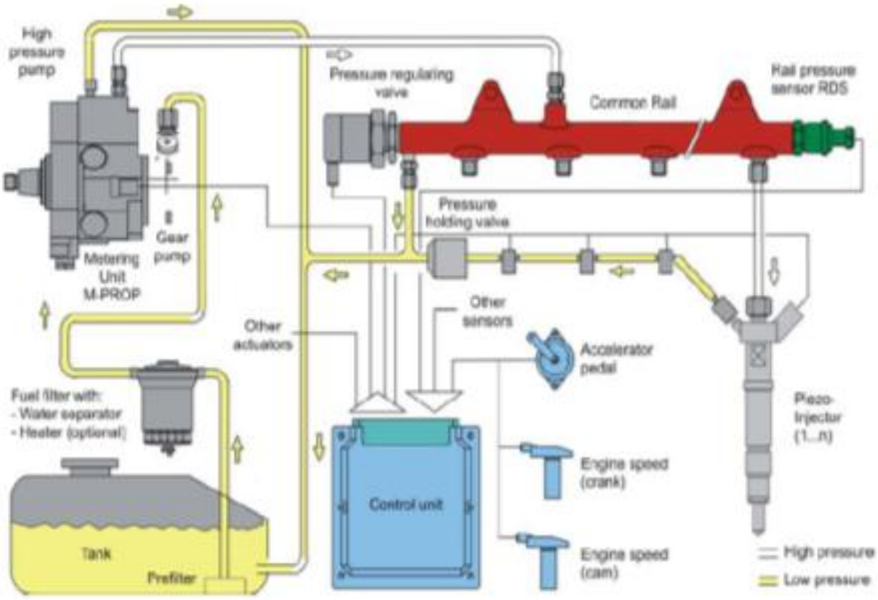
High pressure pump
Pressure regulating valve
Common Rail
Rail pressure sensor RDS
Gear pump
Metering Unit M-PROP
Pressure holding valve
Other sensors
Other actuators
Accelerator pedal
Fuel filter with:
- Water separator
- Heater (optional)
Piezo-Injector (1...n)
Control unit
Engine speed (crank)
Engine speed (cam)
Tank
Prefilter
High pressure
Low pressure

Figure 3.12 : Schematic of a modern common rail system [6].

4. TIMING DRIVE SYSTEMS IN INTERNAL COMBUSTION ENGINES

The main function of timing drive systems on internal combustion engines is to drive the camshaft(s) synchronously with to the crankshaft to provide torque transfer. That is the reason timing drive systems are performed to loading of interactions from driven systems like excitation of different pumps, crank train and valve train systems. There have been different types of timing drive system technologies for the motion and torque transfer for modern engine overhead camshaft drives such as briefly explained in below belt drive systems, gear drive systems and chain drive systems.

4.1 Types of Timing Drive System

There are mainly three technologies used to deliver torque from crankshaft to excited pumps and camshaft(s), which are belt drive, gear drive and chain drive. Durability, package, NVH, efficiency and maintenance costs are depended on the selection for the type of drive system.

4.1.1 Belt drive system

Timing belts are constructed with teeth that fit into a matching toothed pulley. When correctly designed and tensioned, they do not slip and are able to run at profiles of constant speed. By this way, they are generally used to transfer direct motion for excitation or timing purposes.

Belts are commonly used on engines operated with gasoline and relatively low volume diesel engines for passenger cars. A belt drive system illustration in above is shown with Figure 4.1 contents the sub-components which are toothed belt, exhaust pulley, intake cam pulley, crank pulley and several mechanical tensioners. Toothed belt drive usage is a common design way, as it ensures no slip characteristics for belt driven timing systems.

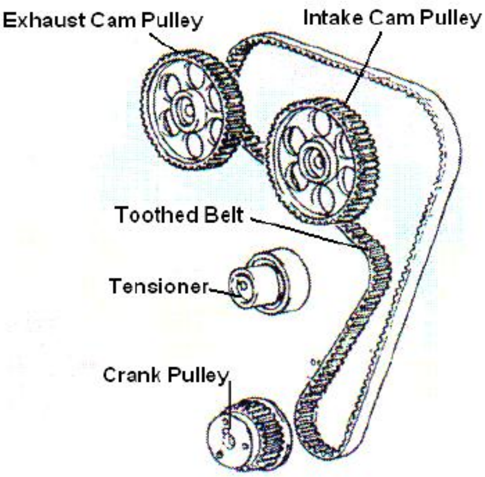
Exhaust Cam Pulley
Intake Cam Pulley
Toothed Belt
Tensioner
Crank Pulley

Figure 4.1 : Typical belt drive system and sub-components [9].

4.1.2 Gear drive system

Gear drives can be performed with very high load a carrying characteristic, which is the reason; heavy-duty diesel engines are commonly using them. Their capability about the high tensile strength prioritizes usage of gear drives with the heavy loading conditions in comparison to the conventional drive systems like chain or belt circuit. As shown in the Figure 4.2 below gear drive system consists of main gear(s) and an idler gear(s).

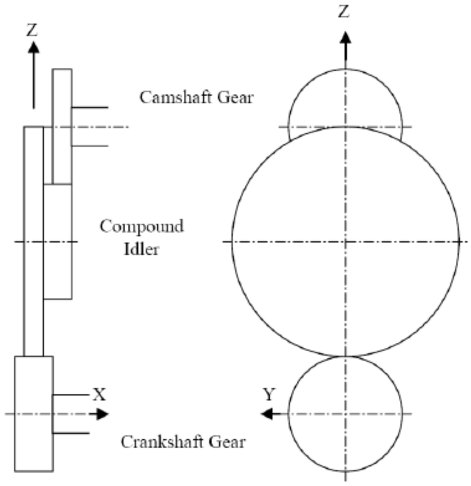
Z
Z
Camshaft Gear
Compound
Idler
X
Y
Crankshaft Gear

Figure 4.2 : Components of gear drive systems [9].

Main gears are generally used for the rotational motion transfer from crankshaft to excitation camshaft(s) by the idler gears and camshaft gears. The system just to transfer torque to the matching gear uses idler gears. An illustration of gear train systems can be seen on Figure 4.2. Another critical item is the determination of the durability of the gear trains; the size and thickness determine the load carrying capabilities of the gears. The structure and size of the gear contact area affects the gear wear properties and NVH characteristics [11].

4.1.3 Chain drive system

A chain is a reliable machine component, which transmits power by means of tensile forces, and is used primarily for power transmission. Chain drives are commonly used in commercial vehicle engines due to low maintenance costs. Special design chains are always valid for specific applications but there are three main types of chain drives available in today's automotive market that are bush, roller and inverted tooth chains which are also known as silent chains [11].

Additionally, guides and tensioners are used to maintain the tightness and degree of stress of the chain under any dynamic condition preventing vibration and dynamic resonances. The illustration shown in below that component of chain drive system is shown in Figure 4.3. Basic construction and system include crankshaft sprocket, camshaft sprockets, plastic guiding elements, and the tensioner.

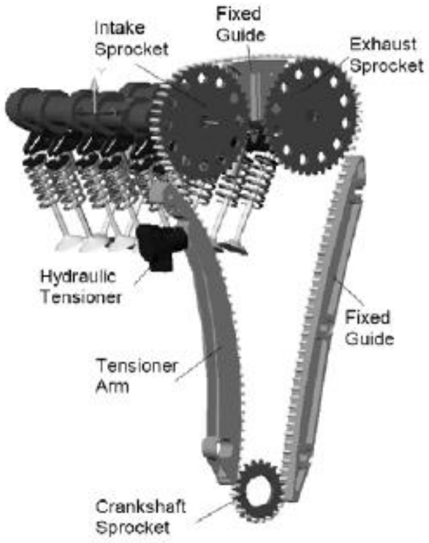

Figure 4.3 : Components of chain drive system [9].

Torque is transferred by the teeth of the sprocket meshing with the holes in the links of the chain and hereby-rotational motion input from crankshaft to camshafts and other adjacent drive systems is transferred [11]. A fuel injection pump or a water pump can be arbitrarily driven with the timing chain.

Here are the sub-components of the timing drive systems explained in following sections.

4.1.3.1 Timing chain

Generally, bush and roller chains are assemble and combination of bushings, pins, links and/or rollers, as presented in Figure 4.4**.** Pins make rolling and sliding motions within a certain range of tolerance while motional contacting the bushes, which is the reason, both components also need to have sufficient strength and wear resistance against frictional effects.

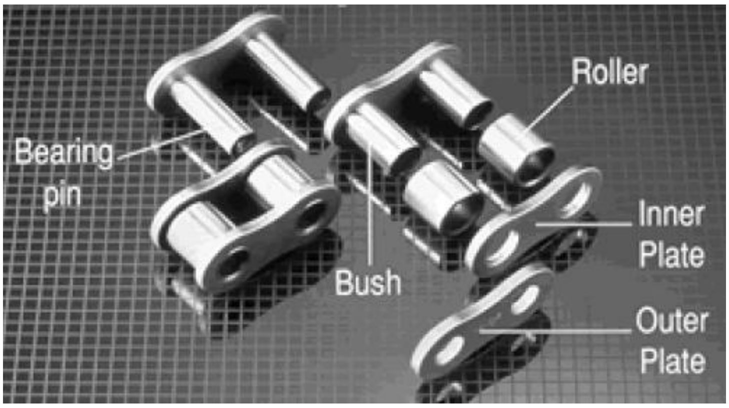

Figure 4.4 : Sub-components of timing chain [11].

Chain inner and outer links provide the linkage between pins and are in contact with sprocket teeth. Therefore, the area that contacts the plastic guides of the driving system should have good surface roughness. By this method, it enables to reduce friction and also wear on plastic guides.

Rollers are used in roller chains. They get in impact contact with sprocket therefore needs to have resistance to impact fatigue. The basic function of rollers is to convert the sliding motion between the bushing and sprocket teeth to rolling contact as the rollers are free to rotate over bushings [11]. Bushing chains and also subcomponents are the common used type of chain especially on various diesel applications. The general chain package offers different types of sizes and standards, which can easily be adaptable to timing drive layouts. You can see the general layout of bush chain, on Figure 4.5. Silent chains or inverted chains are the kinds of applications in order to reduced NVH characteristics are expected.

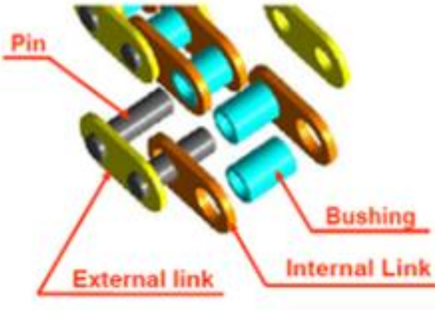

Figure 4.5 : Sub-components of bushing chain [11].

An illustration in below is given in Figure 4.6 consists the sub-components of silent chain [11].

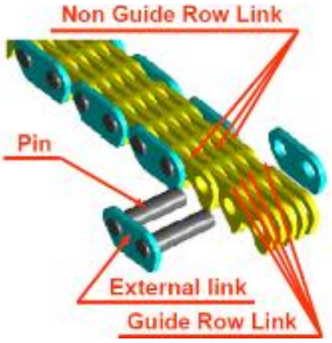

Figure 4.6 : Sub-components of silent chain [12].

As emphasized in the illustration in above, link plates contact to the sprocket teeth at a defined angle, the impact energy is comparably low on silent chains compared to roller and bush chains. By this methodology, it can be achievable for optimized noise behavior of the inverted tooth type chains and supports for the reduction of the polygonal action and its effects on NVH characteristics.

4.1.3.2 Guides

Fixed and tensioning guides are being used by characteristical chain drive systems . Plastic or a metal base fully constraines them with a plastic shoe.

Guides and tensioner arm with their geometries and locations operate as guidance to the chain that needs to follow a predefined driving circuit. They maintain the chain drive dynamic stability on all operating conditions and obtain dynamic condition preventing vibration and dynamic resonances.

4.1.3.3 Tensioners

Tensioner’s are one of the key sub-components of timing drive systems which main operation is to perform the required tension on the chain to supply provide sufficient take up on stress and thus elongation of the chain and also the dynamical stability. Tensioners as mentioned; can be either mechanical or hydraulic type. Further to this, hydraulic tensioners are commonly used on timing drive chain systems, especially with diesel systems [11].

4.1.3.4 Sprockets

With the enagegement of the sprockets, the chain enables converting pulling power to rotation power. Sprockets have many engagement profiles between teeth and profile of the teeth which is fundamental for the relative motion and contact forces. Design of the sprockets is critical as they exert the optimum loading and inertial characteristics on the chain drive. By this reason, proper optimization for dynamic compatibility NVH and wear performances can be achievable with sprockets teeth profiles. Besides, weight optimization for inertial effects is also critical for the design of the sprockets.

4.2 Modeling and Simulation Theory

In order to model the timing drive system Ricardo VALDYN simulation program is used. The theory and equations discussed in this section covers the working principle of VALDYN. Valves have to be actuated synchronously by the camshafts concerning the piston’s motion. Timing chain drives are intended to transfer motion from the engine’s crankshaft to the camshaft with a constant ratio. Therefore, precisely two crankshaft rotations are needed for a single camshaft rotation. Timing chain is the load carrying part in a timing drive system and it has contact with sprockets, plastic guides, and the parts creating the chain has contact in itself, as well. Friction loses are unavoidable where a contact between two parts take place, even lubricants present in the engine environment. Friction loss can be simulated in software thus, simulation tools are used extensively in the design of timing chain drives [11].

As the basic approach, each chain link is modeled by a single rigid body and connected to the adjacent chain links with spring and damper elements. Then the resulting multi-body system is simulated based on the Newton-Euler laws. The displacement of the chain is computed only in the x-y plane. The motion on the z-axis can be ignored without influencing the validity of the simulation. Therefore, each chain link has three enabled DoFs (degrees of freedom); translations in x and y directions and rotation around z-axis. Sprockets are modeled as generic mass elements with only one DoF, which is rotation about the z-axis. Similarly, plastic guides are modeled as generic mass elements, exclusively fixed guides has no rotational DoFs. Contact contours are defined to reflect the actual shape of the sprockets and plastic guides. An exception for the chain links is the identification of circles around the pins. The smaller circle defines the surface, which contacts the sprocket, whereas the larger circle is the outer surface, which couples the chain links and contacts the sprockets and guides [12].

The chain link forces and contact forces are calculated by VALDYN and defining the friction coefficient between contacting contours obtains the friction loss. As shown in the Figure 4.7, it can be figured out that the contact forces between chain links and the sprockets or guides, and link connection forces between adjacent chain links.

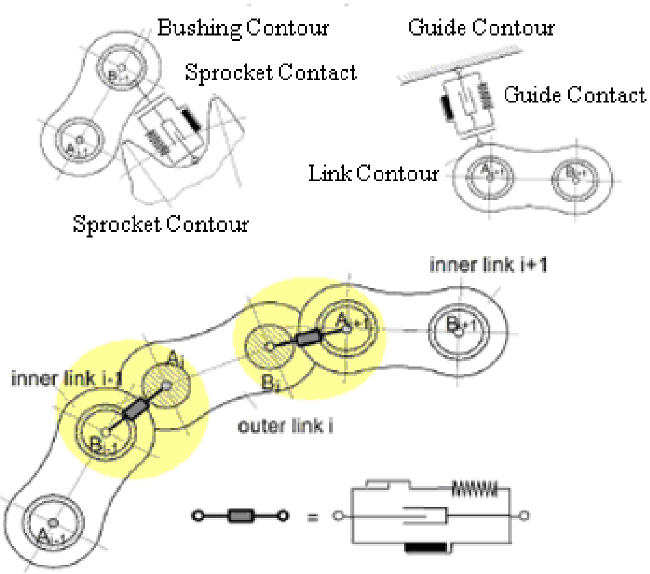

Figure 4.7 : Contact and connection forces in the chain simulation [13].

The contact forces take part when sprocket or guides are contacted by a link. Contact forces can be computed by calculating the intersecting area between the surface profiles of the concerned parts can support to compute the contact forces.

4.2.1 Part modeling

Here are the sub-components modelled according the terms explained in following sections.

4.2.1.1 Chain link modeling

In modeling, the basic approach is to model each chain link as a single rigid body connected to adjacent chain links by means of linear spring and dampers and simulate the resulting multi-body system based on the Newton-Euler laws.

Each chain link is modeled with two displacements and one rotation DoF and center of gravity is defined along the axial link axis as shown in Figure 4.8.

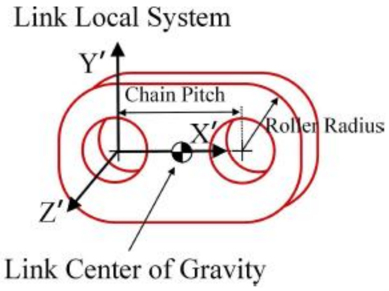

Figure 4.8 : Representation of chain link [14].

Connection between chain links can be gained by defining linear spring and damper elements as shown in Figure 4.3, where k_{link} and c_{link} are the chain link stiffness and damping coefficient, respectively. Location of chain pin centers are denoted by points P_1 and P_2. Every N^{th} link is attached to the neighboring link, N^{th+1}, by connecting the P_2^N and P_1^{N+1} by spring and damper elements. The force F_{link} transmitted by each chain link spring and damper is

$$F_{link} = k_{link}\Delta + c_{link}\dot{\Delta} \tag{4.1}$$

Δ is the relative displacement between the geometric centers of adjacent chain link centers as shown in Figure 4.9 and ($\dot{}$) denotes the derivative with respect to time [11].

Chain connectivity link is detalilly explained and modelled in the simulation corresponding to data in above.

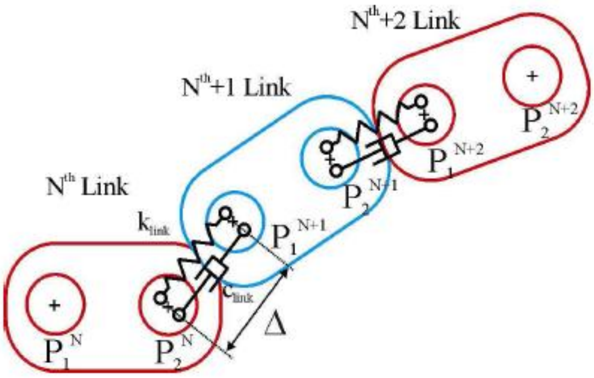
N^{th}+2 Link
N^{th}+1 Link
N^{th} Link
k_{link}
c_{link}
P_2^{N+2}
P_1^{N+2}
P_2^{N+1}
P_1^{N+1}
Δ
P_1^N
P_2^N

Figure 4.9 : Chain link connectivity [14].

4.2.1.2 Sprocket modeling

Sprocket geometry can be defined by means of arcs by defining the tooth profiles as shown in Figure 4.10. The location of the chain link pin is defined by the pitch diameter, R_{pitch}. Roller radius, R_{roller}, define the root radius and borders of the tooth can be denoted by tooth radius, R_{tooth}, and tip radius, R_{out}. The roller contact angle, $\theta_{contact}$ must also be specified. Sprockets are modeled as a rigid body in the plane with two displacements and a rotation.

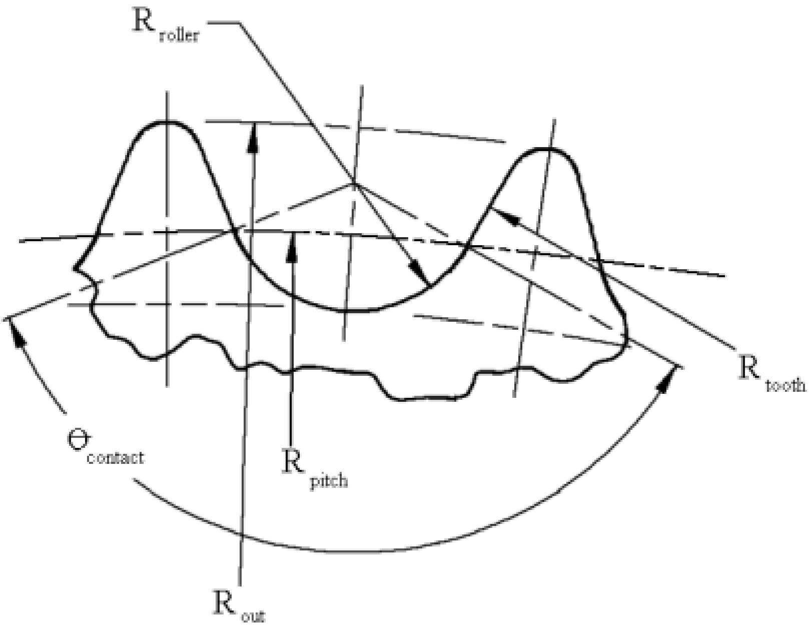
R_{roller}
R_{tooth}
$\theta_{contact}$
R_{pitch}
R_{out}

Figure 4.10 : Sprocket geometry.

Therefore, the connection between sprockets and camshafts is composed of stiffness and damper elements. Consequently, forces, which occur in the X and Y directions, are:

$$F_x = kx + c\dot{x} \tag{4.2}$$

$$F_y = ky + c\dot{y} \tag{4.3}$$

where *k* and *c* represent the shaft stiffness and damping coefficient, respectively; x and y are the relative displacements between the sprocket geometric center and the ground in the X and Y directions, respectively.

4.2.1.3 Guide and tensioner modeling

Guides are modeled similarly to the sprocket tooth profiles by means of arcs. Only difference is the existence of tensioning devices as shown if Figure 4.5 on moving guides. This type of guides generally known as arms and are modeled as rigid bodies with a single DoF. With the force, which does not change its initial direction, applied by the tensioning devices arm can rotate on the hinge point as shown in Figure 4.11 [14].

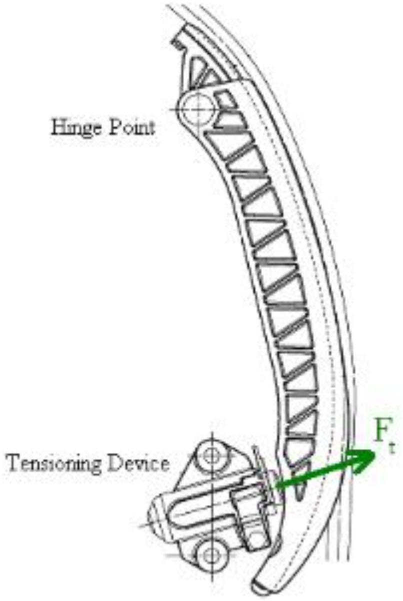

Figure 4.11 : Guide and tensioning devices [11].

Additionally, fixed guides exist in the systems that are modeled as a rigid body to the associated curve.

4.2.1.4 Chain contact kinematics

In this section, contact kinematics equations are simplified by presenting the contact between chain bushings, sprockets and guides, which intermittently occurs.

- Generalized Contact Kinematics

Computation of the contact between the profiles is time dependent and two bodies undergoing intermittent contact is denoted with the superscripts $(.)^k$ and $(.)^l$, respectively, are shown in Figure 4.12.

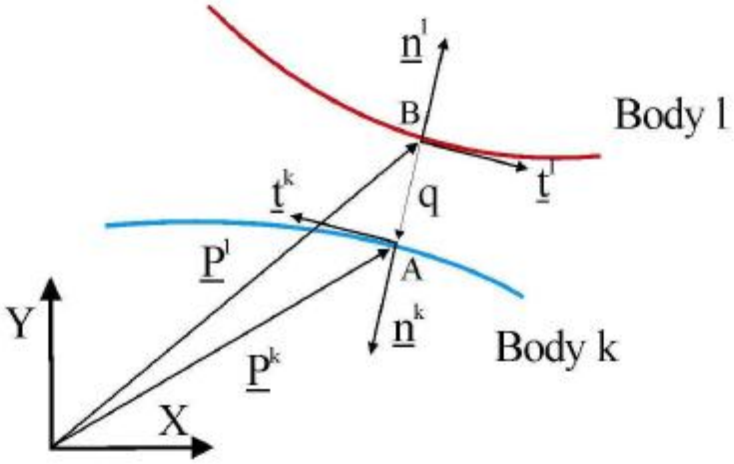

Figure 4.12 : Generalized contact kinematics [14].

In order to investigate the possible contact between point A and B, where $\underline{P}^k$ denotes the position vector of point A whereas $\underline{P}^l$ denotes the position vector of point B, the two conditions that define the position of the candidate contact points are

$$\left(\underline{P}^k - \underline{P}^l\right) \cdot \underline{t}^l = 0 \tag{4.4}$$

$$\underline{t}^k \cdot \underline{n}^l = 0 \tag{4.5}$$

where $\underline{t}$ and $\underline{n}$ are the tangent and normal vectors to the curves.

Equations (4.4) and (4.5) are solved, then the relative minimum distance between the bodies, q, can be computed using Equation (4.6).

$$q = \left(\underline{P}^k - \underline{P}^l\right) \cdot \underline{n}^k = 0 \tag{4.6}$$

The interference between the profiles, a, can be easily computed based on the value of the relative distance.

$$a = \begin{cases} -q & if \quad q \le 0 \\ 0 & if \quad q > 0 \end{cases} \qquad \textbf{(4.7)}$$

Sign of the relative distance, *q*, defines the contact occurrence between the bodies. When *q* is positive, the bodies are not in contact, oppositely contact will occur when *q* is negative.

- Time Derivatives

The tangential and normal velocities can be defined with the time derivative of the relative distance. Then these relative velocities are used in damping and friction models. Taking the time derivative of equation (4.6)

$$\dot{q} = \left(\underline{\dot{P}}^{k} - \underline{\dot{P}}^{l} \right) \cdot \underline{n}^{k} + \left(\underline{P}^{k} - \underline{P}^{l} \right) \cdot \underline{\dot{n}}^{k} \qquad \textbf{(4.8)}$$

The second term in equation (4.8) vanishes considering the equation (4.4), since the time derivative of the normal vector is parallel to the tangent vector. Consequently,

$$\dot{q} = \left(\underline{\dot{P}}^{k} - \underline{\dot{P}}^{l} \right) \cdot \underline{n}^{k} \qquad \textbf{(4.9)}$$

The time derivative of the relative distance is equal to the relative velocity in the normal direction, of two body fixed points that coincide with the contact points. Similarly, the relative velocity in the tangential direction, V_t is given by [11]

$$V_t = \left(\underline{\dot{P}}^{k} - \underline{\dot{P}}^{l} \right) \cdot \underline{t}^{k} \qquad \textbf{(4.10)}$$

Chain link roller and sprocket contact is illustrated in Figure 4.13. The geometry of the chain link roller is show as a circle and the geometry of the sprocket is created by means of circular arcs.

Each chain link roller of radius R_{link} may contact with the center arc of radius R_{roller} or with the left or right flanks of each sprocket tooth, of radius

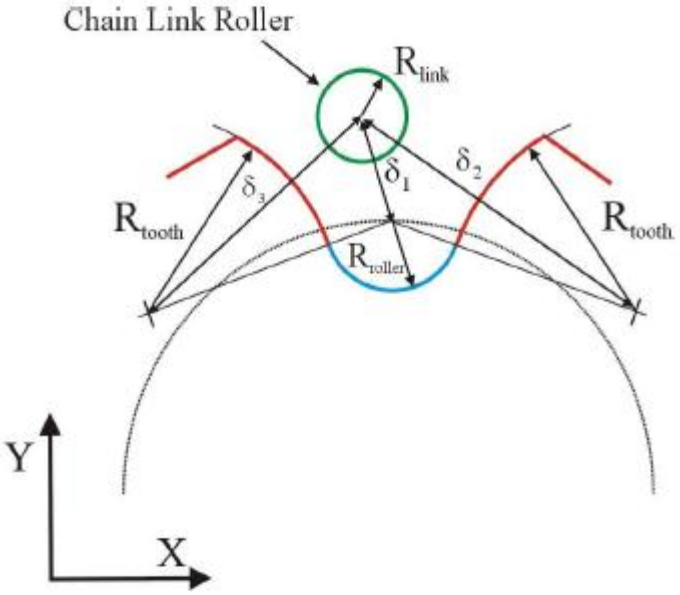

Figure 4.13 : Roller and sprocket contact kinematics [14].

R_{tooth}. Similar contact circumstances are valid to define the relative distance between the chain link roller and each of the arcs is obtained similarly with the equations (4.4), (4.5) and (4.6). Relative distance between the chain link roller and sprocket tooth and flanks can be shown in the form

$$q_1 = \delta_1 + R_{roller} - R_{link} \tag{4.11}$$

$$q_2 = \delta_2 - R_{tooth} - R_{link} \tag{4.12}$$

$$q_3 = \delta_3 - R_{tooth} - R_{link} \tag{4.13}$$

where deltas (δ) are the distance between centers. Clearly, the roller can only contact with only one of the curves, thus, the relative distance q is chosen as the minimum one of the three shown in equations (4.11), (4.12) and (4.13).

$$q = \min\{q_1, q_2, q_3\} \tag{4.14}$$

Then the time derivative of the relative distance *q* is;

$$\dot{q}_1 = \dot{\delta}_1, \dot{q}_2 = \dot{\delta}_2, \dot{q}_3 = \dot{\delta}_3 \tag{4.15}$$

$$\dot{q} = \begin{cases} \dot{q}_1 & if \quad q = q_1 \\ \dot{q}_2 & if \quad q = q_2 \\ \dot{q}_3 & if \quad q = q_3 \end{cases} \tag{4.16}$$

The tangential relative velocities are;

$$V_{t1} = V_{c1} + R_{link}\,\dot{\theta}_{link} + R_{roller}\,\dot{\theta} \tag{4.17}$$

$$V_{t2} = V_{c2} + R_{link}\,\dot{\theta}_{link} + R_{tooth}\,\dot{\theta} \tag{4.18}$$

$$V_{t3} = V_{c3} + R_{link}\,\dot{\theta}_{link} + R_{tooth}\,\dot{\theta} \tag{4.19}$$

WhereV_c is the relative velocity between centers in the tangential direction, $\dot{\theta}_{\text{link}}$ and $\dot{\theta}$ are the link angular and sprocket angular velocities. The tangential relative velocity V_t between link and sprocket is then

$$V_t = \begin{cases} V_{t1} & if \quad q = q_1 \\ V_{t2} & if \quad q = q_2 \\ V_{t3} & if \quad q = q_3 \end{cases} \tag{4.20}$$

In link-guide contact kinematics study, guides are defined by means of circular arcs. Figure 4.14 illustrates the contact between chain roller link and the guide, which is defined by circular arcs. It is necessary to compute the relative distance *q* between the guide and the roller. Also, R guide is contacting to guide with respect to given equation according to (4.21), by this way it is easy to calculate the acting force on the R guide element. An additional info is not required the friction loss of this contact because it can be ignorable from the point of valve train kinematics.

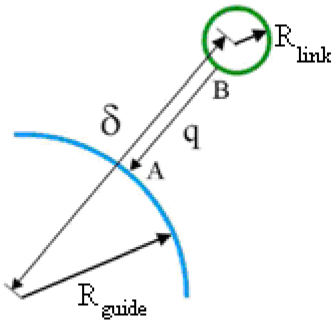

Figure 4.14 : Illustrated roller and guide contact [14].

For guides generated with circular arc, the relative distance between a given arc or radius R_{guide} and the link roller is given by

$$q = \delta - R_{guide} - R_{link} \tag{4.21}$$

where δ is the distance between centers. More than one circular arc can be present in a guide made with arcs, thus, equation (3.21) has to be computed for each arc. The time derivative of the relative distance q is

$$\dot{q} = \dot{\delta} \tag{4.22}$$

The tangential relative velocity V_c is

$$V_t = V_c + R_{link}\,\dot{\theta}_{link} + R_{guide}\,\dot{\theta}_{guide} \tag{4.23}$$

where θ_{guide} is the guide angular velocity.

Clearly, there is no need to solve non-linear equations at every time step by defining the guides by means of circular arcs, since close form solutions exist.

4.2.1.5 Tensioner guide contact kinematics

Figure 4.15 shows the contact kinematics between a tensioning device and a guide. Another important thing is calculation of the force impacting on tensioning device. The formula that explains the force according to tensioner-guide contact is given with the (4.24) in below. In addition, direction may show tendency according to direction of contact. By this way, the acting force direction is important from the point of kinematics of system.

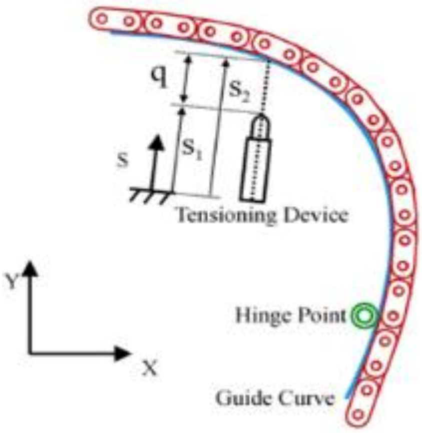

Figure 4.15 : Tensioner and guide contact kinematics [14].

The relative distance and its time derivative are

$$q = s_2 - s_1 \tag{4.24}$$

$$\dot{q} = \dot{s}_2 - \dot{s}_1 \tag{4.25}$$

where s_2 and s_1 denote the positions of the candidate contact points on the guide and tensioner, respectively [11].

4.2.1.6 Chain contact dynamics

Chain contact can occur between the sprockets and guides and within its inner components, as well.

Dynamic motion of the bush elements creates the chain link forces as shown in Figure 4.16 and link force generation depends on the link extension. L denotes the link length, where D denotes the link clearance. d_{ij} is the distance between two adjacent bush.

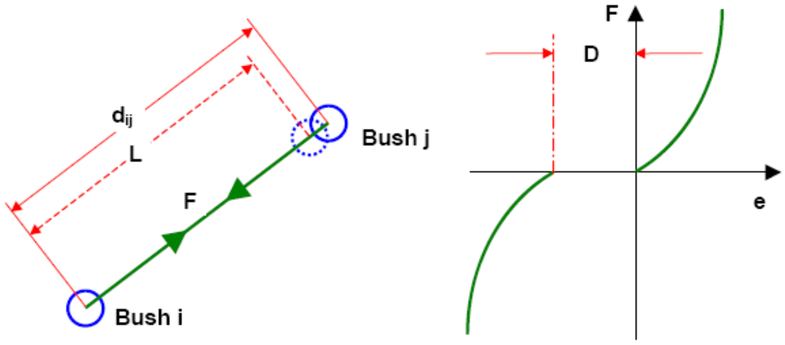

Figure 4.16 : Chain link forces and link extension [15].

Then link extension, e, can be expresses as;

$$e = d_{ij} - L \tag{4.26}$$

Finally, link force can be computed considering the link extension.

$$\begin{aligned}
F &= k_{link} \cdot e + A \cdot e^2 + c_{link} \cdot \left(\frac{de}{dt}\right) && e > 0 \\
F &= 0 && -D \le e \le 0 \\
F &= k_{link} \cdot (e + D) - A \cdot (e + D)^2 + c_{link} \cdot \left(\frac{de}{dt}\right) && e < -D
\end{aligned} \tag{4.27}$$

where k_{link} denotes the stiffnes; A is non-linear stiffness term and c_{link} is the damping coefficient. Then the link force is resolved into x and y components in the global co-ordinate system and applied to the bush x and y nodes.

Chain link bush contact with sprockets or guides results in contact forces and can be computed with the same methodology [11, 14]. Figure 4.17 shows the contact and interference, a, between bush and sprocket or guide face.

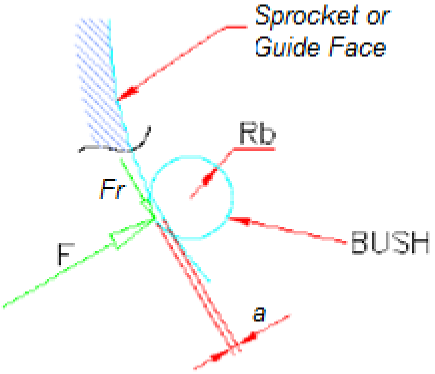

Figure 4.17 : Contact forces - Chain bush and sprocket or guide [15].

Then contact force can be calculated with the help of equation (4.28).

$$F = k_{link} \cdot a + c_{link} \cdot \left(\frac{da}{dt}\right) \tag{4.28}$$

where k_{link} and c_{link} are the stifness and damping coefficients respectively. Then the contact force resolves into x and y components in the global co-ordinate system. Friction force is then computed by calculating the perpendicular force on the contact surface with regards to the local coordinate system and multiplying it with predefined friction coefficient [11].

4.2.1.7 Chain initialization

Chain initialization is needed to start the simulation, therefore wrapping the chain over sprockets and around the guides needs to be properly defined. The aim is to compute the points, which lie on a line that is tangent to the adjacent components. These tangent lines can occur between sprocket and sprocket or sprocket and guide elements. The equations that need to be solved are:

$$\left(\underline{P}^k - \underline{P}^l\right) \cdot \underline{n}^k = 0 \qquad \textbf{(4.29)}$$

$$\underline{t}^k \cdot \underline{n}^l = 0 \qquad \textbf{(4.30)}$$

where P is the position vector of a point that lies in the line that is tangent to both bodies. In order to position the chain over the spans, chain links can be located on the common tangent line that is created by the computed points. In the case of wrapping the chain around the sprockets, interference of the chain bush with the sprocket teeth is avoided by rotating the sprockets. Simultaneously, chain bush is positioned on the closest point to the tangent line [11, 14].

4.3 Engine Specification and Components

Simulated timing chain drive is a primary drive system of an inline 8-cylinder 4.4 L double overhead camshaft diesel engine. Timing chain, sprockets, plastic guides and a hydraulic tensioner are composing the system layout, which is shown by the Figure 4.18. Furthermore, the exhaust and intake camshaft sprockets, a fuel injection pump are driven with the timing chain. The specification of the engine is shown in Table 4.1**.** Also the information about timing drive sub-components is given in Table 4.2. Glass fiber reinforced polyamid is used for plastic guiding elements and their contact profile is defined by means of arcs. . The aim is to compute the algorithms, which lie on a line that is tangent to the adjacent components as shown with the formulas (4.29) in above. The equations are dependent to sprocket and guide connection kinematics for the evaluation of contact bodies.

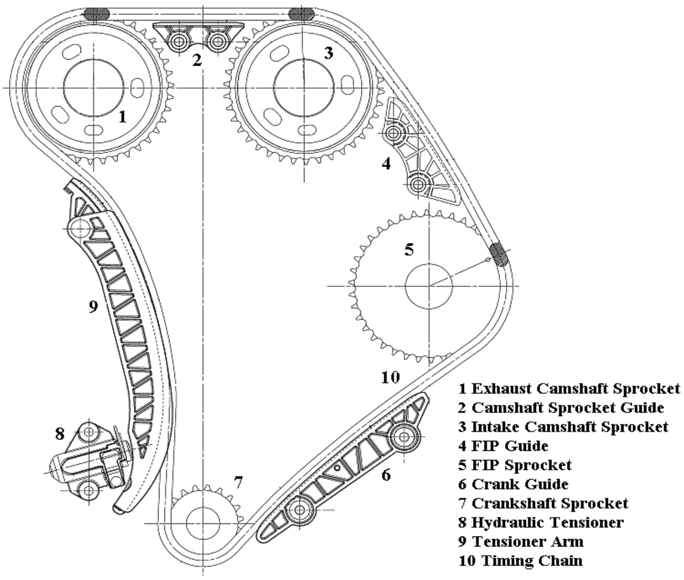
1
2
3
4
5
6
7
8
9
10
1 Exhaust Camshaft Sprocket
2 Camshaft Sprocket Guide
3 Intake Camshaft Sprocket
4 FIP Guide
5 FIP Sprocket
6 Crank Guide
7 Crankshaft Sprocket
8 Hydraulic Tensioner
9 Tensioner Arm
10 Timing Chain

Figure 4.18 : Chain drive layout [11].

Cam sprockets are fine blanked, where fuel injection pump and crankshaft sprocket are forged. With the Figure 4.19, the sketch of valve train system is given, also each tenisoners are shown with different colors.

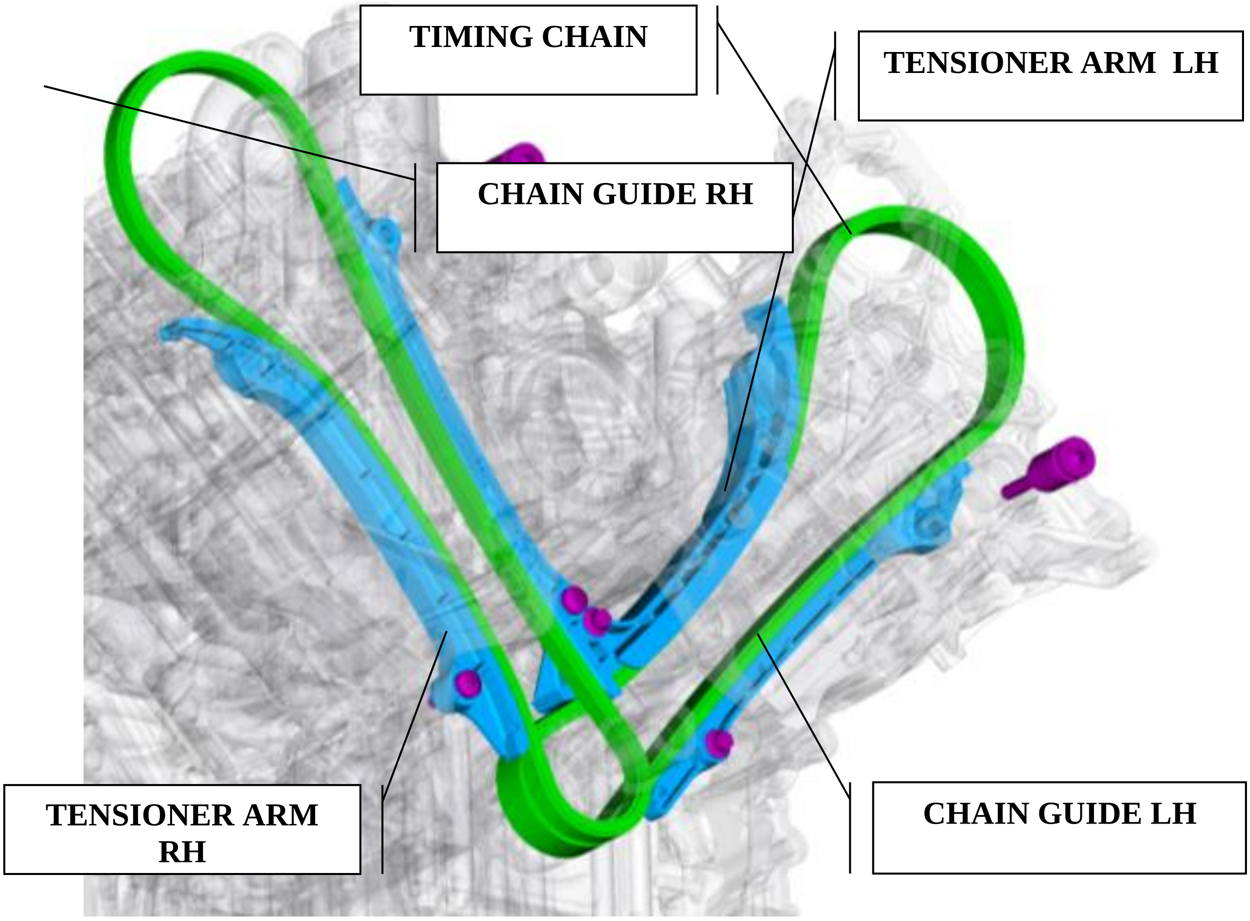
TIMING CHAIN
TENSIONER ARM LH
CHAIN GUIDE RH
TENSIONER ARM RH
CHAIN GUIDE LH

Figure 4.19 : Valve train system schematic with respect to engine package.

The chain modeled in this study is a single strand, bush type chain which has 9,525 mm standard pitch dimension. It is composed of inner and outer links, pins and bushings. Materials are carbon and alloy steel, respectively.

Table 4.1 : Specification of modelled engine.

Item	**Unit**	**Specification**
Engine Type	-	4-Cylinder V-90Diesel
Capacity	Litres	4.4L
Rated Speed	rpm	4200
Max. Torque	Nm	700
Power	PS	313
Emission Level	-	Euro 5
Fuel Inj. System	-	Common Rail

Sprockets' main dimensions, such as teeth number, pitch and root diameter is given in Table 4.2.

Table 4.2 : Timing drive sub-component type and dimensions.

	Type	**Dimension**
Timing Chain	Single Strand, Bushing Quenched and Tempered	9.525mm standart pitch
Hydraulic Tensioner	Oil fed and spring	-
Cam Sprocket	Fine Blanked	38Teeth
FIP Sprocket	Forged	38 Teeth
Crank Sprocket	Forged	19 Teeth
Plastic Guides	Injection Molding	Profile by means of arcs

4.3.1 Chain drive simulation

In this study, Valdyn was used as a simulation program for analyzing the dynamic motion of the subjected valve train system. With the help of the Valdyn's flexible elemental approach, individual parts of the valve train are represented by modeling elements. These elements can be linked together to form the whole valve train model. Each modeling element has been carefully modeled to use the minimum degrees of freedom, whilst retaining sufficient detail to achieve a high level of simulation accuracy. This facilitates model generation and gives short simulation times. Typical single speed simulation times are of the order of seconds for simple models or a few minutes for complex whole system models. Short simulation times make it practical to complete speed sweeps, which give greater understanding of the model dynamics and faster optimization [15].

Three main stages were used to simulate the valvetrain with the help of VALDYN. First, the valvetrain dynamic model was generated. The individual elements were connected together in the desired manner to build the model. Each modeling element has a certain number of required data inputs associated with it (mass, stiffness, damping etc.). Once the model has been generated, the input file for the VALDYN Solver was automatically generated by Graphical User Interface (GUI). The dynamic simulation of the system was performed and output files containing the desired outputs were generated by the Solver. Finally, the results of the dynamic analysis were viewed from the plotter screen [11].

In this section, ‘’Solver Theory’’ is discussed, the solution method in the VALDYN Solver is relatively simple. The model "system state" is described by the node positions and velocities. Numerical integration is used repeatedly to calculate the state at a future time step.

This can be written mathematically as:

State(t) = { Position(t), Velocity(t) }

Given State(0)

Integrate State(t+Δt) = f(State(t))

where "Position" and "Velocity" are vectors with an element for each node in the model.

The function "f" above includes the combined effect of individual modeling element physical equations and an integration strategy, which depends on the equations considered.

Valdyn uses three different strategies depending on the order of the element differential equations.

1- Zero Order Equations: Node position and velocity are an analytical function system state.
2- First Order Equations: Node velocity is an analytical function of system state. Node position is obtained from Runge-Kutta integration of Node velocity.
3- Second Order Equations: Node acceleration is an analytical function of system state. Node position and velocity is obtained from Runge-Kutta-Nystöm integration of node acceleration.

Most of the physical equations in VALDYN are driven by Newton's 2nd law (F=ma) and so are second order equations [15].

4.4 Model Confirmation And Measurements

After a Valdyn model is constructed, the plan is to validate the model with a real world engine testing. All of the critical cases are evaluated and the worst case scenario is taken into accound and done a-backto-back comparison with the simulation results.

As you can see the engine and valve train configuration with the Figure 4.20, after the above sub-components are modelled carefully, the real engine environment is checked to have the same behaviour under identified conditions.

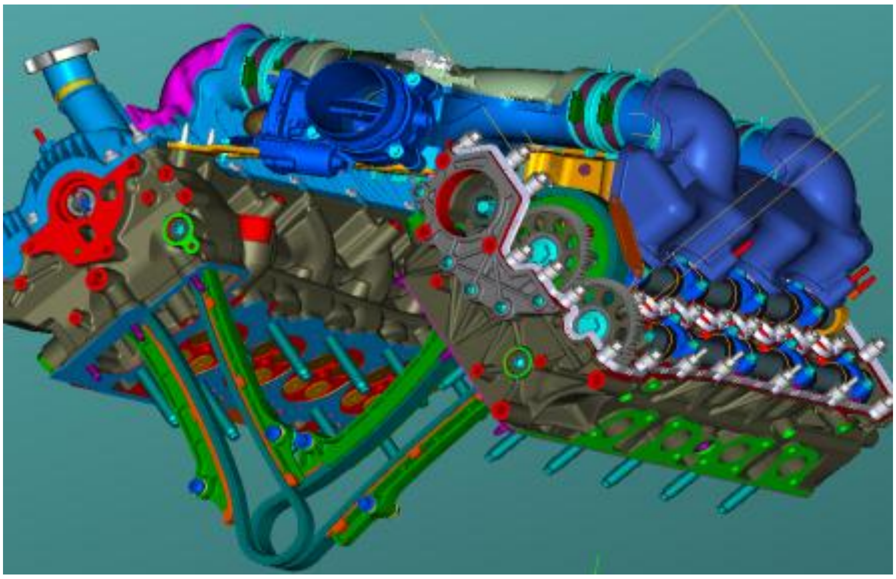

Figure 4.20 : Valve train system of a 4.4L V8 engine with auxilary gears.

In this section, also the methodology of the measurement is briefly explained. Key mechanical responses are recorded and checked with the Valydn results. As a part of type testing of the M1.1 build 4.4L V8 diesel engine Ford Otosan required evaluation of dynamic chain loads on both banks of the timing system. The measurements included simultaneous pressure measurements on both chain tensioners and torsional vibrations of the crank shaft. An overall view of the primary drive layout is shown in Figure 4.21 below.

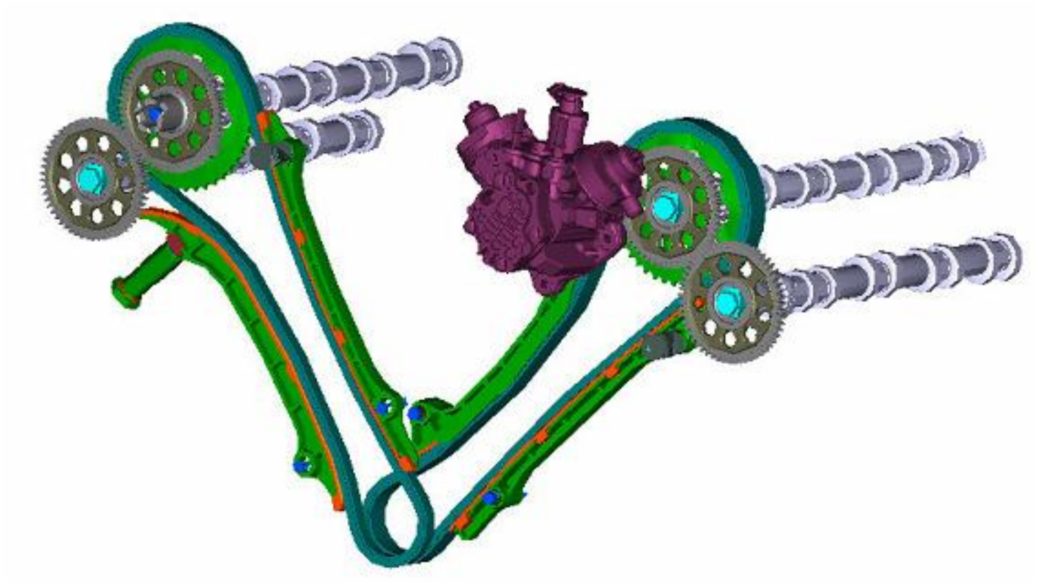

Figure 4.21 : Timing system layout.

Due to high dynamic loads generated by the common rail FIP driven by the LH bank cam gear, the M1.1 engine uses duplex chain on the LH bank and simplex chain on the RH bank.

Team was commissioned to investigate the chain loads on a proto built of the 4.4L, V8 diesel engine. All measurements were simultaneously carried out on two banks; LH Bank driven by a duplex chain and the RH bank driven by a simplex chain. The installation of the measuring system and measurements were carried out at Ford Dunton Engineering Centre.

The objective of these tests was to measure the dynamic chain loads for a proto built 4.4L V8 diesel engine and verify the best fuel injection pump timing configuration and Valdyn model. Testing consisted of measuring the chain loads for speed sweeps from 1000 to 4000rpm, for engine load conditions of 100%, 75%, 50% and 25%. The tests were carried out for the Fuel injection pump shaft indexed from 1 to 11 teeth from its nominal base position.

Maximum dynamic chain loads measured for the duplex chain (LH bank) did not exceed 3400 N and for simplex chain (RH bank) chain dynamic loads did not exceed 2000 N as measured for the fuel injection pump baseline position. The lowest dynamic chain loads measured for both simplex and duplex chains were found for the fuel injection pump phased by 7 teeth from its' base position, with the peak dynamic loads highly reduced to 3100N and 2300N for the LH bank and for the RH bank respectively. The dynamic chain loads measured for the fuel injection pump baseline position are identical to those for the FIP offset 7 teeth. The highest dynamic peak loads were measured for 9 to 11 teeth offset, which resulted in up to 4300 N maximum chain dynamic loads measured on the LH bank (duplex chain).

It is concluded that correct FIP phasing is an important parameter to minimise dynamic chain loads in the timing system and that the base pump position offered the lowest dynamic chain loads throughout all load cases.

4.4.1 Measuring equipment

The principle used in the dynamic chain load analyses and the instrumented sprocket is referred to as the ‘’Rotating Vector Dynamic Chain Strand Load Measurement Technique’’ described in a separate document entitled. Details of the chain geometry and sketches showing the definition of the rotating frame for both banks. All signals were digitally recorded directly on a 16-channel, 16-bit resolution as shown with Figure 4.22. The digitised signals were then translated to UF58 format for subsequent analyses to generate the actual chain loads, measured on the tight and slack spans of the chain on both banks of the engine.

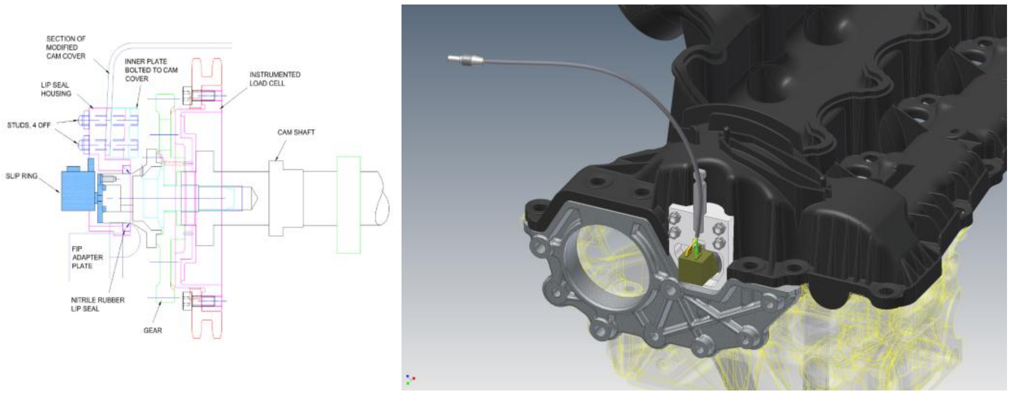

Figure 4.22 : Instrumentation of adapter plate and tensioner around FIP.

Due to the severe restriction of axial space caused by close proximity of the Fuel Injection Pump (FIP), packaging of the instrumentation on the LH bank was very challenging. A CNC machined seal housing replicating the contour of the rocker cover was manufactured together with the stub-shaft, which contained two miniature strain gauge amplifiers. The overall view of the instrumentation package installed on the LH bank is shown in Figure 4.23.

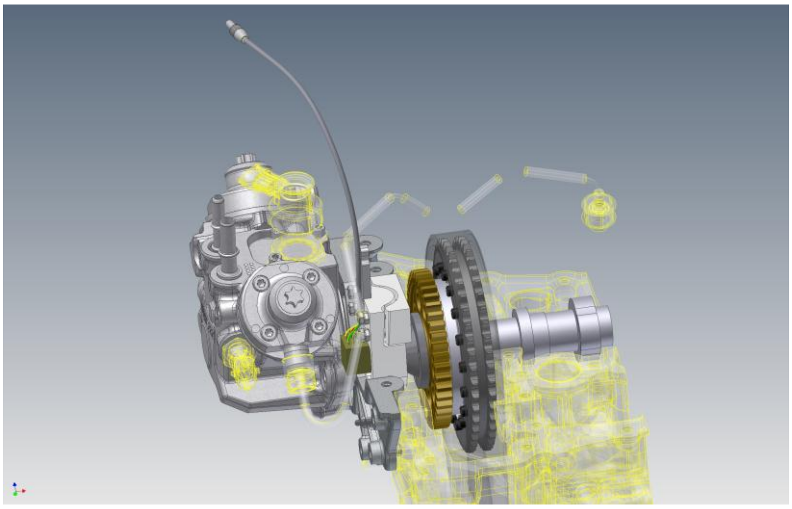

Figure 4.23 : The CAD model of the instrumentation.

Also, other environemntal conditions are checked for a stabil measurement.

4.4.2 LH instrumented chain tensioner

The cross-section of the instrumented chain tensioner is shown in Figure 4.24. A miniaturepressure transducer designed for arduous automotive applications was used to measure tensioner pressure. The nominal input pressure of the above transducer was 210 Bar.

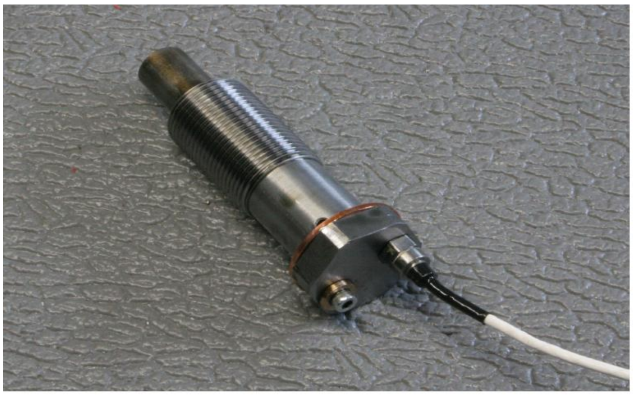

Figure 4.24 : Instrumentation of tensioner.

Internal cavities for wire access and internal pressure channels were manufactured using spark erosion and die sinking technology. Figure 4.25 of section shows an overall view of an instrumented tensioner used on the LH bank.

4.4.3 Instrumented sprocket

To gain axial space on the RH bank, the vacuum pump was removed for the duration of testing. An aluminum blanking plate was manufactured to cover the exposed cavity and provide support for the slip ring, optical encoder and the lip seal - as shown in Figure 4.25. The cross-section schematic view showing RH bank instrumented sprocket is shown in Figure 4.25below.

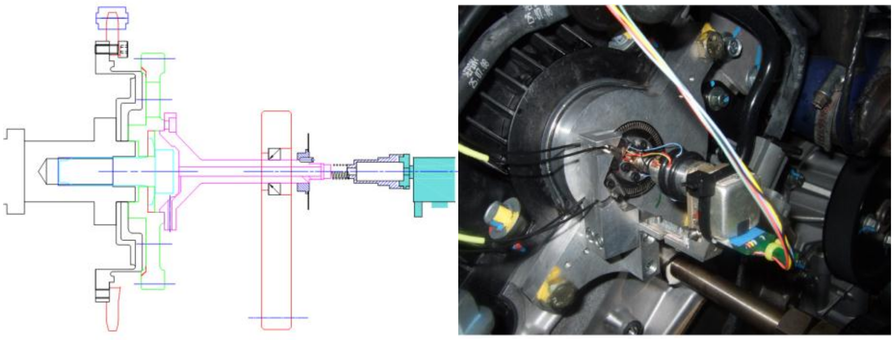

Figure 4.25 : Snapshot of an instrumented tensioner.

4.4.4 RH Instrumented chain tensioner

The chain tensioner used on the RH bank was instrumented to measure dynamic oil pressure inside the tensioner which is proportional (when omitting small contribution of the internal springs) to the load between the chain guide and tensioner plunger. The overall arrangement of the tensioner was similar to the LH bank but no spring load (plunger displacement) was installed due to lower expected load levels on the RH bank. The overall view of the RH bank chain tensioner is shown in the same Figure 4.25with LH instrumented chain tensioner.

4.4.5 Measurement results

Due to regularity of the thesis report, measurement details are shared in the appendices section. Instrumentation location is given with the Figure 4.26.

From the point of engine rear view, the orientation of the system components are shown, cylinder head and adapter plate design assembly is understood.

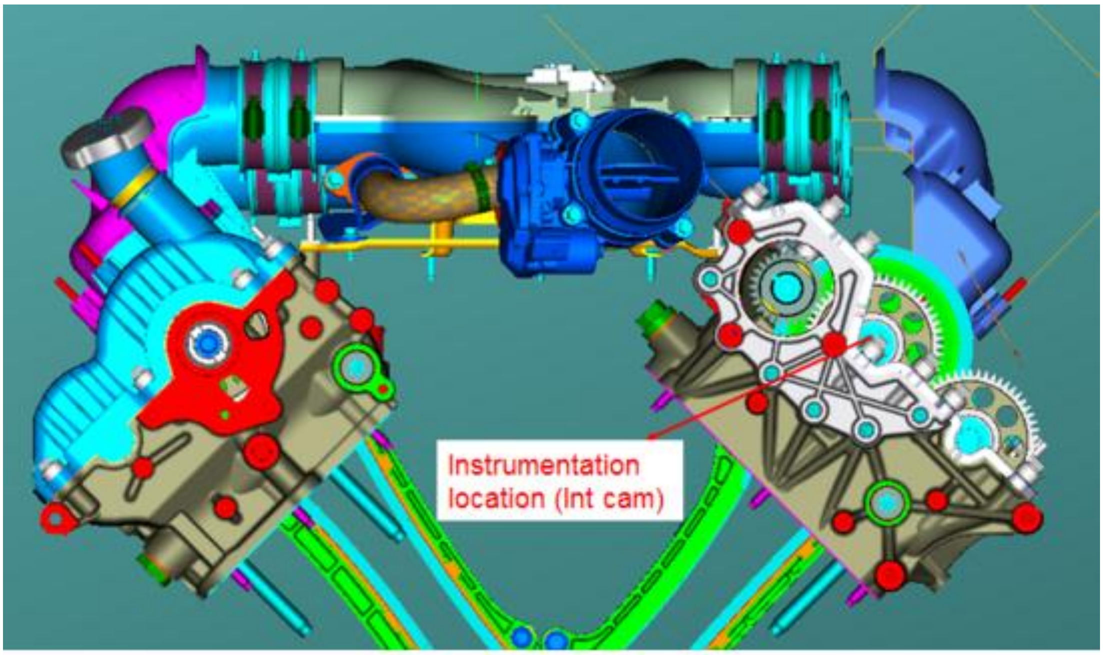

Figure 4.26 : Valve train system according to engine orientation.

From the measurement program carried out on the engine it was found that dynamic chain loads measured for baseline FIP timing were always highest for 100% engine load. That is the reason, 100% data will be shared in the appendices section, and however different cases are also combined with one graph as show in the following sections.

Maximum dynamic chain load measured on the LH bank (duplex chain) increased from 2600 N to 4300 N with the engine running at 25% load and for 100% load respectively as measured for the worst pump timing position as mentioned at the beginning of the section.

For the baseline FIP timing (original FIP position) the maximum tight span loads were measured at 3400 N and 2000 N for the LH bank (duplex chain) and for the RH bank (simplex chain) respectively.

FIP timing has a strong influence on peak dynamic chain loads. The best timing was achieved with FIP in baseline configuration, which resulted in a reduction of maximum dynamic chain loads from 4300 N to 3400 N on the LH bank, and from 2300 N to 2000 N on the RH bank. A close resemblance was observed in the peak dynamic chain loads for the FIP in baseline configuration & 6-7 teeth offset. Whilst both, baseline & 6-7 teeth FIP offset resulted in lowest dynamic chain loads, it is recommended to use FIP in baseline configuration due to apparently less resonant response measured across engine speed as shown with Figure 4.27.

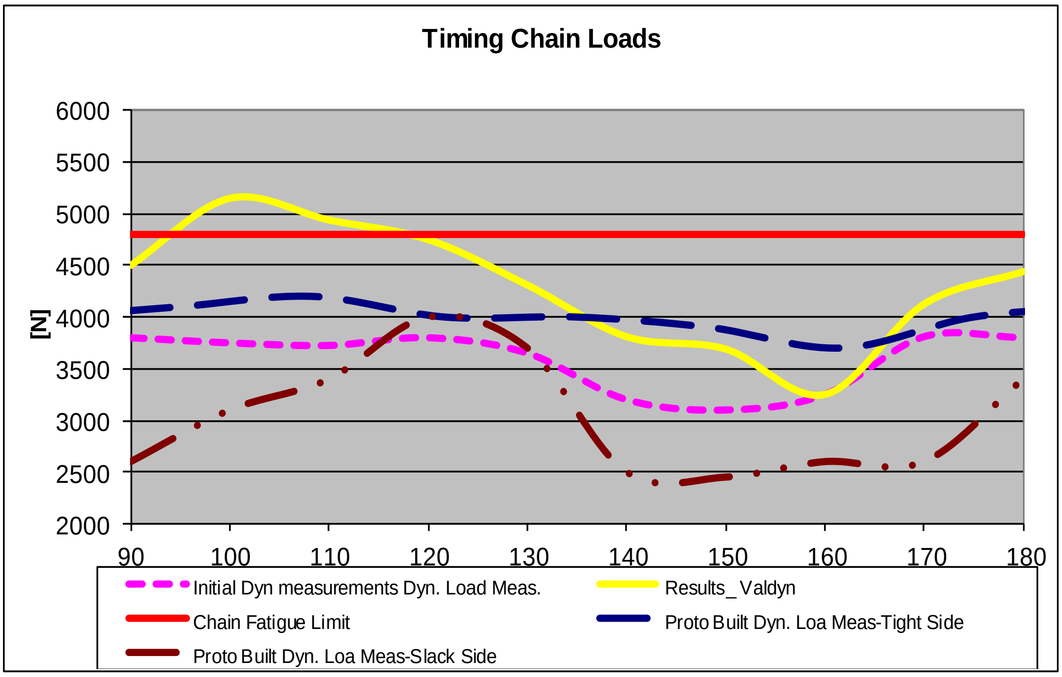

Figure 4.27 : Comparison of different results from simulation and tests.

The highest dynamic chain loads were measured for 2 to 5 teeth offset & 9 to 11 teeth offset, which resulted in up to 4300 N maximum chain dynamic loads measured on the left bank as shown with Figure 4.28.

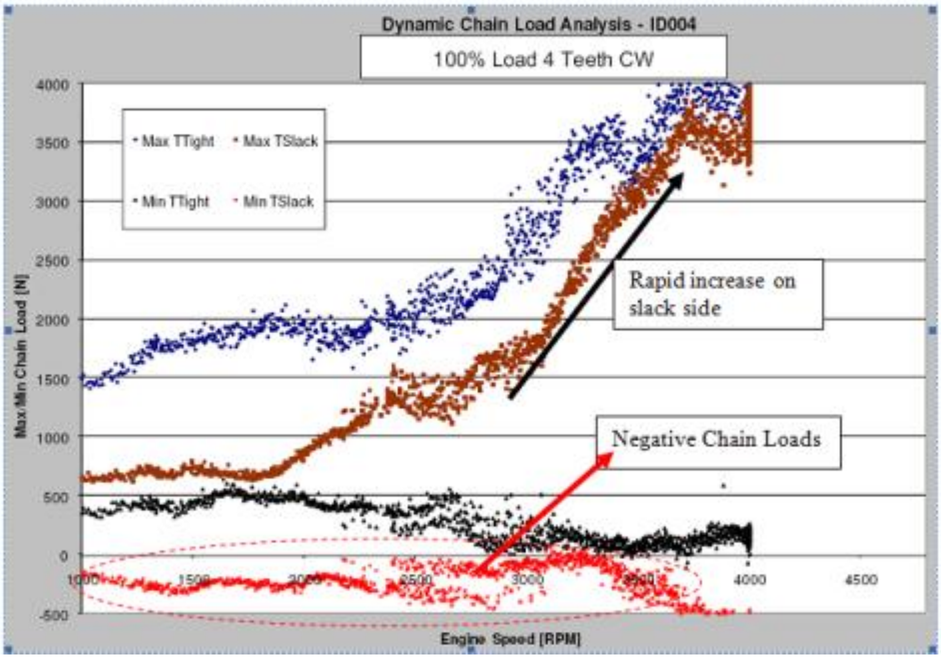

Figure 4.28 : Load distribution according to CW teeth orientation.

Here are the summary of the results of several measurements taken between 25% load and 100% load with the sweep between 1000 rpm and 4000 rpm.

We can conclude that;the “below 0” chain tension measurement is something and the chain tension is likely measured via strain gages. A strain gage will give a below zero value if it senses compression; depending where on the sprocket the strain gage is placed, this may not necessarily be due to “negative” chain load or a tensioner control issue.

Additionally, a negative value could be the result of the method of calibration of the strain gage. The peak slack side load approaching the peak tensile side load would indicate the Tensioner Plunger is pushing harder on the chain, and this is reflected in the oil pressure measurements. This can be also a tensioner control issue as stated in the above paragraph. We cannot really say if we are losing chain control without a measurement of plunger load and movement. Based on these results only, we should stay away from the 2-5 and 9-11 teeth CW rotation of the fuel injection pump gear as illustration shown with Figure 4.29.

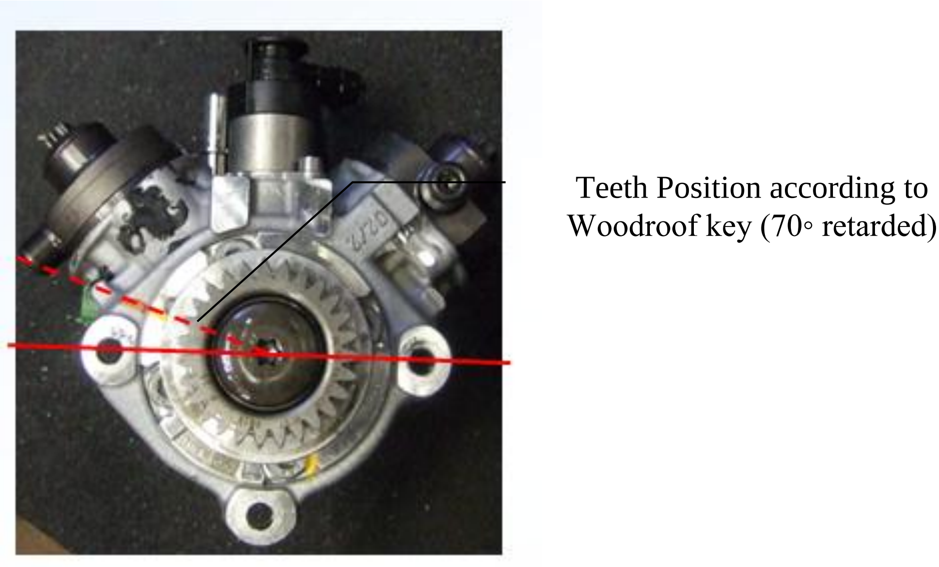

Figure 4.29 : FIP gear orientation according to key.

The chain loads are lower than the fatigue limit of chain. The lowest point still does line up with the measurements and simulations. What is interesting is that the slack side is very sensitive to pump phasing, around 2500N (1500) difference depending on phasing. With the correct timing of the FIP highest dynamic chain loads did not exceed 3400N, which is well below the endurance limit.In every phase setting on proto built engine, chain load is below chain fatigue limit (6000N+1.2SF) as it can be learly figured out from Figure 4.30.

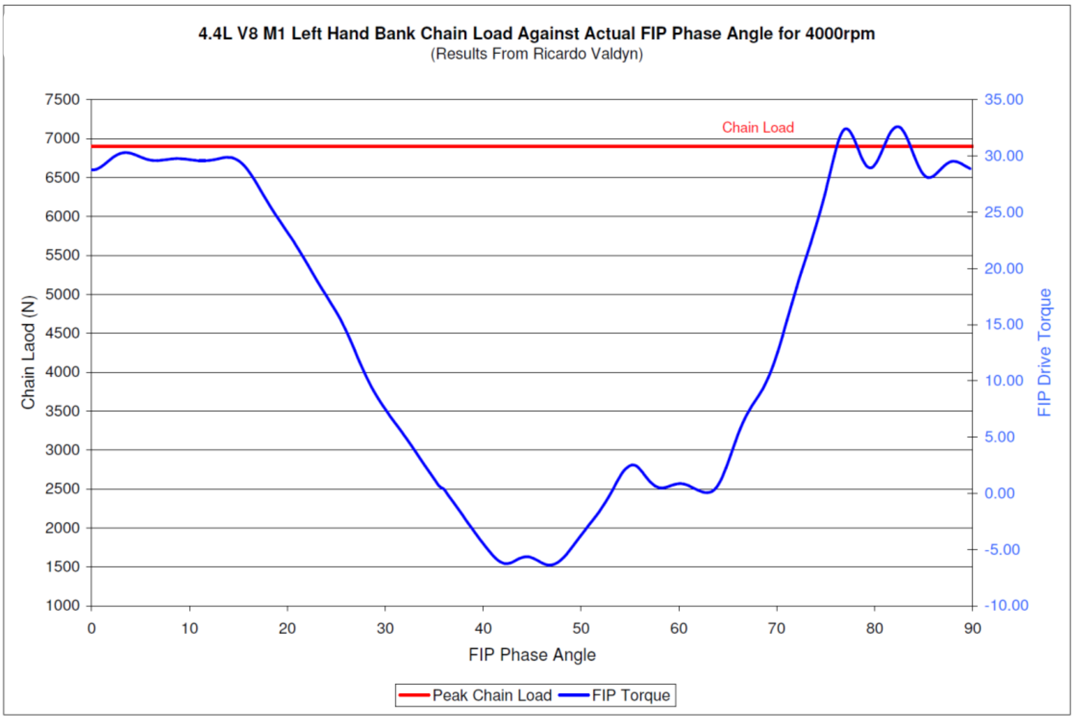

Figure 4.30 : Chain load distribution according to FIP drive torque.

As a result, Valdyn model constructed for V8 diesel engine is confirmed by several test cases, this means the model output can be applicable with the other programs which will be explained in the following sections.

5. FIE SYSTEM SIMULATION

High-pressure fuel pump is developed for a 4.4L V8 common rail diesel engine and used a hydraulic simulator program GT-Fuel to design it. A plunger design is the major trend for high-pressure fuel pumps because of its simple structure and small size. However, the single plunger causes large pressure pulsation and an unstable flow rate, especially at high engine speed. Therefore, a fuel pipe layout that inhibits the pressure pulsation and a flow-rate control that stabilizes the flow are the most important challenges in pump design [16].

Main target is to develop hydraulic simulator which the capability of the model can evaluate the dynamic characteristics of a total fuel supply system regarding with high pressure pump mechanism, which consists of pump and required pipes as shown in Figure 5.1.

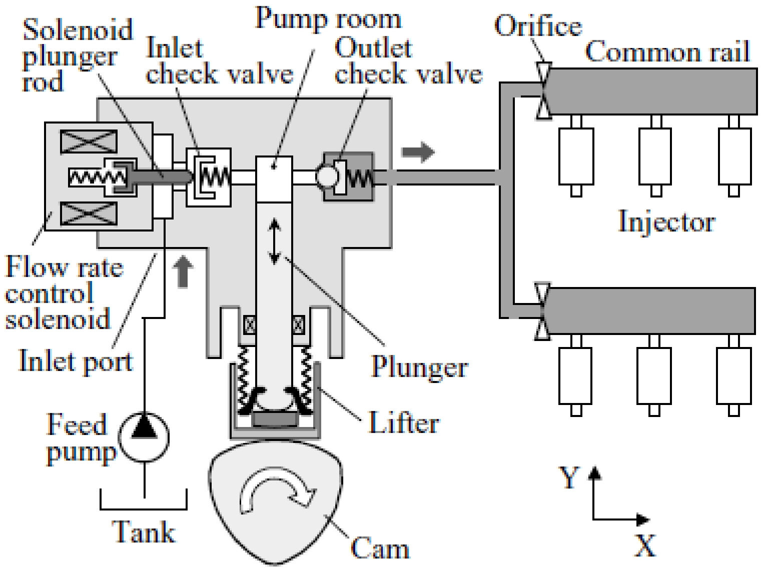
Solenoid plunger rod
Inlet check valve
Pump room
Outlet check valve
Orifice
Common rail
Injector
Flow rate control solenoid
Inlet port
Plunger
Lifter
Feed pump
Tank
Cam
Y
X

Figure 5.1 : Structure of single plunger fuel pump and fuel line system [16].

With the usage of this simulator, it enables to control improved fuel flow by optimizing the outlet check valve lift and the cam profile, and Simulation results are agreed well with our experimental results as explained at the end of this section.

Consequently, mechanical forces and hydraulic influences will be reviewed according to each case, the purpose of this study focuses on.

This model demonstrates the use of flow, mechanical, and fluid-mechanical templates to build a model of a radial high pressure pump with a relatively high level of detail. The interaction between the hydraulic and mechanical components is modeled through GT-Fuel fluid mechanical templates. The inlet and outlet valve dynamics are thus predicted based on valve geometry.

Leakage past the plunger is modeled using the leakage connection template. The radial clearance is varied as a function of pressure. The connection has an option to include the effects of eccentricity, but that has been ignored in this example (eccentricity = 0).

Flow comes from a pressurized tank to the pump inlet volume (chamber of the eccentric shaft). Parts created from the ‘’cam profile’’ template impose the motion of the lifter (and plunger). The kinematic cam lifter reference object is used to calculate the lift profile of the lifter based on geometric inputs such as cam shape and lifter diameter. The output of the kinematic lifter profile object is used as the lift profile entered in the cam profile template representing the lift profile of the lifter.

The motion of the plunger will alter the volume of the pump chamber due to the connection to the fluid piston template. As the pump chamber volume increases, the pressure decreases, and the inlet valve opens to allow fluid to flow from the pump inlet to fill the pump chamber. As the plunger lifts and the pump chamber volume decreases the fluid is compressed and pressure rises, causing the inlet valve close. When the pressure inside the chamber is high enough to overcome the outlet valve spring the valve opens and allows fluid to go to the pump outlet volume. The working fluid is ISO-4113 test oil.

An embedded shows some of the interesting plots such as instantaneous and mean flow rate, fluid temperature increases due to compression, and chamber pressures. With this kind of model it is possible to investigate the pressure pulsations, flow ripples generated by the pump and the volumetric efficiency of the pump.

In this model the cam lift template has been replaced by a full cam shaft and cam lobe. This model is set to run the cam shaft in rigid mode, per the settings in the 'CamAnalysis' part. It could easily be changed to torsional or bending for more detailed analysis. The shaft bearings are also modeled. The lifter is modeled as a 2D inertia, but is currently constrained to only translate along its axis through a 'PrismaticJoint' connection for simplicity. If desired, this constraint could be removed and the rotation and guide friction could be predicted. The 2D contact between the cam and the lifters has an optional tribology reference object which can be used to automatically calculate stiffness solution.

To view results, please run the model and view the prepared results file CR-HPpumpWithCamshaftResults.gu. It contains the same flow related plots shown in CR-HPpump.gu (the model without the cam shaft). In addition it includes an animation of the pump mechanics as well as plots for bearings, cam torque and power loss, as well as cam to lifter contact plots.

The fuel flow as mentioned in above occurs under the reciprocating pumping of the fuel by a positive displacement pump plunger element driven by a camshaft with a known profile. Profile details are also directly regarding with the lifter characteristics.

The input variables to the fuel system are the position of the cam/plunger. The mechanical diesel fuel-injection system is constructed with a high pressure fuel pump presented in above Figure 5.1 below.

The injection pump produces the required pressure for fuel injection. The fuel under pressure is forced through the high-pressure fuel-injection tubing(this tubing physical properties are not important) to the constant volume high pressure rail.

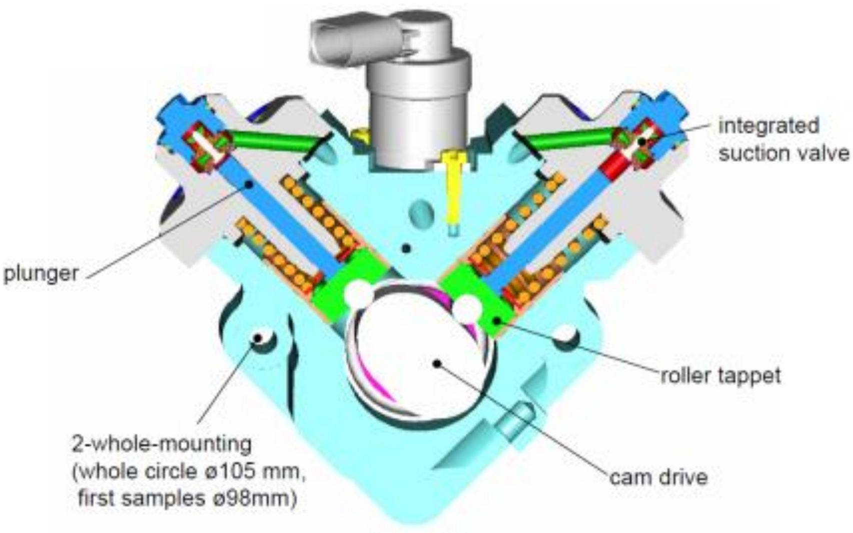

Figure 5.1 : Cross section of a FIP including cam shaft and plungers.

1. Cavitation is not considered. There is no column separation during the transient event, i.e. the pressure is greater than the liquid vapour pressure.
2. Free gas content of the liquid is small such that the wave speed can be regarded as a constant.
3. Flow in the pipeline is considered to be one dimensional with the velocity/flow and the pressure uniform at a section.
4. The leakage in the plunger chamber is partially neglected.
5. The feed pressure (supply pressure) is constant.
6. In all the hydraulic chambers, pressures and densities are considered partially uniform (except the long injection line).
7. Pipe wall distension due to pressure increase is neglected, i.e. flow passages are considered completely rigid.
9. Structure-induced pressure changes are small compared to the water hammer pressure wave in the liquid.
10. The discharge coefficient is assumed constant. The pressure drop or friction caused by flow area changes (expansion or contraction from one module to another) is considered included in the discharge coefficient [17].

For the fuel pump, the rate of volume change is obtained from the motion of the piston that is driven by the fuel injection system cam. The pump plunger velocity is proportional to the cam angular velocity through the cam profile as:

$uplunger = u(degCam)\omega cam$ (9)
where ωcam (= 360×rev/s [deg/sec])
is cam angular velocity and. The cam velocity is assumed to be constant.At the beginning of the report, the importance of the common rail system is explained. The injection pressure rates are getting higher and higher. The high pressure fuel pump is the key component in the fuel system and also in engine auxiliary drive system, supplies highly pressurized fuel to each injector. The pressurized fuel is collected in a constant volume called a common rail as explained in the fuel injection system explanation, and sprayed by the injector into the combustion chamber. The pressure provided to the injection system should be at higher profiles and needs stability to spray fuel during the compression stroke [17]. Because the simulator connects these block elements on a personal computer display and creates a model, model creation and changes are easy to do, and the correspondence between the model and the actual

parts is clear. Moreover, the element model is modified with knowledge obtained via research and development of hydraulic operated circuit breakers.

5.1 Pump Elements

We can split into 3 sections for the model of high pressure pump which are; plunger, cam shaft and its bearings and fuel delivery and transfer system.

5.1.2 Plunger and subcomponents

Pumping operation, a recorded cam profile rotates with the drive shaft, causing the pistons to reciprocate. During its suction stroke, each lobe and piston is filled through its inlet check valve. During compression, the inlet check valve closes and pressure in the pumping chamber rises until it exceeds load pressure. The outlet checkball then lifts off its seat and fluid is pumped out of the chamber. Mechanism is shown with the Figure 5.2.

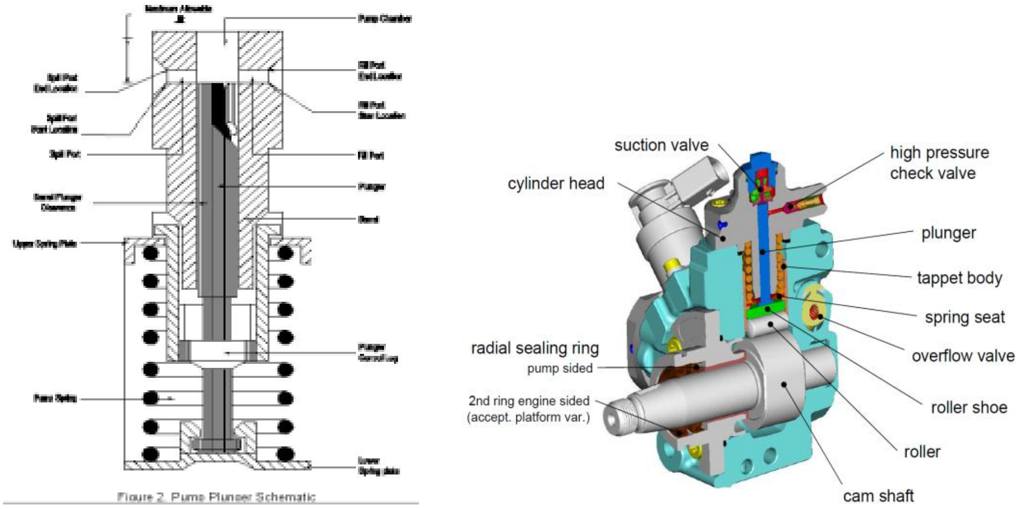
Pump Chamber
Spill Port
Fill Port
Plunger
Barrel
Upper Spring Plate
Figure 2. Pump Plunger Schematic
suction valve
high pressure
check valve
cylinder head
plunger
tappet body
spring seat
radial sealing ring
pump sided
overflow valve
2nd ring engine sided
(accept. platform var.)
roller shoe
roller
cam shaft

Figure 5.2 : Cross Section of a plunger mechanism and position in FIP.

5.2 General Plunger Equations

Rigid Plunger element has only one degree-of-freedom (translation in x direction. Elastic Plunger has two DOFs: translation along x axis for input and output end, separately.

Standard connections can be defined in x-direction only. On input end, a mechanical connection to e.g. Cam Profile element has to be defined as representation stated on Figure 5.3. Multiple mechanical connections to the same element are not allowed (all connections except the first will be ignored).

In this case, the geometry of the plunger has to be specified in the respective input dialogs of the connected elements of the valvegroup which is explained in the following sections [18].

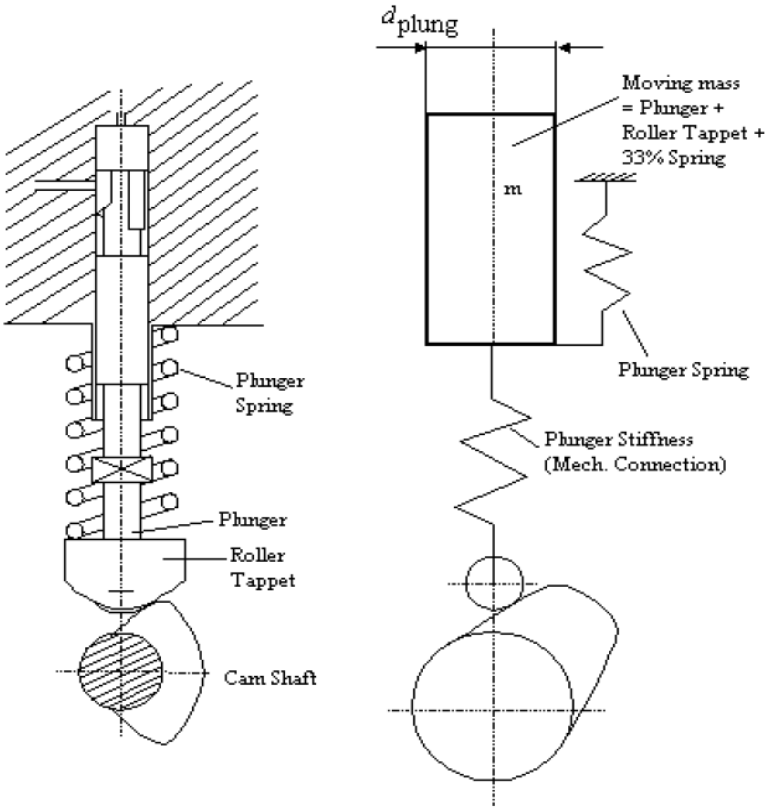
Plunger
Spring
Plunger
Roller
Tappet
Cam Shaft
d_{plung}
Moving mass
= Plunger +
Roller Tappet +
33% Spring
m
Plunger Spring
Plunger Stiffness
(Mech. Connection)

Figure 5.3 : Mechanical model of a plunger [18].

In this case, the geometry of the plunger has to be specified in the respective input dialogs of the connected elements of the valvegroup which is explained in the following sections [18].

The sub-components of a plunger is shown with the Figure 5.4.

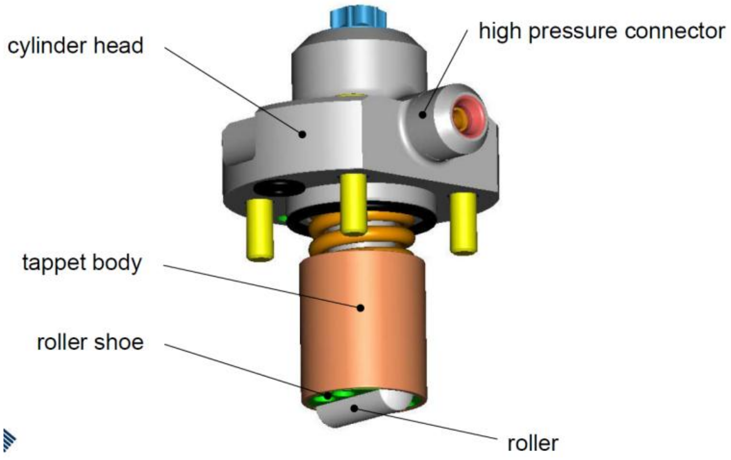
cylinder head
high pressure connector
tappet body
roller shoe
roller

Figure 5.4 : Sub components of a plunger mechanism.

Motion of Rigid Plunger in local coordinate system is governed by the following equation on (5.1):

$$\begin{aligned} m\ddot{x}+c_0\dot{x}+k_0x+\sum_{i=1}^{n}c_i(\dot{x}-\dot{x}_i)-\sum_{j=1}^{l}c_j(\dot{x}-\dot{x}_j)+\sum_{i=1}^{n}k_i(x-x_i)-\sum_{j=1}^{l}k_j(x-x_j)= \\ -F_0+\sum_{i=1}^{n}F_{0i}-\sum_{j=1}^{l}F_{0j}-F_{hyd}-F_{frict}-F_{shear} \end{aligned} \tag{5.1}$$

Forces on right side of equation are defined in local x-direction on (5.2):

n, m number of mechanical connections on input and output ends

$$F_{hyd}=(p_{out}-p_{in}-p_{cam})\frac{\pi}{4}d^2{}_{plung} \tag{5.2}$$

5.2.1 Annular leak connection

In some flow situations, arising for example in fuel injection components, there is a leaking annular flow, e.g. around moving pistons. Leakage volumetric flowrate is calculated using a Poiseuille / Couette flow solution for flow between parallel plates, and thus is only valid when δ << D on (5.3) [19].

$$Q=M\left[\pi D\delta\left(\frac{\delta^2\Delta_p}{12\mu L}-\frac{1}{2}U_{wall}\right)\right] \tag{5.3}$$

Note that the sign convention for all vector quantities above (Q, Δp, Uwall) is that the positive direction is in the direction of the linking arrow through the Figure 5.5.

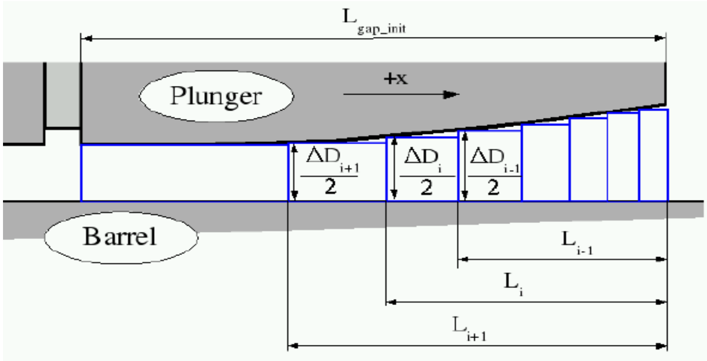

Figure 5.5 : Geometry of user defined variable gap [18].

The effect of plunger eccentricity on the flow rate can be accounted for by setting the Eccentricity Ratioto a non-zero value. The thickness of the annular passage, shown as δ above, is modified based on the eccentricity by the formula shown below on (5.4):

$$\delta_e = f\delta \tag{5.4}$$

However, we don’t have an eccentric plunger that is the reason we will not explain the mathematical equation of correction factor on (5.4) [19].

5.2.2 Flow splits

Flow splits are specifically designed to account for conservation of momentum in 3-dimensions, even though the code is otherwise nominally one-dimensional. The flow solver in GT-SUITE is based on a solution of a 1-D version of the Navier-Stokes equation. In pipes, the scalar equations (mass, energy) are solved at the centers of finite volumes, and the vector (mass flow) at the boundaries between them. When a finite volume has several openings it forms a flow split.

The solution of the flow split is similar to the pipe. The scalars are solved at the center of the volume, while the solution of the momentum equation is carried out separately at each of the volume openings (ports). For the momentum solution, the flow split geometry is characterized for each port by its expansion diameter (the diameter into which the flow will expand after entering the flow split), characteristic length (the distance from the port plane to the opposite side of the flow split) and the port orientation (relative angle of the port).

Of course, a conventional 1-D treatment will not adequately capture the interaction of the flow through ports with arbitrary orientations. Therefore, the flow split momentum solution is specially adapted for this situation. A characteristic velocity vector is calculated for the flow split based on the contributions of momentum flux from all of its ports. The momentum flux out of the flow split is calculated by using the component of the characteristic velocity in the direction of the ports. The directions are corrected according to Figure 5.6 which shows the key input needed for angular data.

Default Roughness Value (mm) for the calculation basics;

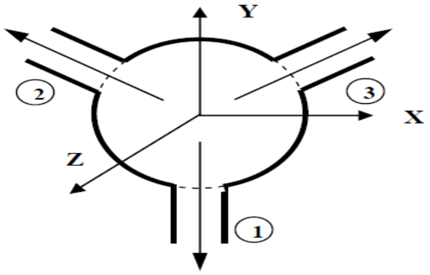

Simple 2D Flow Split Example

Port Number	1	2	3
Angle wrt X-axis	90°	140°	40°
Angle wrt Y-axis	180°	50°	50°
Angle wrt Z-axis	90°	90°	90°

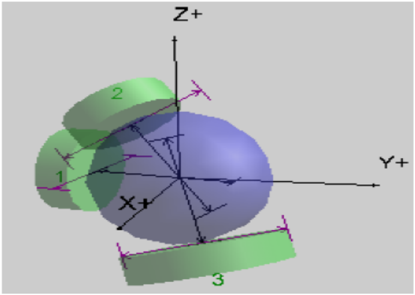

Complex 3D Flow Split Example

Port Number	1	2	3
Angle wrt X-axis = A	100°	110.7°	72.6°
Angle wrt Y-axis = B	170°	127.8°	72.6°
Angle wrt Z-axis = C = ϕ	90°	45°	155°
θ	-100°	-120°	45°

Figure 5.6 : Schematic of a throttle with respect to angular connection [19].

Volumetric flow rate through Tee Junction is calculated from the continuity equation on (5.5):

$$\rho_x \mathrm{Q}_x + \rho_y \mathrm{Q}_y = \rho_z \mathrm{Q}_z \tag{5.5}$$

Two known flow rates are taken from the connected Line elements. The unknown flow rate at the Pressure Port is calculated from equation 203.

Pressure in Pressure Port is taken from the neighboring Volume element (real or virtual) or through inverted connection to the Line element.

The flow resistance coefficient is the ratio of the total pressure loss (drop) to the velocity (dynamic) pressure over an arbitrary flow section. It is determined as the sum of the coefficient of local section resistance ξloc and the friction coefficient ξfr .

$$\xi = \xi_{loc} + \xi_{fr} \tag{5.6}$$

$$\xi = \frac{\Delta p_{fr}}{\rho_{op} W^2 / 2} \tag{5.7}$$

= is the friction loss coefficient in the given flow section of junction

$$\xi_{loc} = \frac{\Delta p_{loc}}{\rho_{op} w^2{}_{op} / 2} \tag{5.8}$$

= is the coefficient of local resistance of the given flow section. Flow resistance coefficient is calculated according to the flow type in the Junction. There are four different flow types (cases). For each Flow Case, different equations for the resistance coefficients (two flow sections) are used [20].

5.2.3 Fluid piston

This object is used to model interaction between flow and mechanical systems, and is commonly used in hydraulic and pneumatic applications. Specifically this template models the following:

- Force on the attached mass due the pressure in a chamber
- Volume change of the chamber due to the mass displacement

The equations used by this template are shown below. The user can choose the icon which is most descriptive for the part of the system being modeled (i.e. open or closed end) by right clicking the part on the map and going to "Choose Part Icon…". Note that poppet mass and flow volume are not modeled in this template. The flow port of this template should be connected to a 'FlowSplit*' flow part. The mechanical port of this template should be connected to a live mass ('Mass' or 'MassWithContacts') either directly or through a series of other fluid-mechanical design templates. The 'Mass' component represents the motion of the poppet, and that information is passed to the mechanical port of the 'FluidPiston' template. The forces computed from the 'Fluid Piston' part will also be passed on the 'Mass'.

Direction of force due to the pressure. Two options:

- Positive: pressure force is in the positive direction. This also means that a positive mass displacement will result in a volume increase.
- Negative: pressure force is in the negative direction. This also means that a negative mass displacement will result in a volume increase.

Force calculations of pistion,the force transferred to the mass is due to the pressure with the equation (5.9) [19].

$$F = jP\left[\frac{\pi(D_{\rho}^{2} - D_{r}^{2}}{4}\right] + F_{ext} \tag{5.9}$$

5.2.4 Spring - massless spring connection

The 'Spring' object is a massless standard spring that can be used to connect component parts with translational degrees of freedom.

Behavior of Spring Force, Spring Force calculation and Conventions: The Spring Force is calculated using the following equation shwon with Figure 5.7:

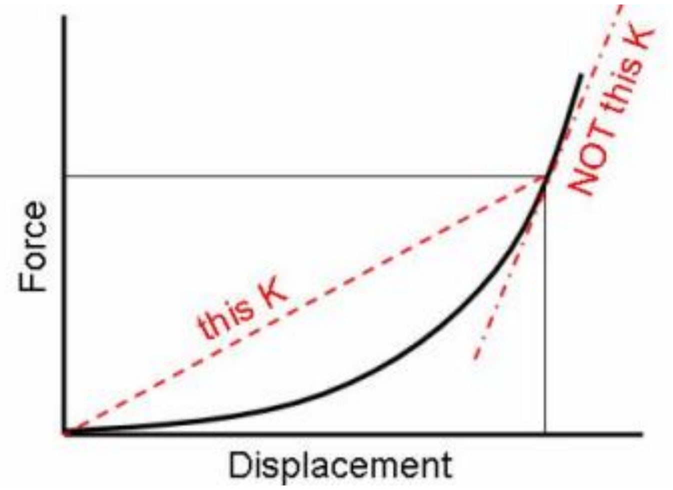

Figure 5.7 : Spring behaviour with respect to force.

$$F = k*(x1-x2) - F_p \tag{5.10}$$

Note that, if the Force versus relative displacement (x = x1 - x2) is known, then the stiffness can be calculated as k = (F + Fp)/ x, independently of whether the spring is linear or not [19].

5.2.5 Ball valves

A ‘BallValveConn’ connection may be placed between two flow components at any point in the system. ‘BallValveConn’ objects require the user to input an array of discharge coefficients versus angle in both forward and reverse directions for the range of valve’s position. It is often convenient to specify the angle by a parameter name so that the angle may be easily set at run time for each case. The angle may also be specified as a time-dependent transient profile using a ‘ProfileTransient’ reference block to simulate the opening or closing of the valve within a given case. This object shown with Figure 5.8, is used to model a ball poppet with a conical seat for hydraulic or pneumatic applications.

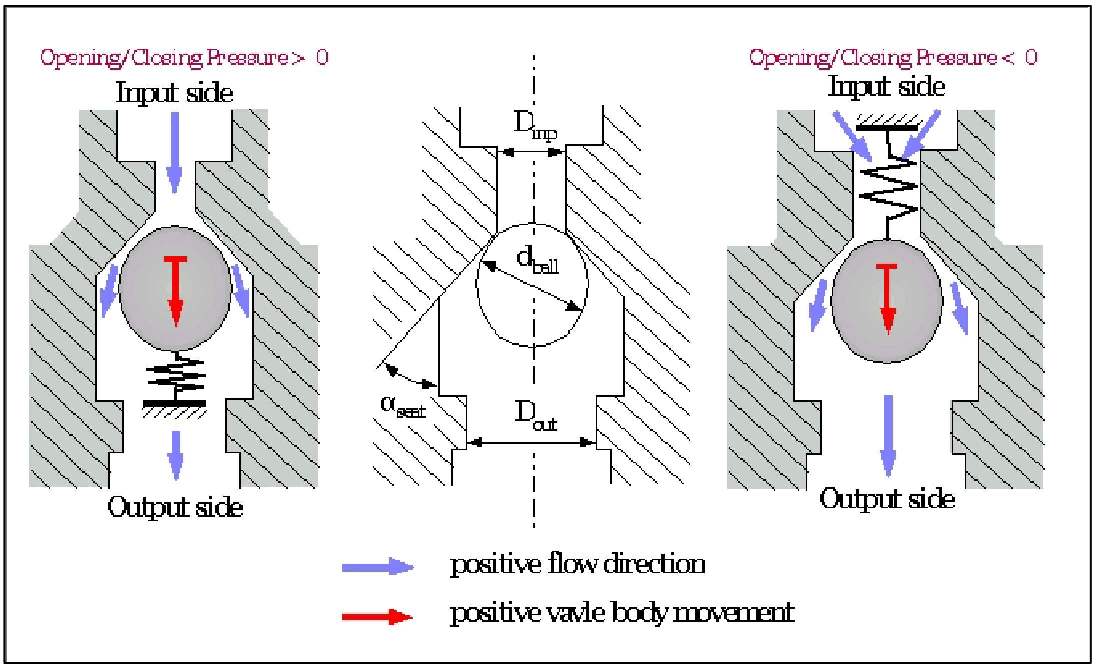
Opening/Closing Pressure > 0
Input side
Output side
Dinp
dball
αseat
Dout
Opening/Closing Pressure < 0
Input side
Output side
positive flow direction
positive vavle body movement

Figure 5.8 : Ball valve schematic and explanation of equation [18].

This template calculates the change in flow area as a function of lift of the poppet, the pressure forces on the poppet, and the redistribution of volume of attached flow components due to poppet lift. Note that poppet mass itself is not modeled in this template. The mechanical port of this template should be connected to a live mass which represents the motion of the poppet. [18].

Motion of Check Valveball in local coordinate system is governed by the following:

$$m\ddot{x}+c_0\dot{x}+k_0x=-F_0-F_{hyd}-F_{frict}-F_{in\_st}-F_{out\_st} \tag{5.10}$$

Preload force *F0* is calculated from the valve opening/closing pressure:

$$F_0=p_0\frac{\pi}{4}\left(d_{ball}\cos\alpha_{seat}\right)^2 \tag{5.11}$$

where *p0* is the opening/closing pressure, *dball* is the ball diameter and α*seat* is the half-angle of valve seat.

Hydraulic force *Fhyd* is calculated from the equation:

$$F_{hyd}=\frac{\pi}{4}\left(p_{out}-p_{in}\right)\left(d_{ball}\cos\alpha_{seat}\right)^2 \tag{5.12}$$

where *pin* and *pout* are the actual pressures on input and output end. Pressures *pin* and *pout* are taken from the connected hydraulic elements (volumes or hydraulic boundaries). Fluid damping force is calculated from Equation (5.13). Forces from input and output stops *Fin_st* and *Fout_st* are calculated identically.

5.2.6 Delivery valve

Volumetric flow rate through Check Valveis calculated from Bernoulli equation:

$$\dot{Q} = \sqrt{\frac{1}{\xi_{eq}} \frac{2(p_{in} - p_{out})}{\rho}} \tag{5.13}$$

where *Q&* is the flow rate, ξ*eq* is the equivalent flow resistance coefficient and ρ is the fluid density.

5.3 Cam Lobe and Cam Shaft

The 'CamLobe' object is used to describe the properties of a cam lobe. The cam profile, cam angle defining the start of the lift event, and lobe properties such as inertia, stiffness and damping are defined by the attributes below. The cam lobe coordinate system, see Figure 5.9, coincides with the camshaft system as described in the 'Cam Analysis' template. In the absence of a 'Cam Analysis' and camshaft assembly, the 'CamLobe' is positioned at the Global Coordinate System Origin [19].

This element serves to define the Cam Profile by follower acceleration or lift data (grinding coordinates for reciprocating follower).
Cam Profileacceleration/lift data implies the acceleration/lift of the roller center of the reciprocating Cam Profilefollower, provided the connection between the cam profile and the roller is rigid [19].

Positive angle implies that from the calculation start up to the shaft rotation angle, less than specified shift angle, the follower (roller tappet) rests on the cam base circle. Hence, if positive shift angle is defined, the initial conditions of the follower must be equal to zero. This mechanism is shown with Figure 5.9, specify the shift angle of cam profile relative to the start position. Negative shift angle implies the calculation start from the cam profile value corresponding to the shift angle value in the cam profile table. With this way, the mechaism stiffness coefficient can be considered with different values that are appropriate with real life data.

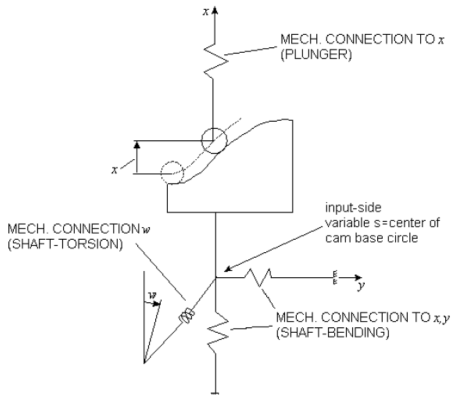
x
MECH. CONNECTION TO x
(PLUNGER)
x
input-side
variable s=center of
cam base circle
MECH. CONNECTION w
(SHAFT-TORSION)
w
y
MECH. CONNECTION TO x,y
(SHAFT-BENDING)

Figure 5.9 : Mechanical representation of a cam profile [19].

In this case, the appropriate number of rows in the table will be skipped until the row with the cam angle equal to shift angle is given with Figure 5.10 [19].

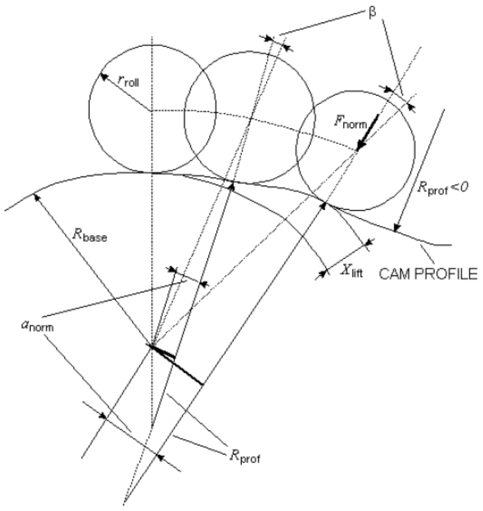
β
r_{roll}
F_{norm}
$R_{prof}<0$
R_{base}
X_{lift}
CAM PROFILE
a_{norm}
R_{prof}

Figure 5.10 : Geometry of cam profile [19].

w-coordinate of cambody (rotation angle)

$$w = \dot{\varphi}_{cam} t = i_{tr} \dot{\varphi}_{ref} t \tag{5.14}$$

w-coordinate (rotation angle) of cam base body. If Cam Profiles a boundary element (i.e. an input mechanical connection in *w*-direction does not exist), rotation angle of cam profile is the product of Reference speed *ref t* transmission ratio *tr i* and time interval from the beginning of calculation *t* :

Torsional distortion angle corresponds to *Δ*β in equation (5.16) 3. It is used to correct the cam angle in order to maintain permanent contact between cam contour and follower (roller),

$$\Delta\beta = \alpha_{tabl} - w \tag{5.15}$$

where α*tabl* is the angle in 1st column of Cam Profiletable and *w* is rotation angle of the cam body (camshaft). Δβ is equal to 0, if input mechanical connection does not exist.

Reaction force normalto cam profileResistance force normal to cam profile *Fnorm* (5.17). It is calculated from the reaction force of the cam follower (e.g. plunger) in x-direction *Fx* according to the formula:

$$F_{norm} = \frac{F_x}{\cos(\beta + \Delta\beta)} \tag{5.16}$$

Torsional vibrational velocity and angular velocity of cam body relative to stationary rotation. Torsional vibration velocity is the difference between actual angular velocity in *w*-direction and reference speed, which is defined in Calculation It is nonzero only if an input mechanical connection in w-direction exists [19].

5.3.1 Hertz stress at camroller contact

Hertz stress at cam-roller contact is calculated from the formula and shown with Figure 5.11.

$$p_{Hertz} = 0.418\sqrt{\frac{E_{cam}F_{norm}}{b_{roll}}\left(\frac{1}{R_{prof}} + \frac{1}{r_{roll}}\right)} \tag{5.17}$$

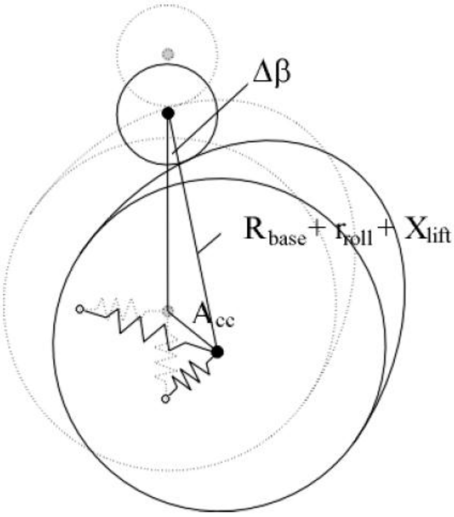

Figure 5.11 : Amplitude of cam center and torsional cam distortion [18, 19].

To connect cam profile to a shaftelement three mechanical connections (in x, y, and w directions, respectively) are necessary as shown in Figure 5.12.

To denote a rigid (or almost rigid) connection between the cam and shaft, the respective connections must possess very high stiffness (e.g. comparable to the shaft bearing stiffness).Preload, stiffness and damping of input mechanical connections from shaftelement in *x* and *y*-directions have to be defined in global coordinate system.

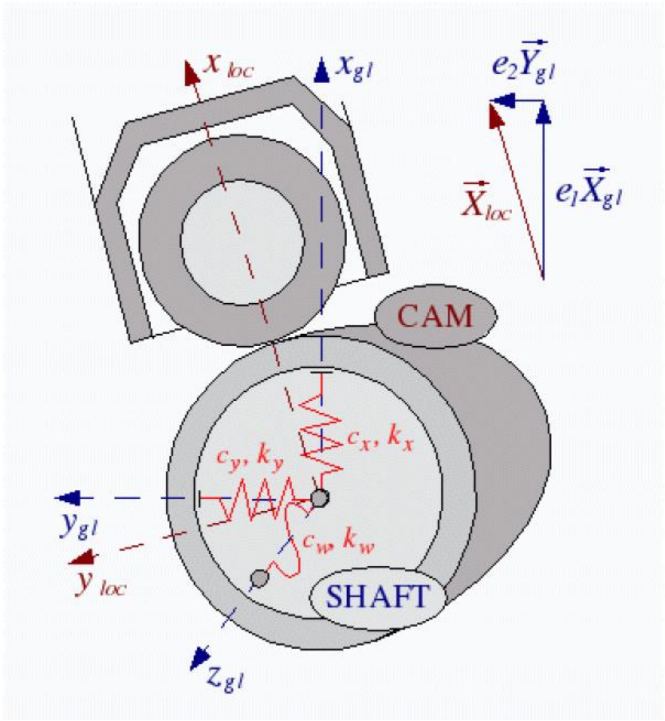

Figure 5.12 : Cam profile with connections to shaft [18, 19].

Local coordinate system of Cam Profileand connected elements (with their connections) can have only translational motion with respect to each other and the global coordinate system. The motion of Cam Profileis governed by the following equation on (5.19):

$$\begin{aligned}
&\sum_{i=1}^{n_x} c_{xi}(\dot{x}-\dot{x}_i)-\sum_{j=1}^{l_x} c_{xj}(\dot{x}-\dot{x}_j)+\sum_{i=1}^{n_x} k_{xi}(x-x_i)-\sum_{j=1}^{l_x} k_{xj}(x-x_j)=\sum_{i=1}^{n_x} F_{oxi}-\sum_{j=1}^{l_x} F_{oxj},\\
&\sum_{i=1}^{n_y} c_{yi}(\dot{y}-\dot{y}_i)+\sum_{i=1}^{n_y} k_{yi}(y-y_i)=\sum_{i=1}^{n_y} F_{oyi}+F_y,\\
&\sum_{i=1}^{n_w} c_{wi}(\dot{w}-\dot{w}_i)+\sum_{i=1}^{n_w} k_{wi}(w-w_i)=\sum_{i=1}^{n_w} T_{oi}+T_{Fx}
\end{aligned} \qquad \mathbf{(5.18)}$$

Reaction force *Fy* is calculated from the equation:

$$F_y = F_{norm}\sin(\beta + \Delta\beta) = F_x \tan(\beta + \Delta\beta) \qquad \textbf{(5.19)}$$

where *Fnorm* is the reaction force normal to cam profile at its contact point with the roller, *Fx* is the resultant force from output mechanical connections in *x*-direction (follower force), β is the pressure angle between force vectors *Fnorm* and *Fx* without consideration of the cam center motion and Δβ is the correction of pressure angle due to the motion of cam center in *x* and *y-direction*s (refer to Figure 2) .

5.3.2 Journal

Journal' parts are used to define the main journals in a crankshaft, camshaft or general shaft assembly. Listed below are the attributes that define the 'Journal' object. Journal properties are defined in its local coordinate system. For crankshaft systems, the journal coordinate system (see Figure 1) coincides with the crankshaft system as described in the 'Crank Analysis' template. Similarly, for camshaft systems, the journal coordinate system (see Figure 2) is identical to the camshaft system as described in the 'Cam Analysis' template. For general shaft assemblies, like a balance shaft as shown with Figure 5.13, the 'Shaft Analysis' template and coordinate systems is applied.

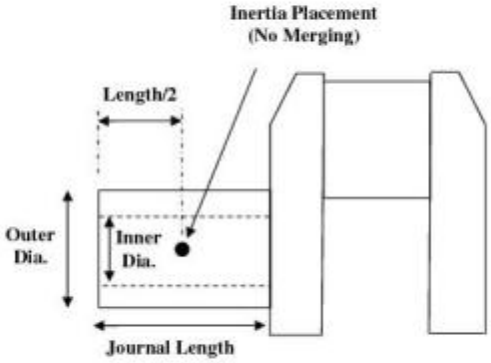

Figure 5.13 : Journal dimensional basics [19].

The impedance technique predicts the forces and torque transferred at a journal bearing joint between two parts as a function of the states of the parts. Forces and torque transmitted in a journal bearing are functions of oil pressure and shear stress distribution in the bearing oil film, arising from the relative motions of the journal and the bearing, which are in turn determined from the solution of equations of motion for components containing the journal and bearing. The oil film pressure distribution is governed by the Reynolds Equation, a partial differential equation derived by application of the Navier-Stokes equations to thin films. Time and the axial and tangential coordinates in the film are the independent variables. The solution domain is the entire film, axially extending from one end of the bearing to the other and wrapping 360 degrees around the shaft as shown with Figure 5.14. The pressure of the lubricant (e.g. oil or air) outside the bearing constitutes the boundary condition for the solution of the equation.

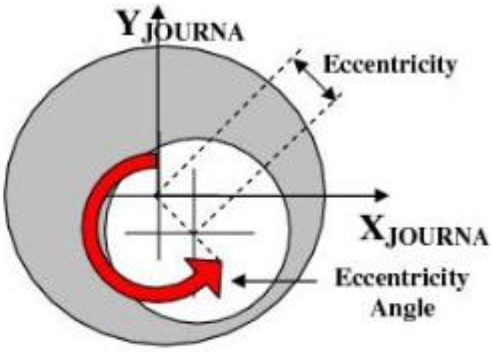

Figure 5.14 : Journal bore eccentricity [19].

The relationship between the equivalent linear velocity and angular velocity is shwon with Figure 5.15;

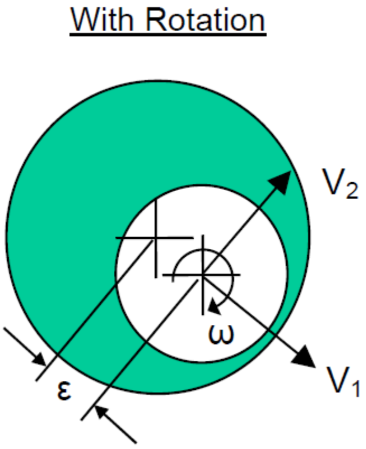

Figure 5.15 : Journal eccentricitiy with rotation [19].

The relationship between the equivalent linear velocity and angular velocity can be expressed as:

$$V_{eq} = -\frac{|\omega|}{2} \bullet \varepsilon \tag{5.20}$$

This eliminates the need of accounting for the angular velocity parameter, and reduces the number of parameters needed to predict the forces and torque,

$$V = \sqrt{V_1^2 + (V_2 + V_{eq})^2} \tag{5.21}$$

When the Reynolds equation is non-dimensionalized, three *dependent* dimensionless groups emerge for the integrated forces and torque: one involving the force in the direction of eccentricity, one for the dimensionless force in the direction perpendicular to the eccentricity, and one for the dimensionless(bearing friction) torque. All three are functions of two *independent* parameters only, namely: i) the normalized eccentricity (ε/c); and ii) translational motion angle (β): [18, 19].

$$F_1^* = \frac{F_1}{\mu VR}, F_2^* = \frac{F_2}{\mu VR}, T^* = \frac{T}{\mu VR^2} \tag{5.22}$$

F1* represents the dimensionless force parallel to the direction of eccentricity, F2* represents the dimensionless force perpendicular to the direction of eccentricity, T* represents the dimensionless torque. The impedance maps relate these three groups to normalized eccentricity ε/c and velocity angle β. [18, 19].

5.4 Simulation Results and Modeling Details

According to formulas and mechanical calculations shared in above, reference engine speed and load cases are ran with GT-FUEL simulation program.
Engine speed is 4000 rpm which is the same speed profile we considered during the measurements of valve train system. Engine load is full load (%100) which means the highest volumetric flow from high pressure fuel pump to injectors. This volumetric data is another cross check reference for the model confirmation.

First of all, the high pressure plunger of hgih pressure fuel pump is modelled. As you can see in Figure 5.16 all of the mechanical and hydraulical components are carefully installed. Geometrical and mechanical inputs are filled. All of the details of these components are explained in the previous section.

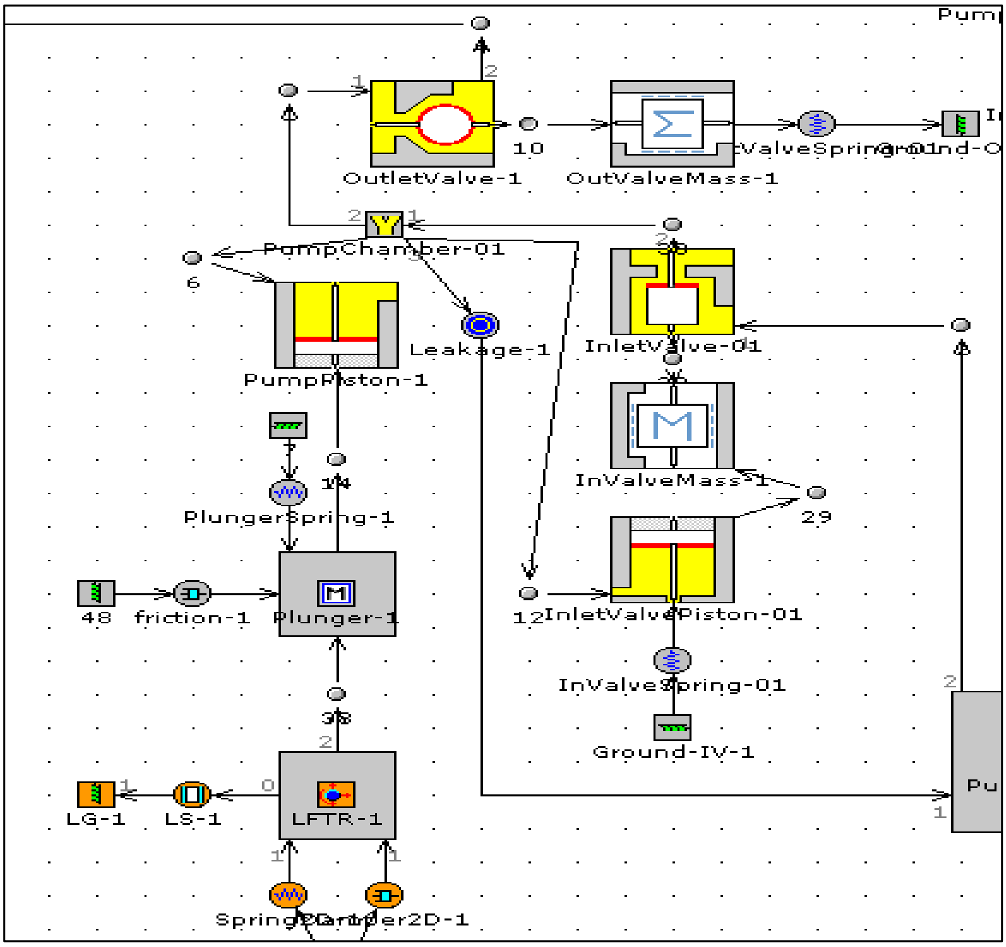
Pum
OutletValve-1
10
OutValveMass-1
ValveSpring-01
Ground-O
PumpChamber-01
6
Leakage-1
InletValve-01
PumpPiston-1
InValveMass-1
29
14
PlungerSpring-1
48
friction-1
Plunger-1
12
InletValvePiston-01
InValveSpring-01
38
Ground-IV-1
LG-1
LS-1
LFTR-1
Pu
SpringDamper2D-1

Figure 5.16 : Plunger model snapshot from GT fuel.

After the simulation of mentioned engine conditions, we can review the results of the simulation; here is the Figure 5.17 below the high pressure pump piston force graph according to pump shaft per cycle.

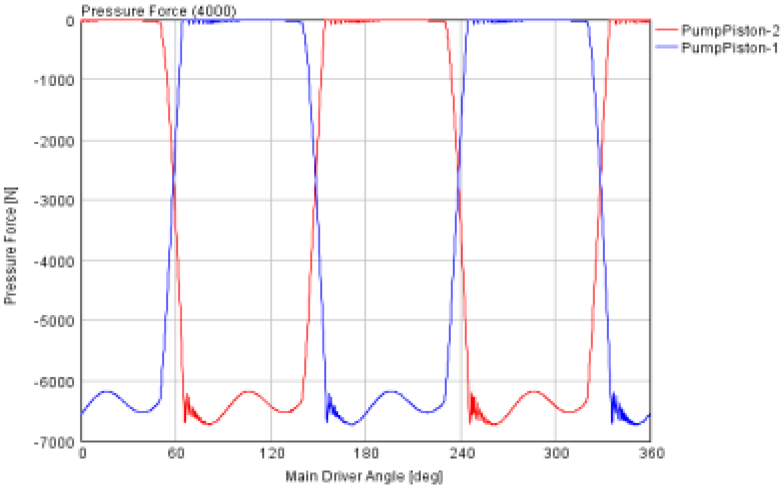

Figure 5.17 : Plunger forces acting on pistons respectively.

As known, the force has a harmonic distribution corresponding to main driver angle. Displacement of the plunger is another key data which need to also consider for the confirmation of cam profile which we derivated from geometrical data as shown in Figure 5.18.

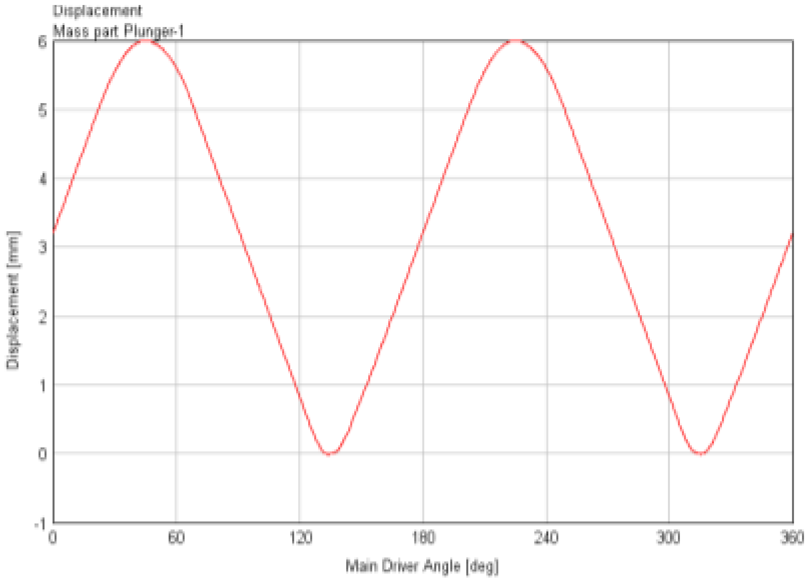

Figure 5.18 : Cam profile lifting characteristics of plunger.

The displacement is also changing between 0 to 6 mm corresponding cam shaft rotational angle as mentioned for the pump piston graph.

As you can see the graph with Figure 5.19, cam contact forces are another key data which we can easily evaluate the effect of frictional force on the movable parts which are modelled with high pressure plunger.

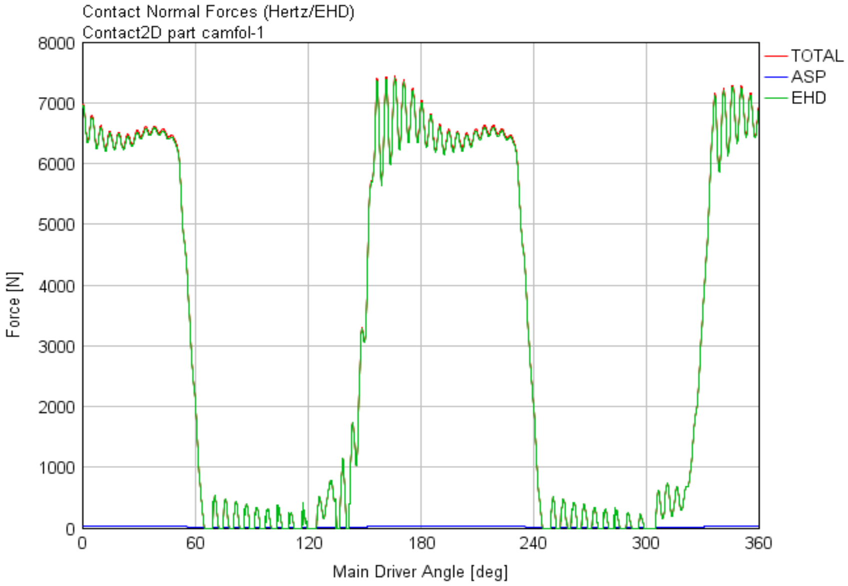

Figure 5.19 : Cam contact force distribution drived by plungers.

The frictional force is directly related with the friction coefficient of the standard fuel which we stated at the previous section. Also, the force distribution of contact force on cam shaft is almost same with the force characteristics of high pressure piston element as previously shared the results.

Frictional forces can be also ignored with reference to the results of high pressure plunger forces, as given Figure 5.21.

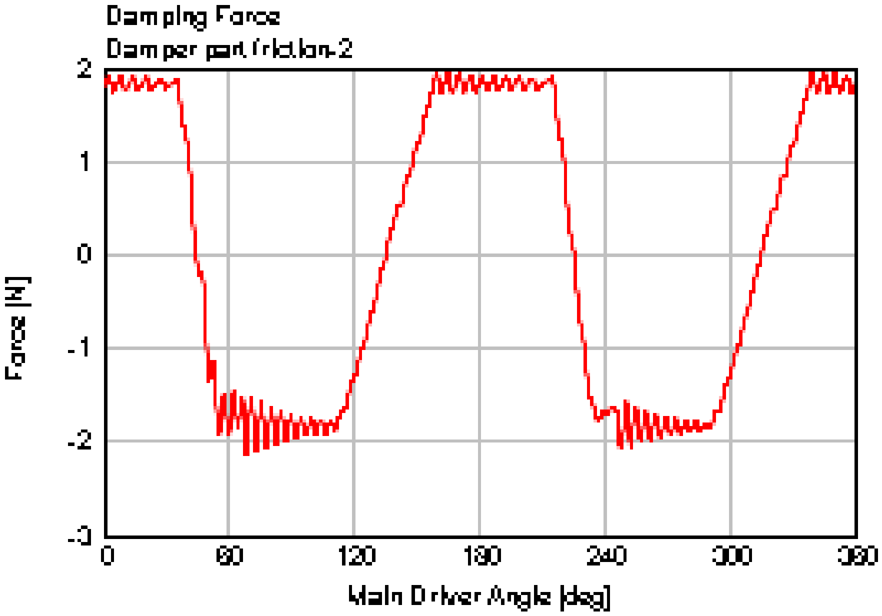

Figure 5.20 : Damping force variation with respect to cam angle.

So the multi body model will not consist the frictional force effect on the high pressure plungers.

Furthermore, total mass flow through pump outlet orifice is given in the Figure 5.21 below. This data is a reference for the confirmation of plunger geometrical input.

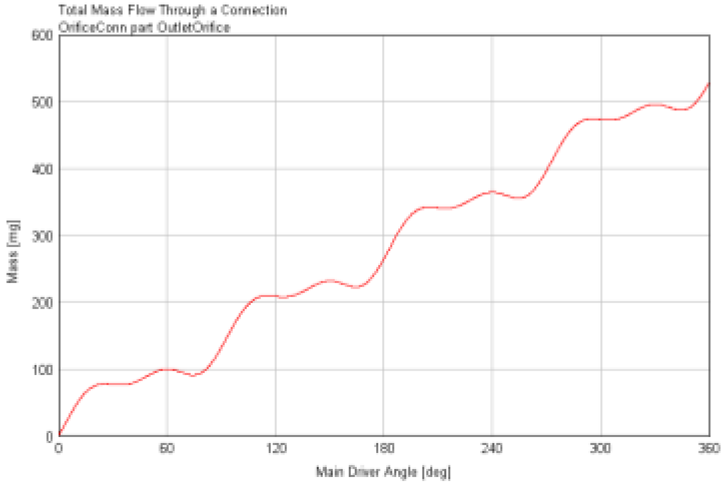

Figure 5.21 : Total flow rate with respect to cam angle.

The accumulated fuel content is demonstrated with one rotational cycle of the cam shaft of high pressure pump. Also this data is calculated according to agreed engine speed and load conditions. As explained, engine speed and load conditions have an effect on the delivered or required fuel quantity on injectors. This reality is given in the in Figure 5.22 below.

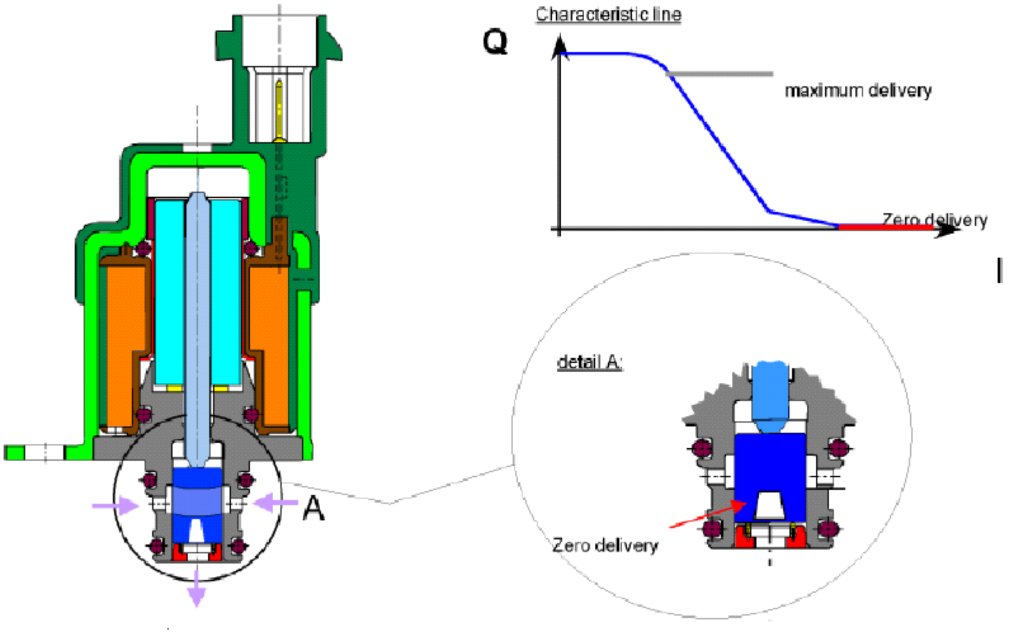

Figure 5.22 : Metering unit function for total fuel delivery [10].

Metering unit means, MeUn is regulating the pressure, This form of pressure control means, for the overall system, that the high-pressure pump always delivers as much fuel as the system needs to maintain the pressure, or to increase or decrease it. This means that the pump only takes on the required power from the engine and compresses only as much fuel as necessary.

For full load, the system is usually designed in such a way that the MeUn is fully opened and the delivered quantity is sufficient for attaining the maximum pressure.

As Figure 5.23 states in below, Input and Output torques are very critical from the point of high pressure fuel pump mechanical behaviour. The torque excitation is the key limitation for the valve train system. The more required torque means the more effect on system stability. The required torque is also related with the required fuel flow quantity on injectors as metering unit functionality explained in the previous section.

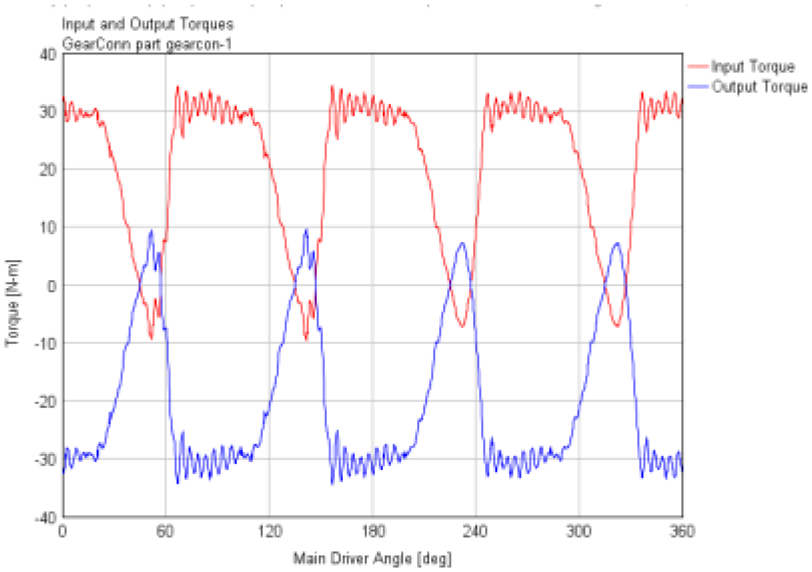

Figure 5.23 : Input and output drive torque required for pump excitation.

Also, cam shaft and bearings simulation model is shared in Figure 5.24 below, all of the mechanical part details are explained in the previous section.

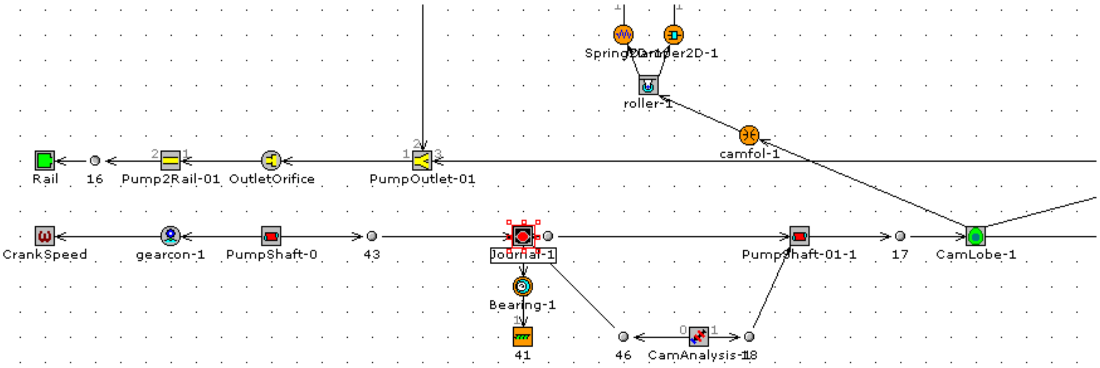
Spring2D-1
Damper2D-1
roller-1
camfol-1
Rail
16
Pump2Rail-01
OutletOrifice
PumpOutlet-01
CrankSpeed
gearcon-1
PumpShaft-0
43
Journal-1
Bearing-1
41
46
CamAnalysis-1
18
PumpShaft-01-1
17
CamLobe-1

Figure 5.24 : Cam shaft and dynamical journals representation from model.

Cam shaft directly contacts with two plungers which have 90◦ positioning between eachother. As previously mentioned, cam profile and cam shaft geometrical data are installed in the simulation program and as you can see in Figure 5.25.

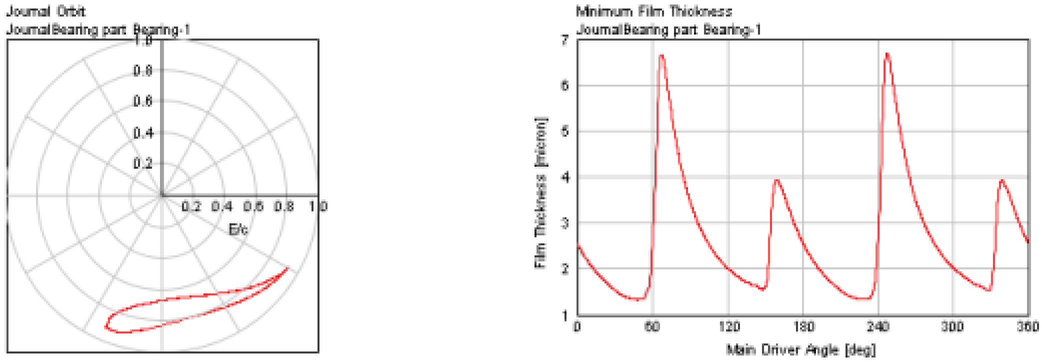

Figure 5.25 : Dynamical journal force distribution.

Also, density of the cam shaft (High Speed Steel) already introduced to the progmram material library.

Eventhough the pressure and force distribution are not our target for the 3D modelling, these info are also beneficial and suggestive from the point of 1D modelling advantages. If there is a further study continued, the detailed properties such a frictional coefficient, viscosty and density may effect on the journal mechanical outputs as can be figured out from Figure 5.26.

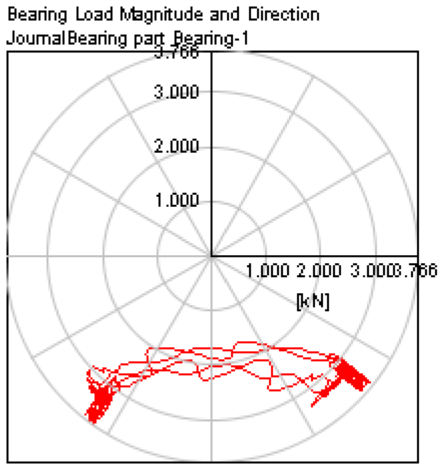

Figure 5.26 : Bearing load magnitude with respect to both directions.

Also frictional force distribution and journal load reaction are dependly related with eachother. The force magnitude also depends on the force and mechanical variability on the cam contact surface force reaction. So, every change on plunger and cam shaft may result in marginal change on journal and bearing mechanical output.

5.5 Measurement Equipment

The measurement results are taken from a similar test bench from full service supplier. So, all of the key simulation result will be compared with the measurement results from these test becnhes.

As you can see from the picture of the test bench in Figure 5.27, it has several functionalities as; Test each cylinder's oil supply capacity at various rotation speeds, test point and interval angle of oil supply of injection pump is calculated according to set conditions of run cycle. Adjustment and check of the mechanical governors are calculated and measured with reference to rotational angle of pump cam shaft speed. Also, the rig is capable to measure vibrational outputs in case of necessity.

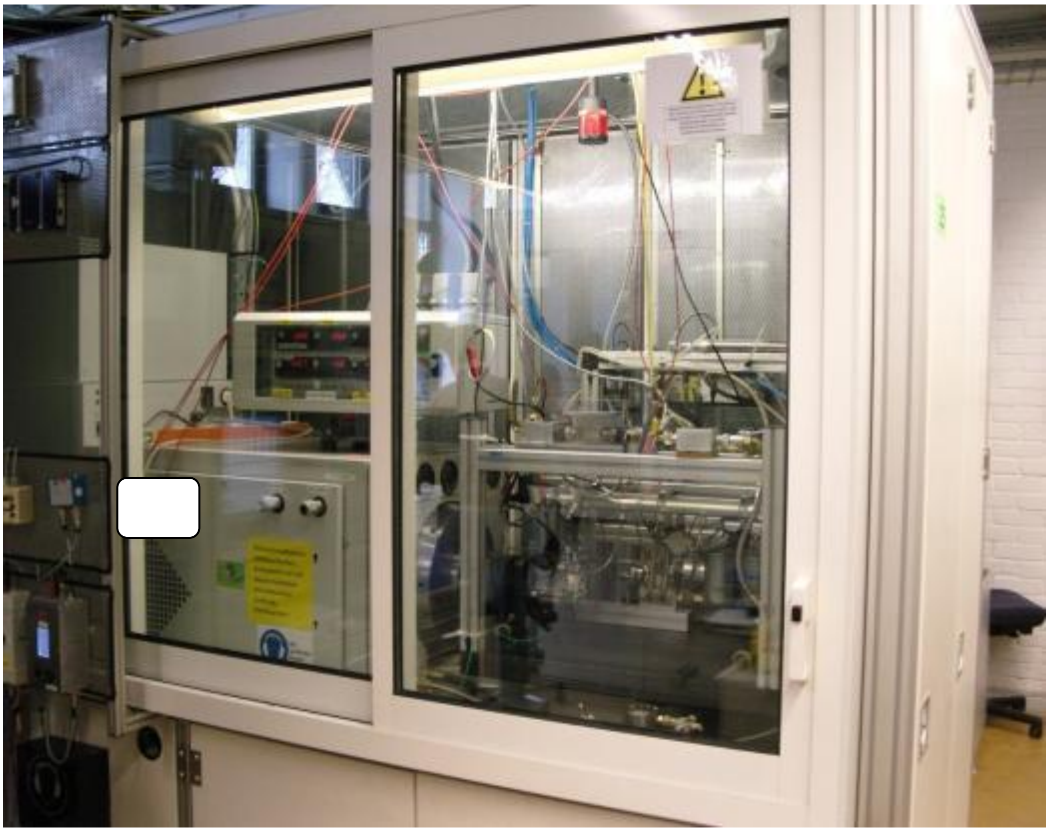

Figure 5.27 : Bench Ttest of a fuel injection pump [5].

Another capability of these testing rigs are measuring the sealing performance of injection pumps and testing the negative pressure performance of pneumatic speed regulators embedded in it as it can be figured out from the illustration given with the Figure 5.28. As it can be seen, this is a typical equipment used by several manufacturers in the field.

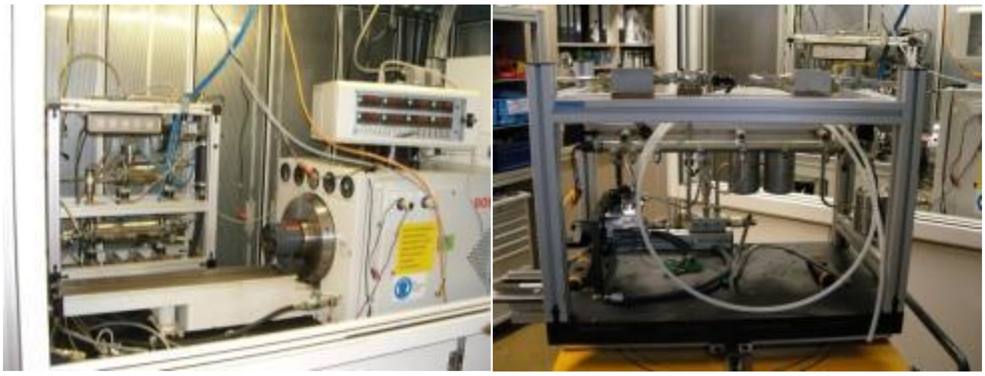

Figure 5.28 : Fuel injection pump rig test [10].

There are also an integrated suction pump installed on testing bench. The testing fluid is selected in paralell to compatible fuel which we also recommended in the field usage.

5.6 Measurement Results and Model Confirmation Discussion

As you can clearly figure out from the Figure 5.29, 2000 bar is the worst case scenario from the point of required torque. As we did with your simulation results, measurement results will be evaluated for 2000 bar and 3750-4000 rpm profiles.

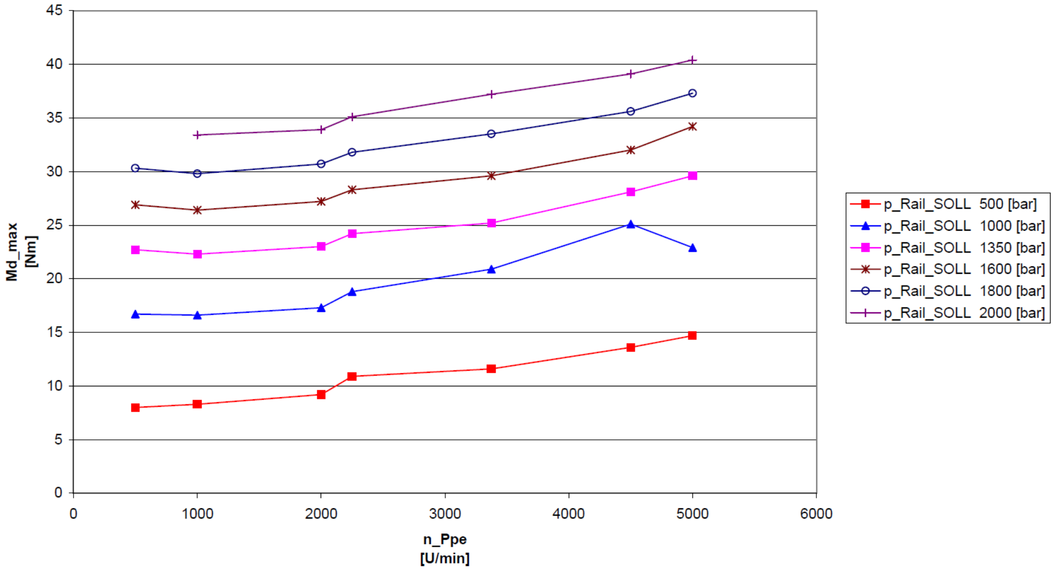

Figure 5.29 : Excitation torque required respect to different FRP profiles.

Inlet pressure at pump inlet is 5 bar (absolute) and the temperature profile at pump inlet is 40◦C. These physical properties have marginal effects on mechanical output.

The torque measurements of rig data is shown in red with the Figure 5.30 in below.

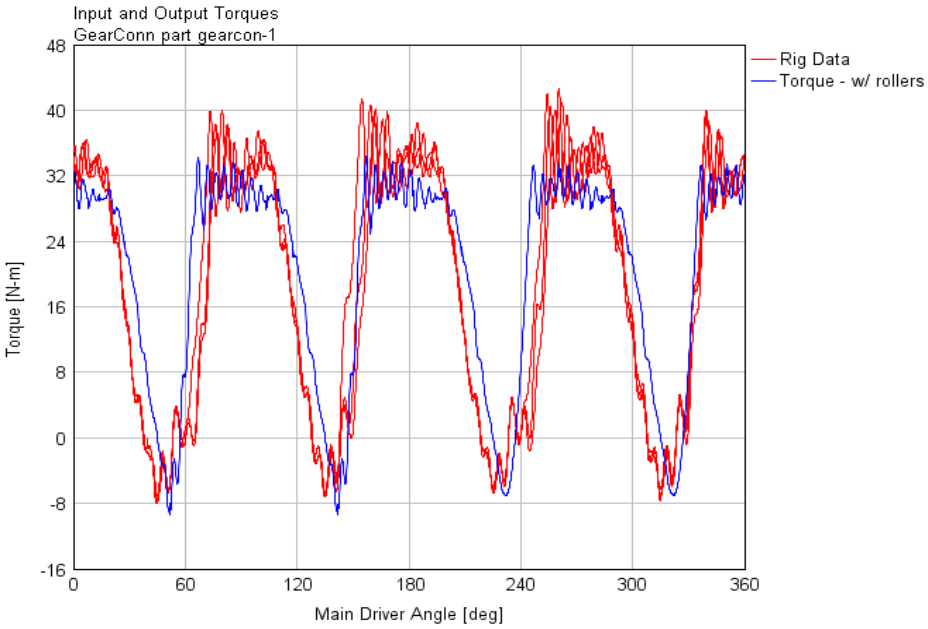

Figure 5.30 : Back to back comparison of rig tests and simulation results.

You can see from Figure 5.31, a comparison of the new results to the rig data below. Still included a shift in the x data to match the rig data, but this change is very common and accepted when comparing simulation to measured data.

Also, the previously presented torque values exported from simulation program is shown in blue in the graph. As you can see there is a consistently increasing and decreasing curves to eachother.The rig measurements of both left and right plunger piston are given in below figure, by the reason the pistons of the plungers orientation to eachother. Force distribution can be explained as the angular position of the cam shaft.

If you can browse the Figure 5.31 piston force measurements, force variation and characteristics show consistency to eachother.

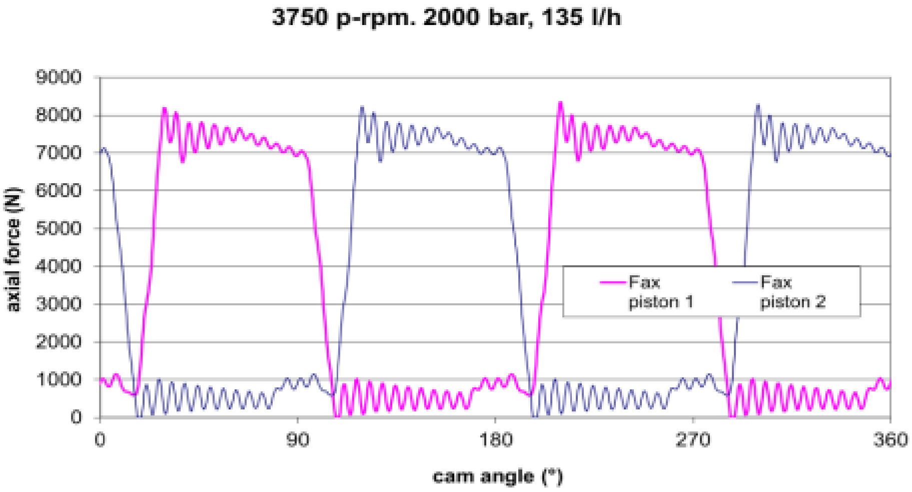

Figure 5.31 : Real world plunger force measurements.

In this paragraph, the cam profile is confirmed with the simulation results. In the Figure 5.32 shown in below, shows a certain coherent with the test rig measurements. The simulation result is given with the Figure 5.19 and the lift profile is changing between again 1 mm to 6 mm.

As a last data which we can use for the model confirmation is the total mass flow delivered from high pressure fuel pump. As you can browse from the previously given Figure 5.32 from the simulation results, the total flow quantity are coherent to eachother. Thus, the volumetric efficiency of the both simulation and measurements are within same range.

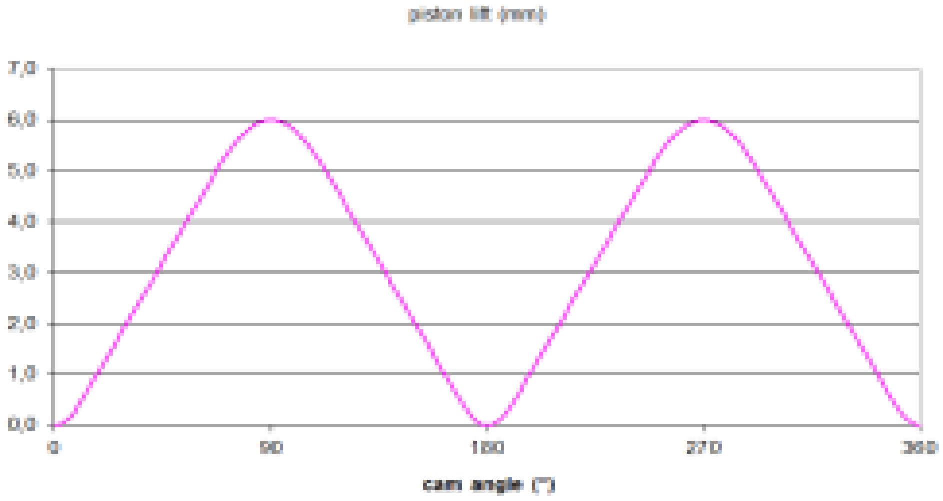

Figure 5.32 : Testing of lifting profile measurement results.

Here is the volumetric efficiency data given by measurements in below.

(Plunger diameter)²* π/4 * (Plunger stroke) * (Cam lobes) * Cylinder

If we roll up the calculation for our system, the simulation result was 500 mg per once cycle. This shows consistency to fuelling data of the engine.

So, all of these data shared in below shows the consistency between the real world model and simulation model. By this way, we can use our 1D pump model outputs with the following sections of the thesis project. Especially, cam shaft load and piston forces are easily acquised from pump model to 3D multi body dynamic model.

6. MULTI BODY DYNAMIC PUMP MODEL

Currently, engine development is pushing on the limits. The need to reduce fuel consumption and increase the mechanical efficiency, while increasing or maintaining power and torque, is indeed challenging. Furthermore, the development of product development system from the point of timing has decreased in recent years and it is expected that this trend will be continued. Consequently the engine development process is one of compromise. One side, each of the fuel injection components within each generation have to be optimized to reach the technical goals especially fuelling, bsfc target etc. To survive with these mentioned challenges within the engine design process, it is important to have access to modern design tools. One of these tools is multi body system simulation allows a flexible handling of technical questions by preoptimizing components and their functions in the concept and design phase, and also allows optimization of systems already in standard production. Within this section of study, the use of commercial software MSC Adams, its place within the design process, its handling and its capacities are demonstrated and verified.

This section describes the modeling and dynamic simulation of a high pressure diesel fuel pump. It integrates a physical and conceptual model, a mathematical model describing the system dynamics, algorithm selection and numerical solution of the equations, and then a computer program is developed using a modular approach to investigate the behavior of the system dynamics [17].

The high pressure fuel pump build and engine conditions are required as input data and results are presented with the results section in the following sections. The high pressure pump model consists of detailed geometry definitions for the cam lobes (including rotational inertia),camshaft support stiffnesses, high pressure plunger stiffness and mass, additional valves stiffness and mass, plunger spring definition. All of the elements described in above have data associated with them that needs to be either calculated or measured. All of the sub-components are carefully weighted and some of the key component are exposed to modal testing.

Based on the theory of contact motion, the reason of complicated dynamic mechanism is evaluated with muldit body dynamic program which is called ADAMS.We can also investigate and evaluate the Hertz stress between cam profile and plunger roller with the introduction of 3D multi body dynamic model as it can be figured out from Figure 6.1. Also, system methodology is direclty consistent with the shown fiure in below. By this way, capability of MBD program is efficienly used.

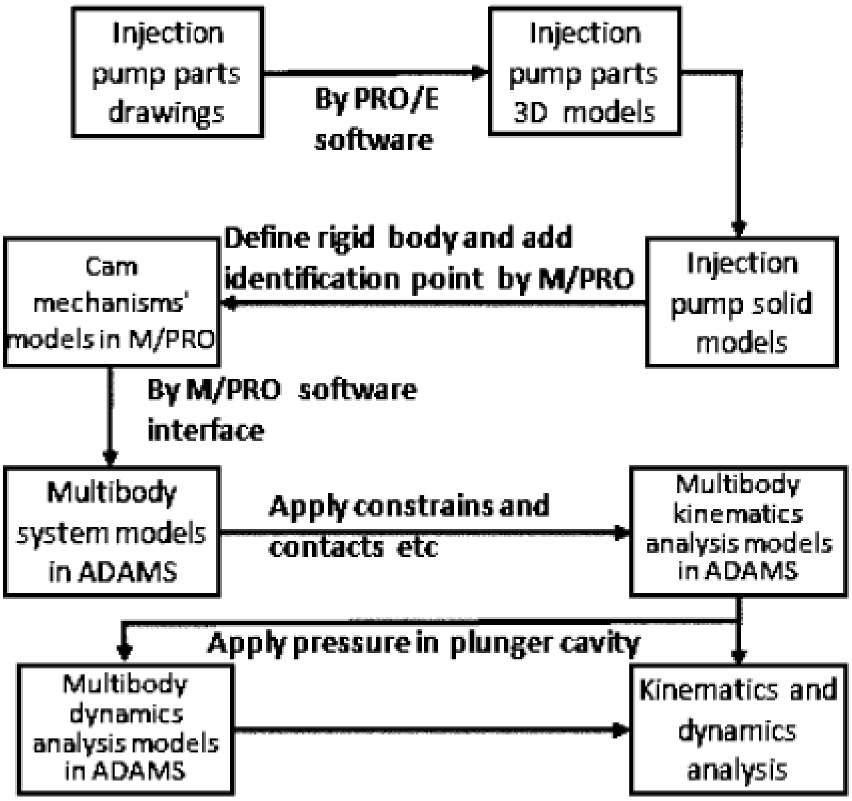
Injection pump parts drawings
By PRO/E software
Injection pump parts 3D models
Define rigid body and add identification point by M/PRO
Cam mechanisms' models in M/PRO
Injection pump solid models
By M/PRO software interface
Multibody system models in ADAMS
Apply constrains and contacts etc
Multibody kinematics analysis models in ADAMS
Apply pressure in plunger cavity
Multibody dynamics analysis models in ADAMS
Kinematics and dynamics analysis

Figure 6.1 : Generic flow chart of Adams simulation [21].

One such process consists of translating a Multibody Dynamics System (MBS) model into an equivalent Finite Element Analysis (FEA) model. Typically,users start with the creation of a MBS model which is set at a desired operating point by means of running simulations in the MBS domain (e.g. dynamics, statics.) The MBS model is then further translated into an equivalent FEA model which is used to perform simulations in the FEA domain (e.g. passivesafety/crash, noise vibration harshness/NVH.) Currently, the translation of the MBS model into a FEA model is done either manually or by means of using a userwritten script. Examples of such algorithm implementation in MSC Adams (Adams) are presented. Currently a FEA model for vibration analysis is generated from scratch without making reuse of the MBS model [22].

6.1 Construction of Adams Model

The methodology for the construction of MSC Adams Model is quite similar to the construction methodology done for 1D model of the high pressure fuel pump. We cam split into 2 basic systems which are plunger and its subcomponents, consequently camshaft and its subcomponents are simulated according to real world measurements. The details of sub-components are shown with Figure 6.2.

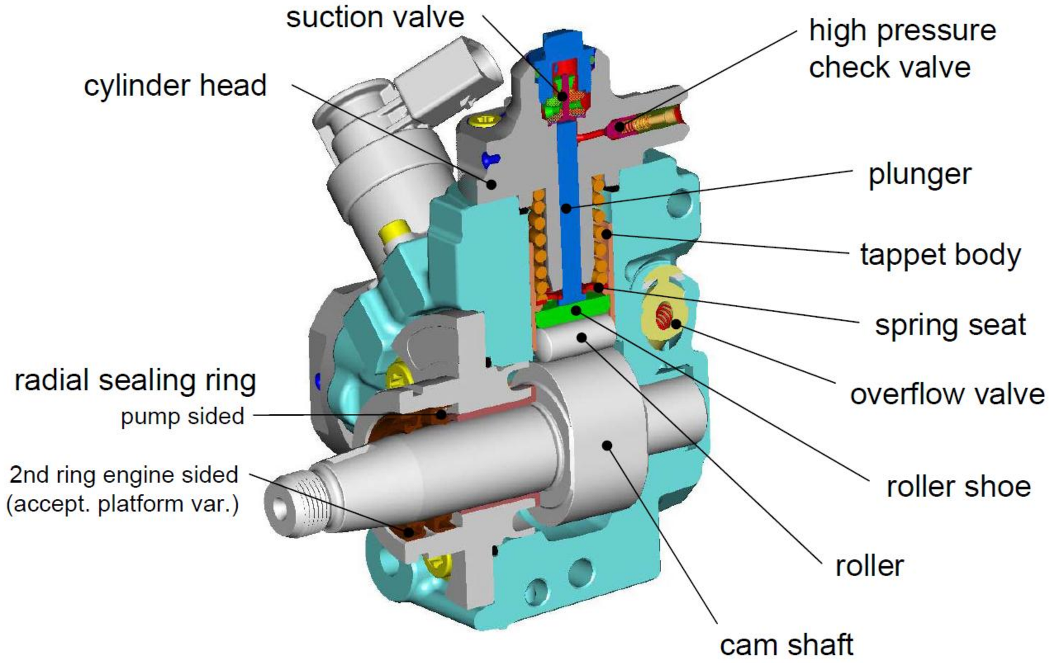
suction valve
high pressure check valve
cylinder head
plunger
tappet body
spring seat
radial sealing ring
pump sided
overflow valve
2nd ring engine sided
(accept. platform var.)
roller shoe
roller
cam shaft

Figure 6.2 : Fuel injection pump sub-components in general.

Furthermore, high pressure fuel pump cover and adapter plate of cylinder head where the high pressure pump is mounted on are considered. This enables to check the stress distribution on the cylinder head coming from the high pressure pump NVH behaviour.

In the following sections, all of these main components are explained according to modelling theory of multi mody dynamics.

6.1.1 High pressure plunger

The high-pressure pump forms the connection between the low-pressure and high-pressure system. It is driven via a fixed connection (clutch, chain or toothed belt) preferably with camshaft speed. The fuel continuously delivered by the presupply pump is compressed and supplied to the rail as it can be seen from Figure 6.3.

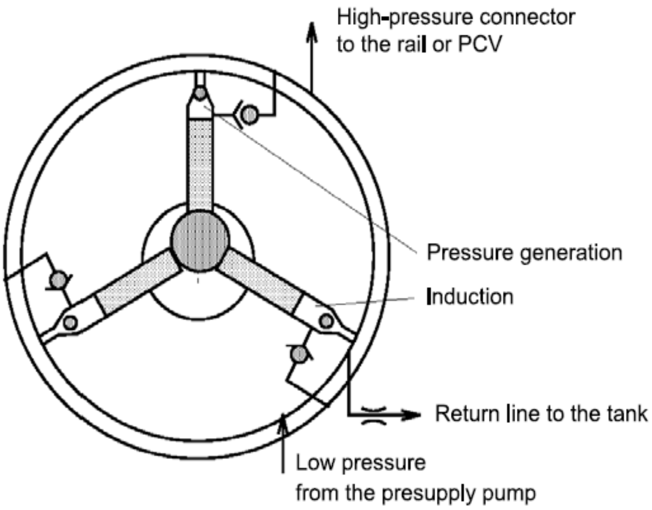
High-pressure connector
to the rail or PCV
Pressure generation
Induction
Return line to the tank
Low pressure
from the presupply pump

Figure 6.3 : Function diagram of a high pressure pump [10].

The drive shaft with its cam shaft and the return spring move the pistons ofthe two pump elements up and down in a sinusoidal movement. The presupply pump presses fuel through the throttle bore of the safety valve into the lubricating and cooling circuit of the high-pressure pump. As shown in Figure 6.4, also, the electrical feed pump can press fuel through the inlet/suction valves into those pump elements in which the piston is moving downward (suction stroke). When the bottom dead centre of a piston is reached, the inlet valve closes due to the pressure drop and the fuel in the pump element cannot escape.

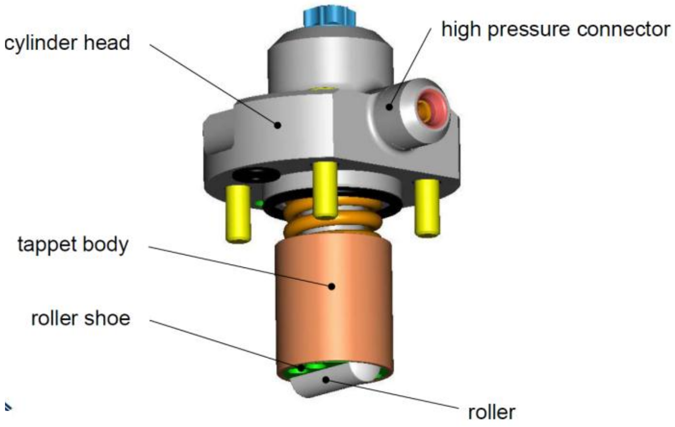
cylinder head
high pressure connector
tappet body
roller shoe
roller

Figure 6.4 : Sub-components of a plunger and basic components.

Now, it can be compressed above the delivery pressure of the electrical feed pump. The pressure building up opens the highpressure valve when the pressure in the rail is reached and the compressed fuel enters the high-pressure circuit. The pump element delivers fuel until the top dead centre is reached (delivery stroke). The high-pressure valve closes due to the resulting pressure drop, that is, the now greater pressure in the rail closes the high-pressure valve.

Consequently, all of the mass measurements are taken. For the mass calculation, MSC Adams is capable to calculate the mass corresponding to its geometrical properties. Thus, the density of the material can be introduced from material library embedded in the program.

Tappet body, roller shoe and roller subcomponents of the plunger entered to the program. As you can see in the Figure 6.5, density properties and real world mass measurements are taken and compared to eachother. Eventhough all of these components can move without any dependence to eachother, from the point of multi body modelling simplification, they can be accepted as one part. Otherwise, we can model as individual part and also can use ‘’fix joint’’ to eachother.

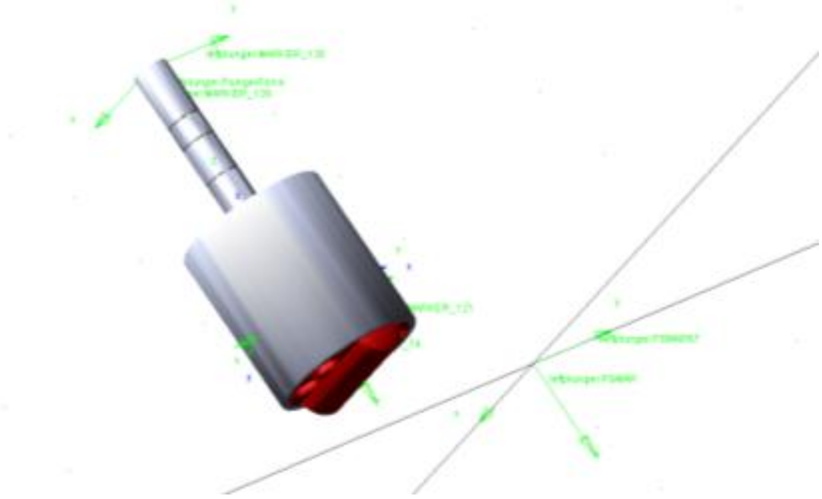

Figure 6.5 : Screenshot from Adams including plunger sub-components.

The spring stiffness coefficient is manually entered to the program according to real worl measurements taken from supplier and installed to program as seen Figure 6.6.

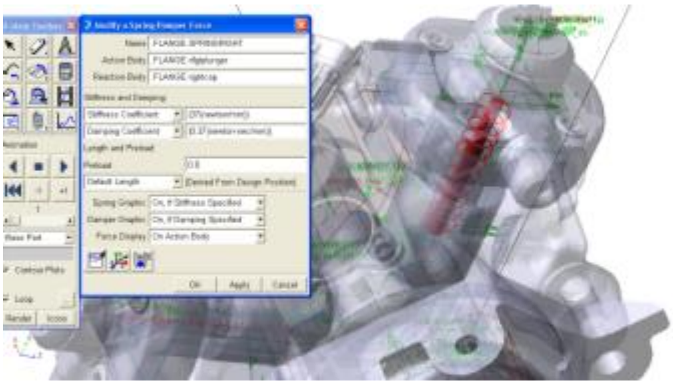

Figure 6.6 : Snapshot from Adams including spring element.

There is a pretension of the spring which is also entered to the model. The geometrical info is also shared by the supplier.

6.1.2 Joints

First of all, due to plunger high pressure piston movement within the cylinder of the high pressure fuel pump, a translational/cylindirical joint is used to connect both of these components to eachother as it can be seen from Figure 6.7.

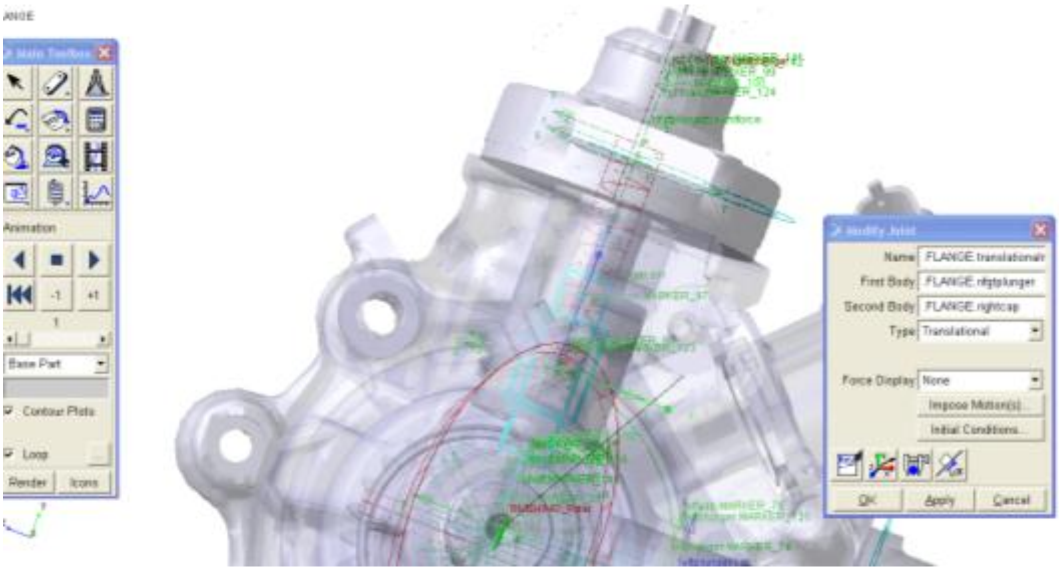

Name: .FLANGE.translational
First Body: .FLANGE.nfgtplunger
Second Body: .FLANGE.rightcap
Type: Translational
Force Display: None

Figure 6.7 : Translational joint representation.

Furthermore, spring is not modelled an individual part, additional prepared spring model coming with the program is used. As mentioned, all of the stiffness and damping coefficients are entered to the spring model coming with the MSC Adams program. Spring model connects, the combination of one part including tappet body, roller shoe and roller to cylinder head of high pressure pump. All of the acting forces on translational element is shown with the Figure 6.8.

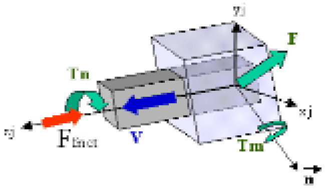

Figure 6.8 : Translational element mechanism details [23].

Joint reaction force (F), bending moment (Tm), torsional moment (Tn), and force preload (Fprfrc) are used to compute the frictional force in a translational joint. You can individually turn off the force effects using switches SW1 through SW4. The bending moment (Tm) is converted into an equivalent force using the Xs block.

Similarly, torsional moment is converted into an equivalent joint force using the friction arm (Rn). Frictional force (Ffrict) is applied along the axis of translation in the direction that the FRD block computes. For more information, see the Block Diagram of the Translational Joint.

6.1.3 Cam shaft

6.1.3.1 Mechanism of common-rail pumps

The plungers of the pump are arranged radially with an adjacent angle of 90° to each other and the plunger springs keep them in contact with the slider. InFigure 6.3, the plungers are actually the plunger-tappet sets (the tappets are combined with the plungers for simplicity). As in a typical piston-crank system, the motions of the three members in the mechanism are different: when the cam/crank rotates with the shaft, the plungers move reciprocatingly with respect to their cylinders, and, being a connecting rod, the motion of the slider is planar, which may be analyzed relatively easily by the motion of the flats of the slider. Take the top flat for analysis. The flat moves reciprocatingly with respect to the contact point of the plunger-end surface with a stroke same as that of the plunger. The plunger-end surface should be slightly spherical in order to avoid the over constraint to the plunger. Because the contact point moves with the plunger, the motion of the flat is a combination of two reciprocating motions orthogonal to each other – along and normal to the centerline of the plunger. In each cam revolution, the locus of the cam center determines the TDC and BDC of the plunger and the left and right limiting positions of the flat. In one half of the cam revolution, the flat moves from the left to the right and in the other half, from the right to the left. The association of the plunger with the cam center is similar to that of the flat with the cam center; [24].

6.1.4 Cam profile and shaft

Cam mechanism is important in the course of Precise transmit of diesel injection pump. In the diesel fuel injection pump, the high pressure oil is pressured through the cam lifting. The fuel oil pressure is directly proportional with the square of velocity of the cam. And the initiation time, pump supply pressure and fuel supply rate, and the maximum operating speed of the fuel oil is affected by cam mechanism. The kinematics and dynamics is stressed in the optimization design of cam mechanism of traditional fuel injection pump to attain compromise between the better fuel supply rate and the lower impact. A series of mature design methods haveformed through long time exploration and practice [25].

Cam profile is achieved from the lifting profile of the plunger. According to given reference at the beginning of cam mechanism kinematics, the plunger mechansism moves in paralell with cam profile eccentricity. Cam material is introduced to the program, all of the mass and other physical properties are matched with the real world measurements. Additionally, cam profile part and camshaft are seperated into two parts which will be very effective and simplified for the flexible modelling. Cam contact joints can not be easily modelled with the commercial programs. Also, our main target is to evaluate NVH characteristics that is the reason, flexible cam profile will not give us an advantage for the vibrational analysis. On the other hand, also cam profile part and cam shaft are fixed together to achieve a representative model as it can be figured out from the Figure 6.9 shown in below.

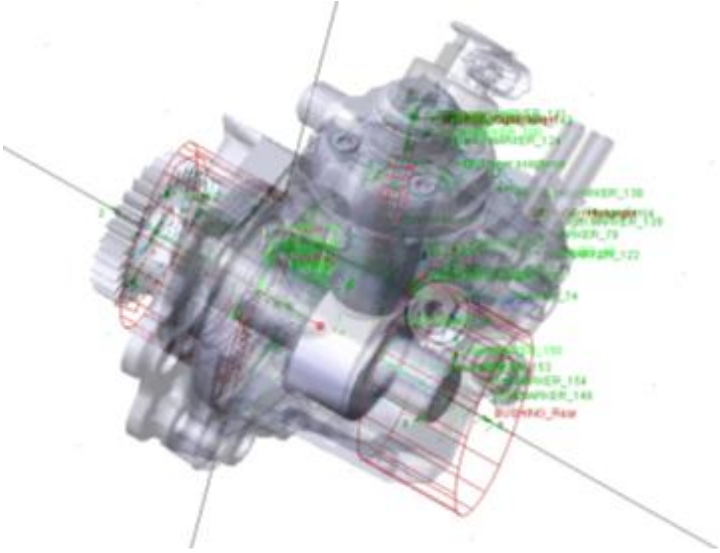

Figure 6.9 : Representation of cam contact with plunger roller.

Cam profile can be understood by the MSC Adams program, so it is sufficient to make a joint with cam contact to another component. With this joint mechanism, it gives an oppurtuntiy to define a stiffness coefficient between the two parts connected with cam contact surface together.

Cam contact profile creates or modifies a contact force between two geometries as shown in Figure 6.10. For solids and curves, you can select more than one geometry as long as the geometry belongs to the same part. The first geometry is called the I geometry and the second

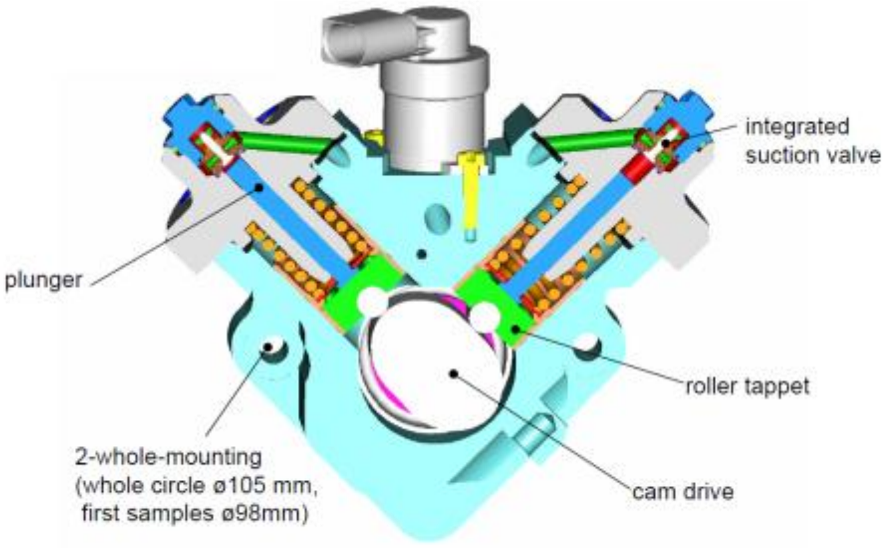

Figure 6.10 : High pressure fuel pump section showing sub-components.

geometry is called the J geometry. For sphere-to-sphere contacts, you can specify that the contact be inside or outside the sphere [23].

6.1.5 Bushings

The simulation of main bearing load plays an important role in engine multi-body dynamics simulation, seemingly influencing the simulation of strength, vibration and acoustics. It is necessary to conduct bench tests to validate the result of simulation [26]. Further attention has been paid to the flexibility of pump cover and cylinder head connections, but not on the installing conditions of engine test bench, such as the stiffness of mounts, the presence of the connecting flange and the elasticity of shaft and plunger mechanism. The target of this study here focuses on the influence of internal components conditions on the multi-body dynamics simulation of a high pressure pump considering again the internal hydraulic effects as mentioned at the beginning of this thesis report. With the comparison of the simulation results of different models,the effects of the connecting flange, the stiffness of internal components and the elasticity of cam shaft are discussed. Also their vibrational effect on pump nvh behavior is also evaluated.

At this point, bushings and cylindrical joints of the cam shaft should be carefully deifned. Stiffness coefficient are defined according to 1D model outputs which are

also corrected according to fuel specification (bulk modulus, temperature, viscost etc.)
The following constitutive equations define how Adams/View uses the data for a linear bushing to apply a force and a torque to the action body depending on the displacement and velocity of the I marker on the action body relative to the J marker on the reaction body [23].

Also, cylindirical Joint for the dynamic journal is defined between the high pressure pump and cam shaft as shown with Figure 6.11. The same fluid properties are carried over from the bushing properties as copied from 1D high pressure pump model.

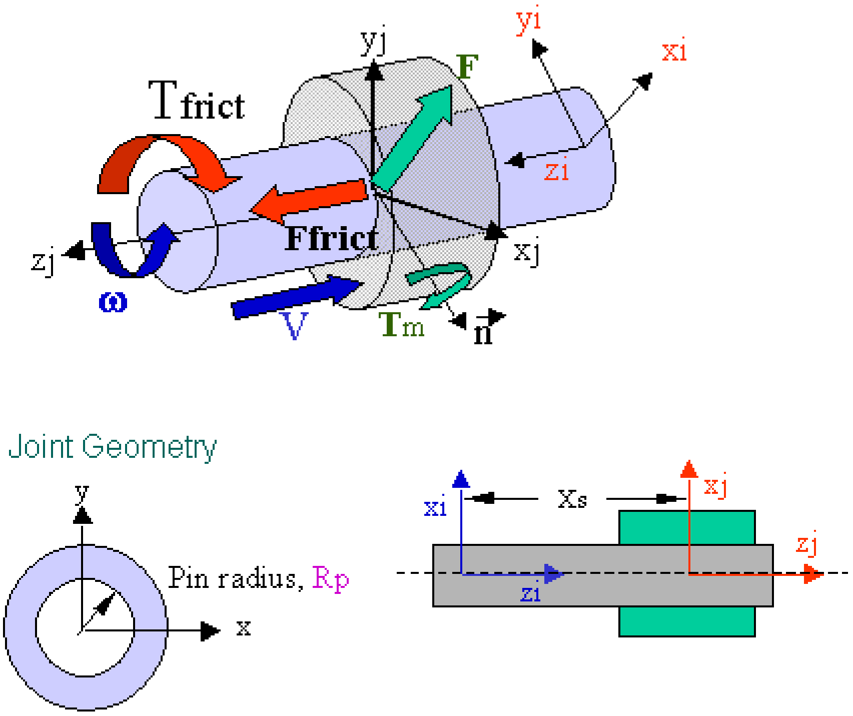

Figure 6.11 : Cylindirical joint details [23].

Joint reaction (F) and reaction torque (Tm) combined with force preload (Fprfrc) and torque preload (Tprfrc) yield the frictional force and torque in a cylindrical joint. As the block diagram indicates, you can turn off one or more of these force effects using switches SW1 through SW3. The frictional force in a cylindrical joint acts at the mating surfaces of the joint. The FRD block determines the direction of the frictional force. Based on the frictional coefficient direction, the surface frictional force is broken down into an equivalent frictional torque and frictional force acting along the common axis of translation and rotation. See the Block Diagram of the Cylindrical Joint [23].

Pump Cover is also fixed to adapter flange as mentioned at the beginning of the section. For the rigid model, this fix joint is sufficient for only kinematic and dynamic force results. For the vibrational results, it should be modelled with a flexible joint which is called RBE2. This element is used for simulation of bolt joints and limitation of degree of freedoms according to structure to structure joints. Further details are given in the flexible modelling section.

6.2 Model Excitation

Revolute joint is defined for the excitation of the cam shaft in order to have same profiles coming from 1D pump and valve train model. The torque profile is defined with respect to cam angular rotational profile. Is is very easy to change the excitation torque by importing the different torque profiles from 1D simulations to multi body dynamic pump model [23].

Total Torque Equations shown in (6.1) for a six-component general force and a three-component torque, the magnitude of the torque is the square root of the sum of the squares of the magnitudes of the three mutually orthogonal torque components, such that: [23]

$$\vec{T}_a = T\,X\hat{x}_{rm} + T\,\hat{Y}\,y_{rm} + T\,\hat{Z}\,z_{rm} \qquad \textbf{(6.1)}$$

Exactly the same kind of study is above is done for the point force on high pressure piston which is the subcomponent of plunger. There is a distributed load defined on pump piston surfaces which are in contact with pressurizing chamber. As similar to cam shaft, 1D high pressure pump model load profile is used for importing the load variability respect to cam angular rotational profile. By this way, whole of the variable load and torque profiles are defined with respect to roration angle of the cam shaft.

You can define force directions in one of two ways:

- Along one or more of the axes of a marker.
- Along the line-of-sight between two points.

If your force direction remains fixed with respect to some part in your model, either a moving part or the ground part, then you can define the force using one vector component and specify only one magnitude and direction.

If you have two or more forces whose directions always remain perpendicular to one another (such as a normal force and a friction force), you can either define multiple single-component forces whose directions are perpendicular or you can use a multiple-component force element. You must define several expressions, one for each of the force magnitudes you need [23].

3D pump model is also available to excite with different engine speed variants which is very important for the NVH behaviour as known. The same 1D model engine speed variants are used for the 3D model. However, it gives an oppurtuntiy to see different speed profiles NVH effect with the conribution of all load ans torqye variation defined according to rotational angle of the cam shaft.

6.3 Rigid Model Results

With respect to accepted engine speed and load profiles, all of the variable drive torque and load profiles are imported to the model. In this section, cam lifting profile, force distribution of cam shaft, rotational movement of cam shaft and spring behaviour under dynami conditions are reivewed. Also, all of these data can be compared with 1D model and also real world data.

As you can see from the Figure 6.12, the lifting profile is again between 0 mm and 6 mm. Also, there is another movement with Y-axis coming by the contribution of spring dynamics and inertia of the moveable parts defined with the model.

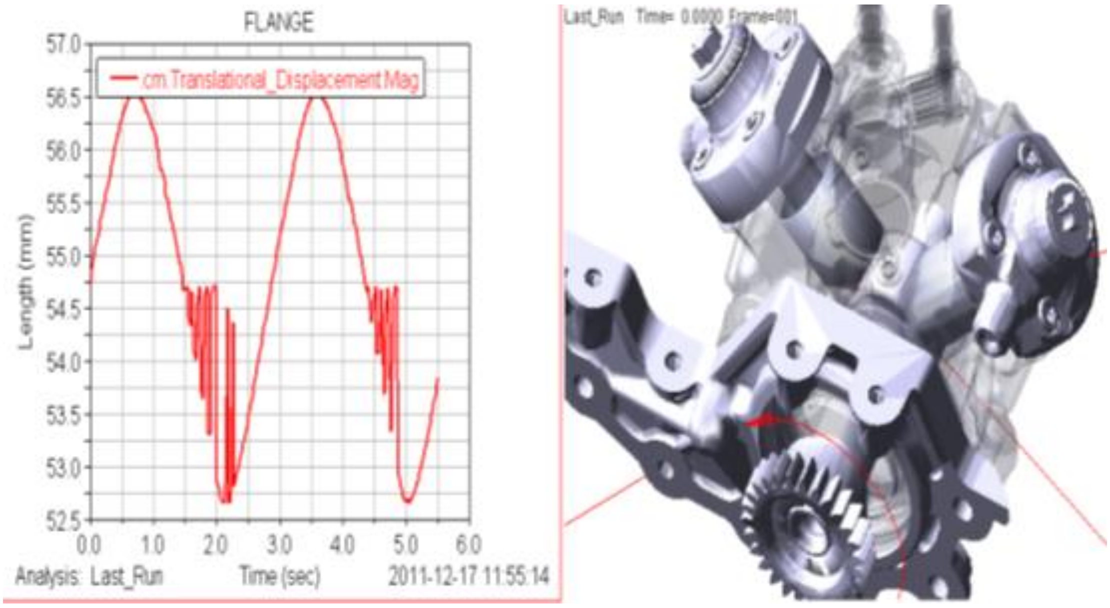

Figure 6.12 : Lifting profile with respect to cam profile.

This is also important to evaluate the design of the spring and effect of changing the mass of the plunger subcomponents. Here represented in the Figure 6.13, the force comparison of both left and right plungers are shown. In comparison to 1D model and real world measurements, it shows consistency with the references given in previous sections.

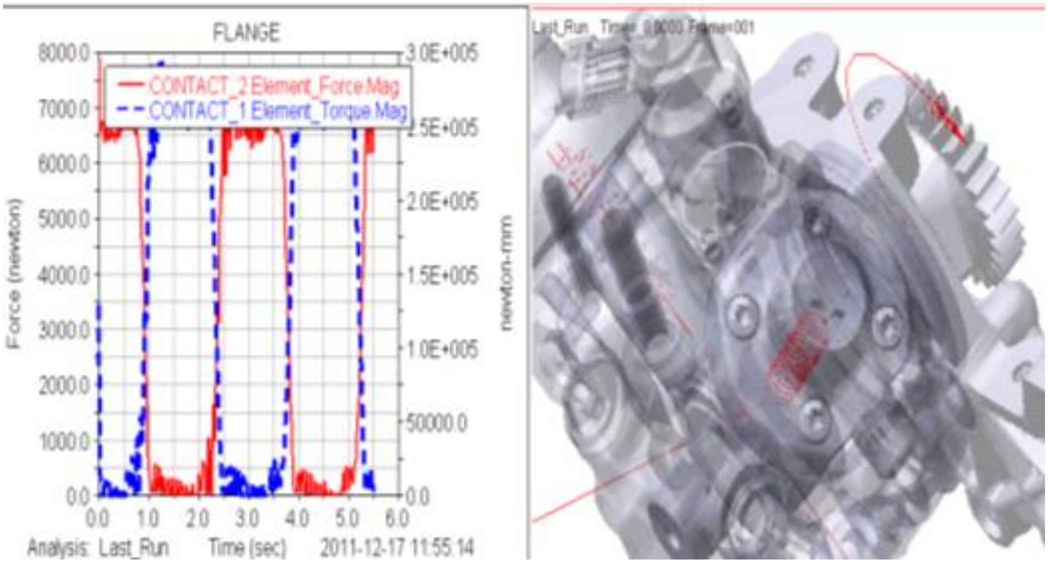

Figure 6.13 : Both of the plunger forces in one graph.

It gives an oppurtunity to investigate contact force and fuel speficiation effect on dynamic behaviour as it can be seen in Figure 6.14. By the reason of cam contact joint, hertzitian effect on cam contact surface is very important for wear robustness and long therm durability.

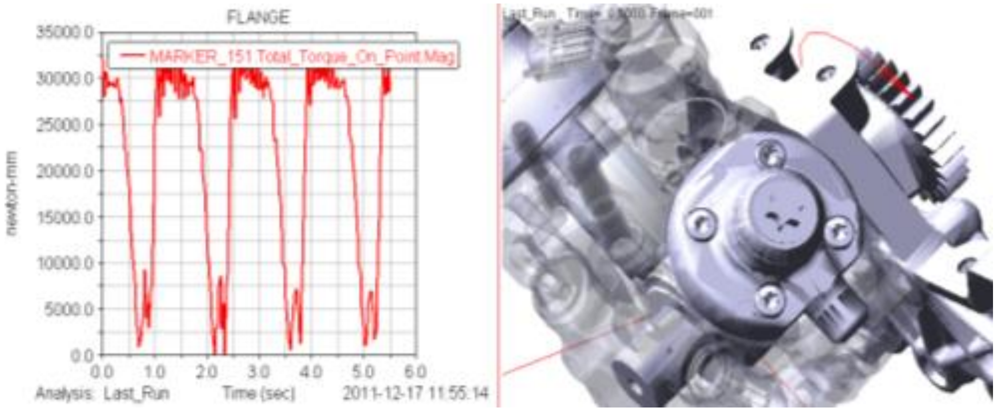

Figure 6.14 : Drive torque for the sufficient excitation of FIP.

In the Figure 6.15 shown in above shows the different parts kinematics. For the dynamic calculation of key parts.

MSC Adams program usage also gives an availability to check maximum speed and acceleration values.

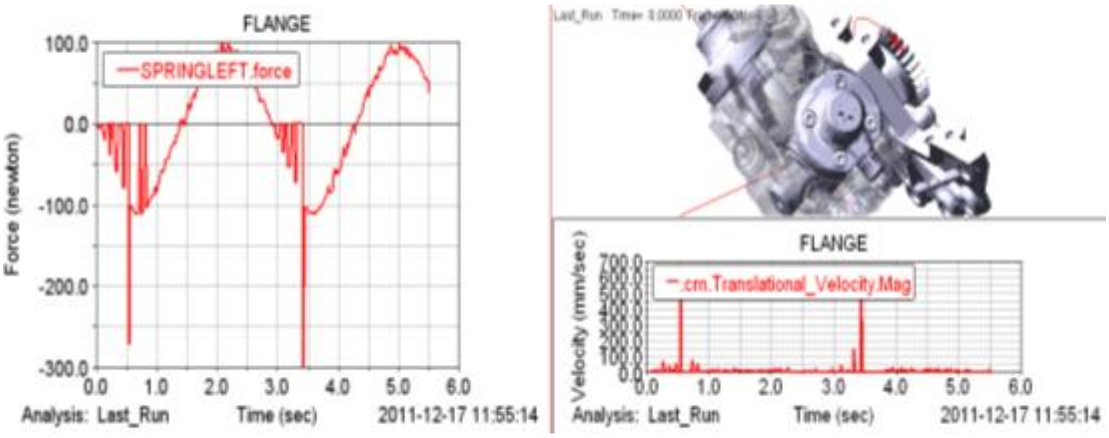

Figure 6.15 : Velocity and force on the plunger roller element.

7. NVH MEASUREMENTS ON ENGINE

Another important data which should be considered is to check the 3D multi body dynamic model with real world engine measurement. As shown in the figure, key locations on pump structure are fitted with accelerometers.Accelerometers were attached to requested components as shown in Figure 7.1 (engine orientations used throughout).

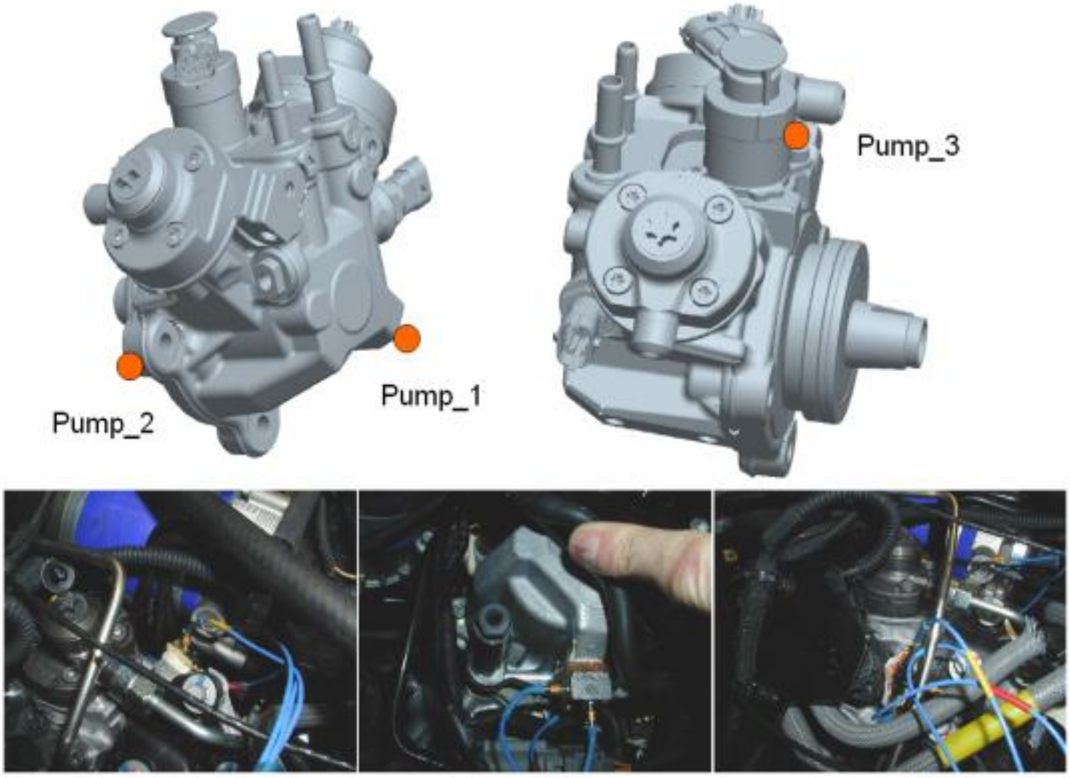

Figure 7.1 : Snapshots of accelerometers from real engine test.

Here are the each accelerometers results with respect to their original positions. Each of data is recorded between engine speed sweeps between 800 rpm and 4000 rpm. With the measurement results, each accelerometers response is carefully evaluated and is shared the critical resonance values.

Full-load sweeps were run taking data from 1000-400 rpm. The data was processed and shown in the form of peak hold, colour map and waterfall graphs. The full-load data was analysed noting all significant peaks with respect to frequency, amplitude, order and engine speed. A table of this data was compiled and can be viewed below with Figure 7.2:

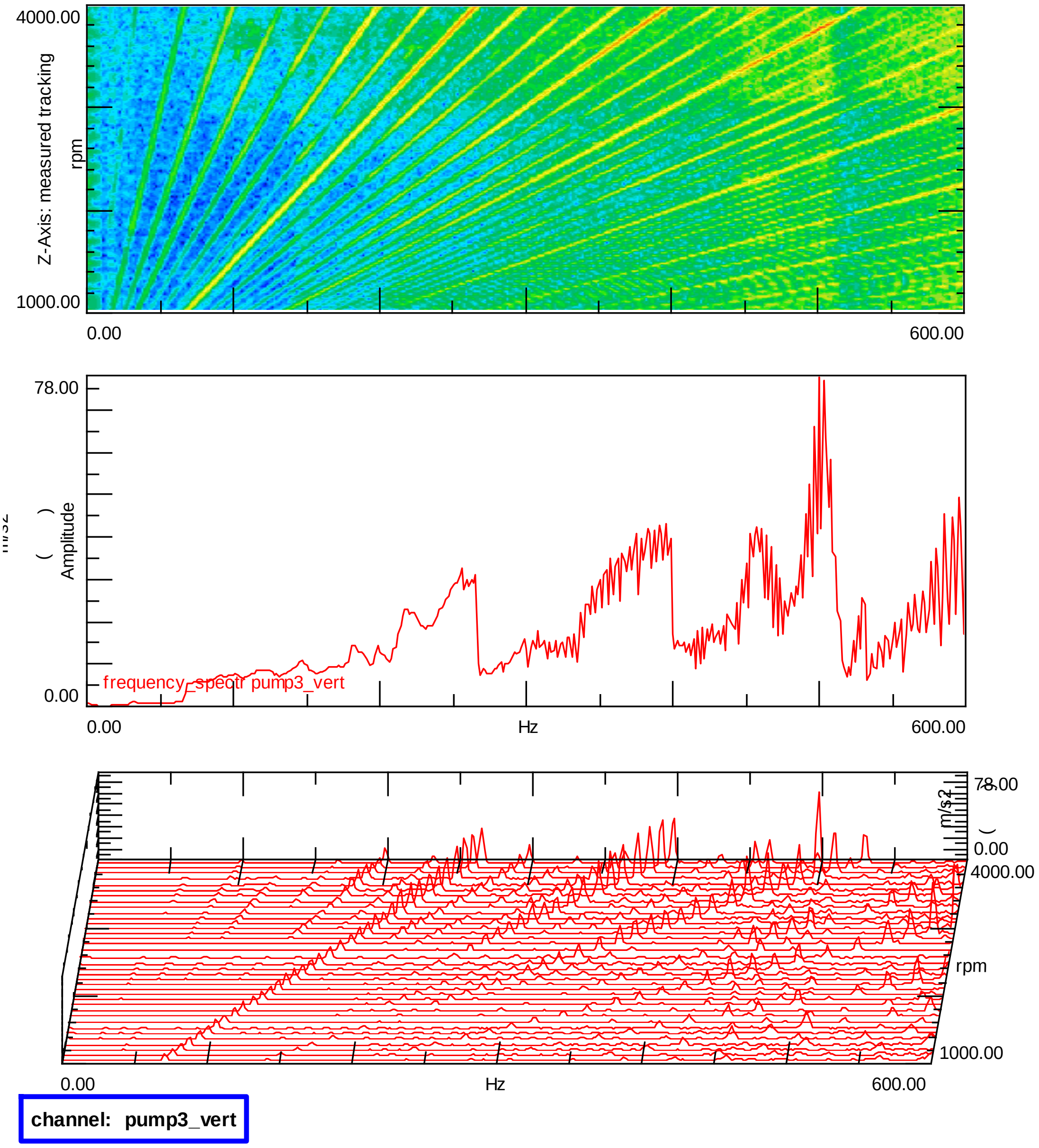

Figure 7.2 : Pump metering unit vertical direction vibration measurement.

In the figure above, the measurement is taken from the metering unit sensor from vertical direction with respect to engine orientation which is the middle of the pump body. Pump_3 location is the representation of the accelerometers position. Also, here are the resonnance profiles shown in below which is caught between 1000 rpm to 4000 rpm in different orders.

Table 7.1 : Vertical metering unit measurement results in table.

Position	Resonance		Order	Amp	Amp
	Hz	check		mm	m/s^2
Fuel_Pump_MROP_vert	200	2000	6	0.019	30.62
	253.1	3797	4	0.012	29.68
	287.5	4325	4	0.012	39.52
	437.5	4372	6	0.011	80.91
	553.1	4150	8	0.011	137.5
	600	4497	8	0.012	196.6

In the Figure 7.3, the measurement is taken from the metering unit sensor from longitudinal direction with respect to engine orientation which is the middle of the pump body.

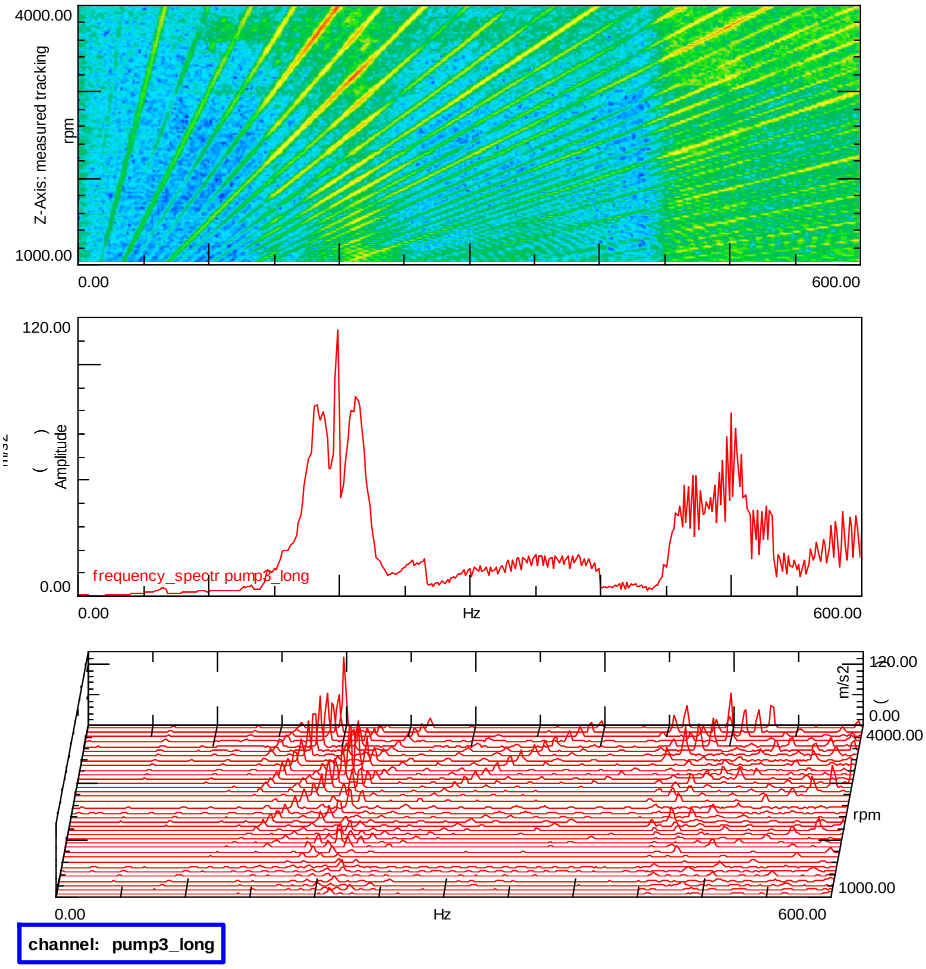

Figure 7.3 : Pump metering unit long. direction vibration measurement.

Pump_3 location is the representation of the accelerometers position. Also, here are the resonnance profiles shown in below which is caught between 1000 rpm to 4000 rpm in different orders.

Table 7.2 : Long. metering unit measurement results in table.

Position	Resonance		Order	Amp	Amp
	Hz	check		mm	m/s^2
Fuel_Pump_MROP_long	187.5	3751	3	0.164	227.2
	200	4000	3	0.144	227.9
	412.5	4123	6	0.011	73.81
	549.9	4099	8	0.008	93.83

In the figure above, the measurement is taken from the metering unit sensor from lateral direction with respect to engine orientation which is the middle of the pump body.

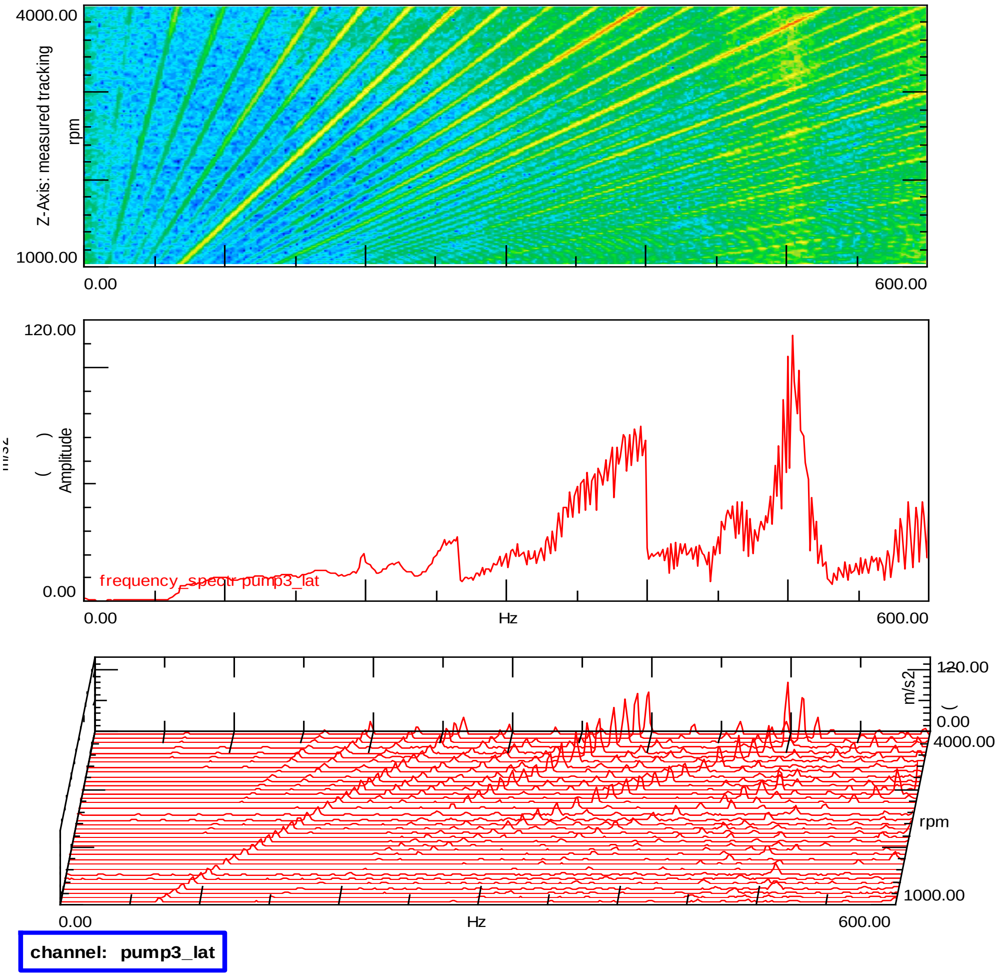

Figure 7.4 : Pump metering unit lateral direction vibration measurement.

Pump_3 location is the representation of the accelerometers position. Also, here are the resonnance profiles shown in below which is caught between 1000 rpm to 4000 rpm in different orders.

Table 7.3 : Lateral metering unit measurement results in table.

Position	Resonance		Order	Amp	Amp
	Hz	check		mm	m/s^2
Fuel_Pump_MROP_lat	203.1	4071	3	0.016	26.58
	256.2	4397	3.5	0.009	24.08
	362.5	3627	6	0.008	39.45
	425	4249	6	0.010	68.26

In the figure above, the measurement is taken from the metering unit sensor from lateral direction with respect to engine orientation which is the middle of the pump body as shown with Figure 7.5.

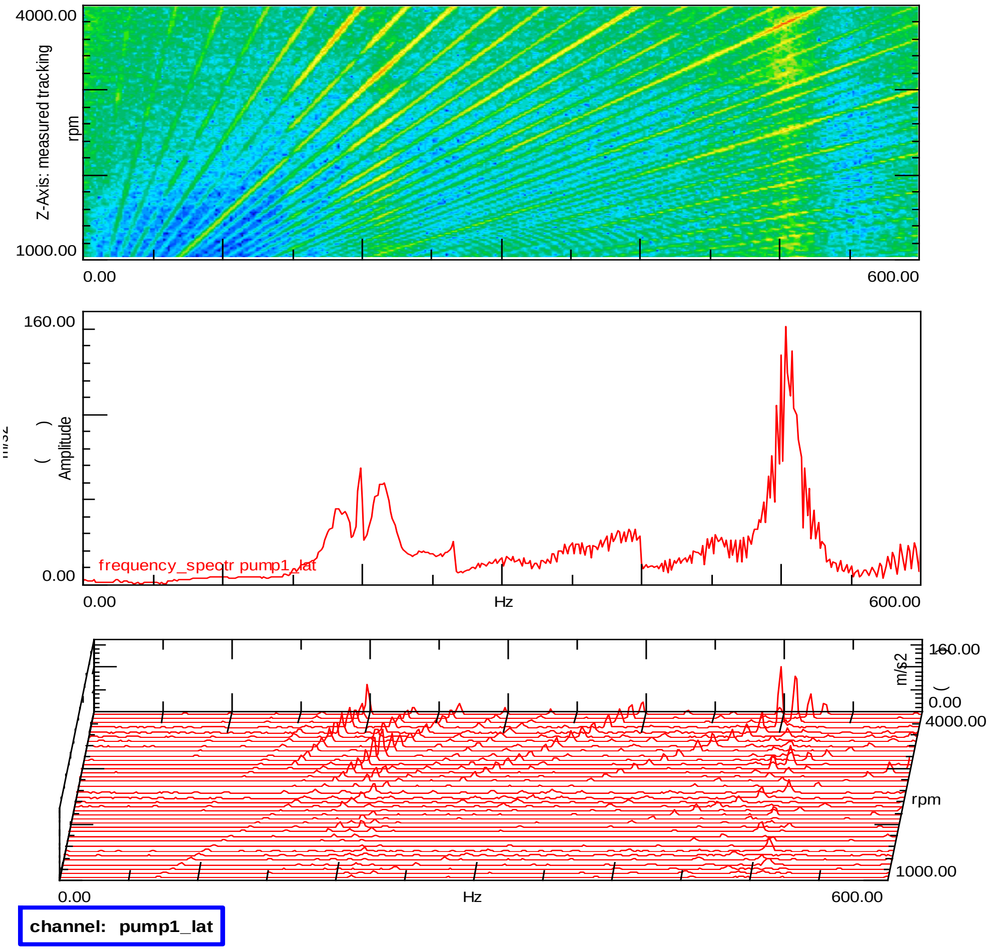

Figure 7.5 : Pump bottom- left lateral direction vibration measurement.

Pump_3 location is the representation of the accelerometers position. Also, here are the resonnance profiles shown in below which is caught between 1000 rpm to 4000 rpm in different orders.

Table 7.4 : Lateral pump bottom-left measurement results in table.

Position	Resonance		Order	Amp	Amp
	Hz	check		mm	m/s^2
Fuel_pump_bolt _lat	187.5	3751	3	0.117	161.9
	200	4000	3	0.100	158.2
	271.9	4071	4	0.022	65.4
	300	4497	4	0.018	63.08
	450	4497	6	0.035	283.2

In the Figure 7.6 in below, the measurement is taken from the bolt located sensor from vertical direction with respect to engine.

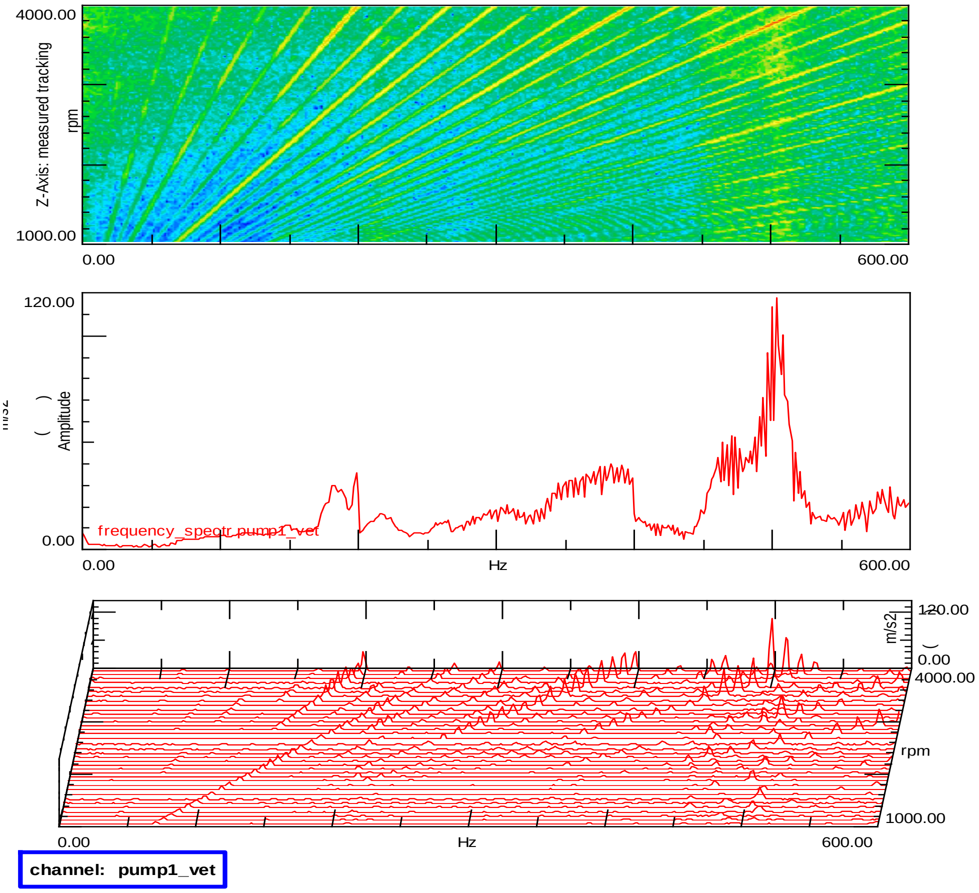

Figure 7.6 : Pump bottom- left vertical direction vibration measurement.

Pump_1 location is the representation of the accelerometers position. Also, here are the resonnance profiles shown in below which is caught between 1000 rpm to 4000 rpm in different orders.

Table 7.5 : Vertical pump bottom-left measurement results in table.

Position	Resonance		Order	Amp	Amp
	Hz	check		mm	m/s^2
Fuel_pump _bolt _vert	187.5	3751	3	0.034	47.3
	200	4000	3	0.029	46.21
	412.5	4123	6	0.014	93.99
	446.9	4473	6	0.030	236.7
	537.5	4024	8	0.008	92.84
	743.8	3674	12	0.024	531.3

In the Figure 7.7 below, the measurement is taken from the bolt located sensor from vertical direction with respect to engine orientation.

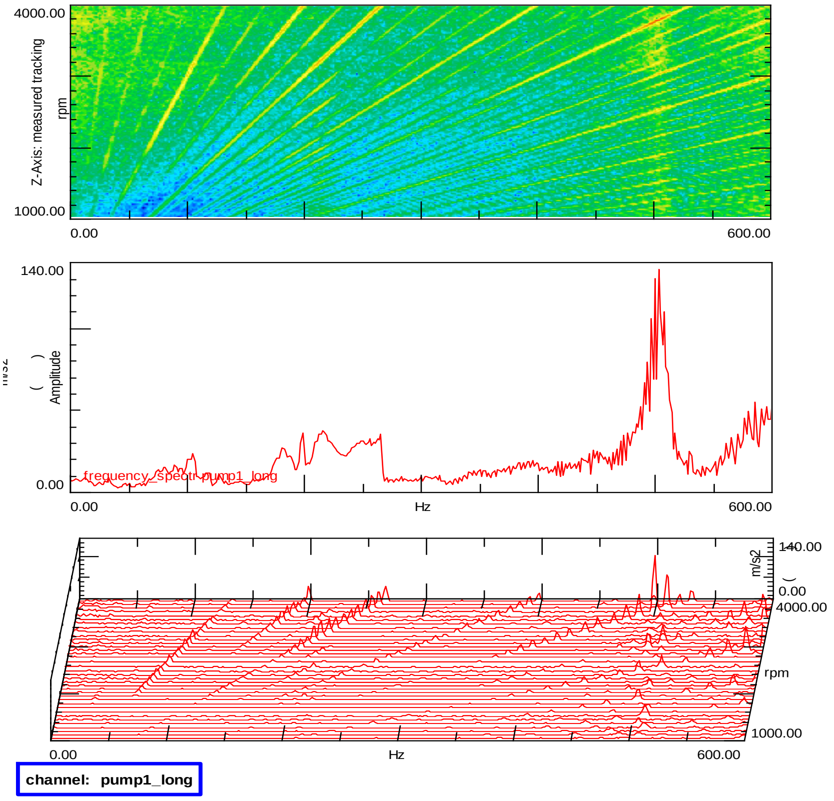

Figure 7.7 : Pump bottom- left Long. direction vibration measurement.

Pump_1 location is the representation of the accelerometers position. Also, here are the resonnance profiles shown in below which is caught between 1000 rpm to 4000 rpm in different orders.

Table 7.6 : Long pump bottom-left measurement results in table.

Position	Resonance		Order	Amp	Amp
	Hz	check		mm	m/s^2
Fuel_pump_bolt _long	203.1	4071	3	0.010	16.6

8. MODAL ANALYSIS AND NVH EVALUATION

As a third control data is typical modal analysis conducted with Altair Hyperworks commercial program, also it gives an oppurtunity to compare the typical modal analysis with dynamic multi body model analysis.

The details of the analysis are the mass details are defined according to real world data as done for dynamic analysis. Also, typical algorithms are used for modal analysis. In case of necessity, details of analysis can be shared. Here are the results of high pressure pump including the adapter plate component NVH evaluation.

First mode is detected with the 227Hz, also magnitude distribution is mostly intensified on the left plunger cap location which is up to 8,28 E-01 as shown with Figure 8.1. Effect on the adapter plate is not considerable.

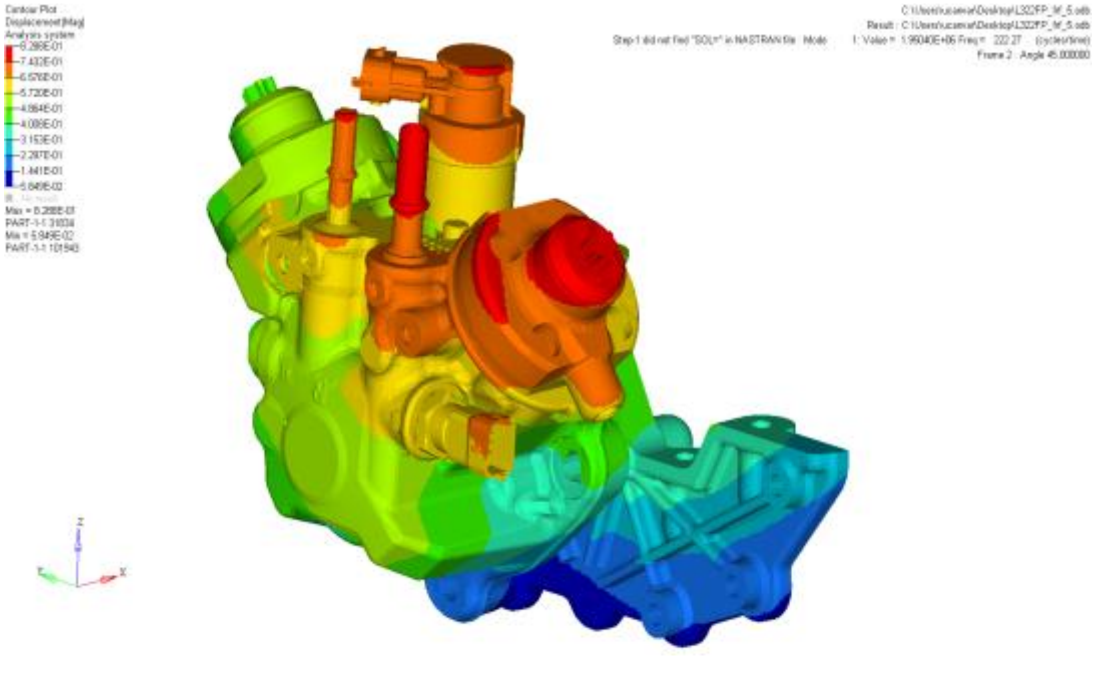
Contour Plot
Displacement(Mag)
Analysis system
8.288E-01
7.432E-01
6.576E-01
5.720E-01
4.864E-01
4.008E-01
3.153E-01
2.297E-01
1.441E-01
5.849E-02
Max = 8.288E-01
Min = 5.949E-02
Step-1 did not find "SOL=" in NASTRAN file : Mode
1 : Value = 1.99040E+06 Freq = 222.27 (cycles/time)
Frame 2 : Angle 45.000000
Z
Y
X

Figure 8.1 : 1^{st} mode modal analysis results.

Second mode is detected with the 466Hz, also magnitude distribution is mostly intensified on the right plunger cap location which is up to 3.92 E-01 as shown with Figure 8.2. Effect on the adapter plate is not considerable.

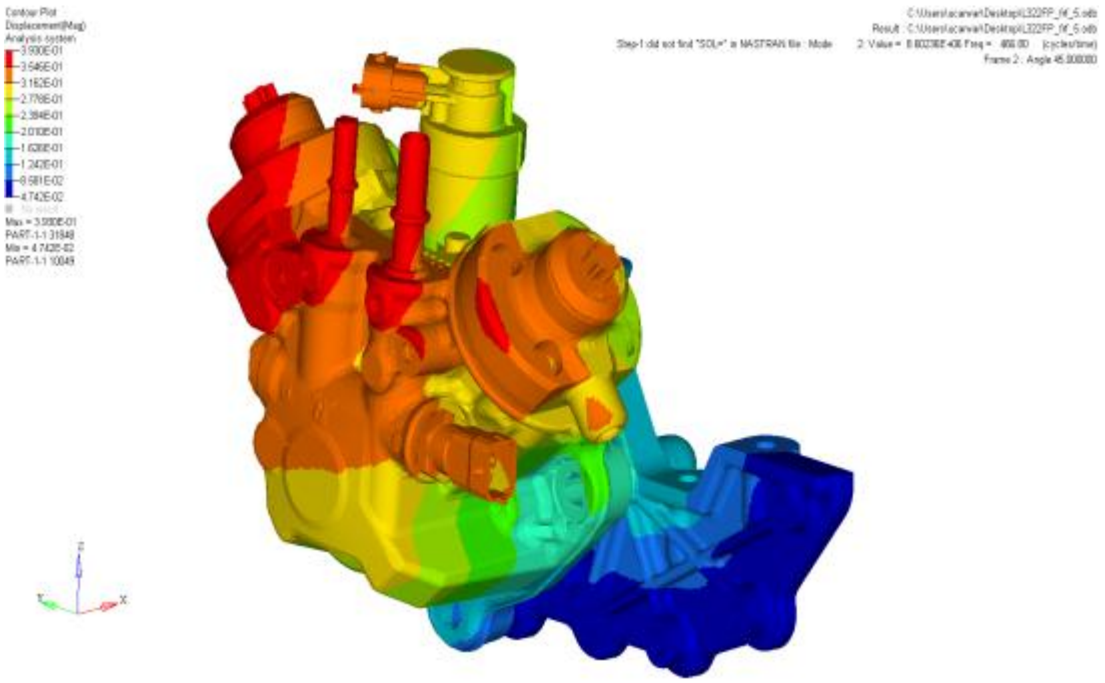

Figure 8.2 : 2nd mode modal analysis results.

Third mode is detected with the 516Hz, also magnitude distribution is mostly intensified on the left plunger cap location which is up to 1,60 E-01 as shown with the Figure 8.3. Effect on the adapter plate is not considerable.

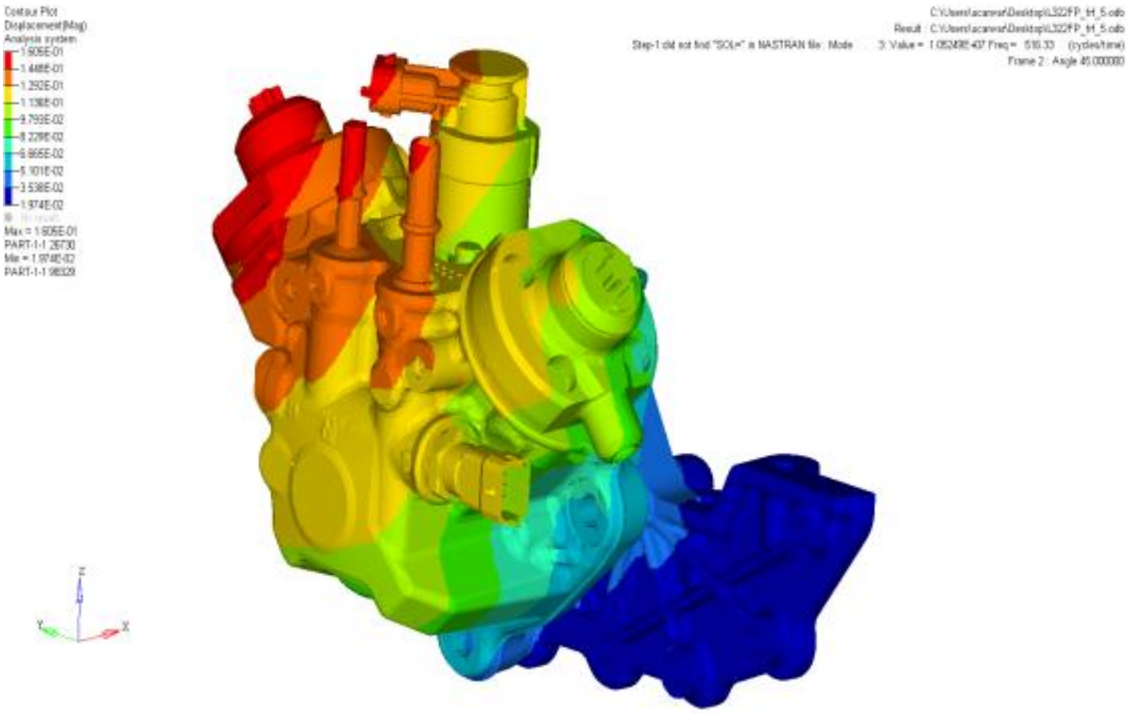

Figure 8.3 : 3rd mode modal analysis results.

Fourth mode is detected with the 571Hz, also magnitude distribution is mostly intensified on the Pump Cover bottom location which is up to 8,82 E-02 as shown with Figure 8.4. Effect on the adapter plate is not considerable.

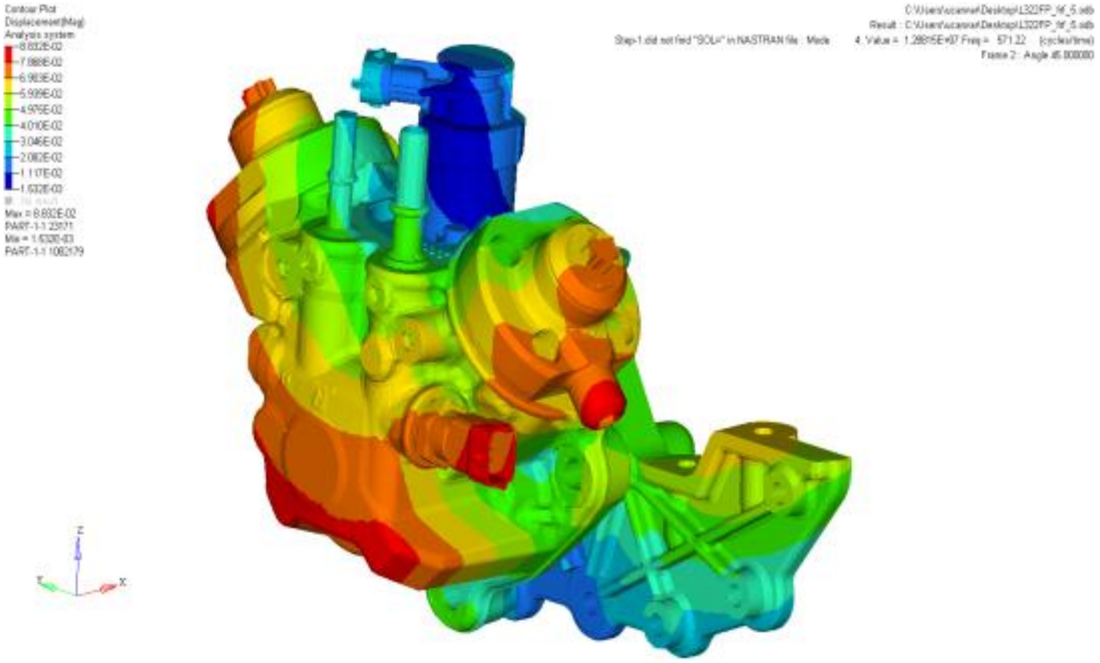
Contour Plot
Displacement(Mag)
Analysis system
8.832E-02
7.868E-02
6.903E-02
5.939E-02
4.975E-02
4.010E-02
3.046E-02
2.082E-02
1.117E-02
1.532E-03
Max = 8.832E-02
PART-1-1 23071
Min = 1.532E-03
PART-1-1 1082179
Step-1 did not find "SOL#" in NASTRAN file : Mode
4. Value = 1.28815E+07 Freq = 571.22 (cycles/time)
Frame 2 : Angle 45.000000
Z
Y
X

Figure 8.4 : 5th mode modal analysis results.

9. MULTI BODY DYNAMIC FLEXIBLE MODEL

In this section, preparation of flex model is explained. As you can figure out from the previous sections, a confirmed rigid pump model is validated and constructed. Now, the conversion from rigid model to flexible model is done by additional features as mentioned in the following sections. As shwon with Figure 9.1.

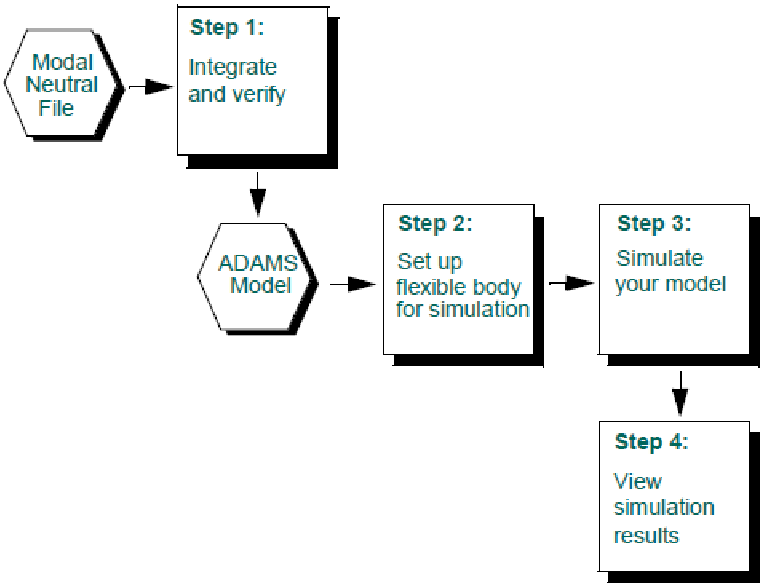
Modal Neutral File
Step 1:
Integrate and verify
ADAMS Model
Step 2:
Set up flexible body for simulation
Step 3:
Simulate your model
Step 4:
View simulation results

Figure 9.1 : Flexible modal analysis steps.

Building a flexible model needs the modal neutral file (MNF) defining the body and creates the necessary Adams/View geometry for displaying the flexible body. Generating a modal neutral file from a finite element model requires that you perform a special analysis on the model in the finite element analysis program and then translate the output of the analysis to an MNF. Generating an MNF is usually performed by a finite element analyst or an Adams user with experience running a finite element program. When you generate a modal neutral file, you must specify which units were used in the FEA program. This units information is stored in the MNF. An improperly constrained finite element model can seriously misrepresent the component. That is the reason, key components are carefully converted from rigid to flexible model as the process is explained with Figure 9.2 shown in below.

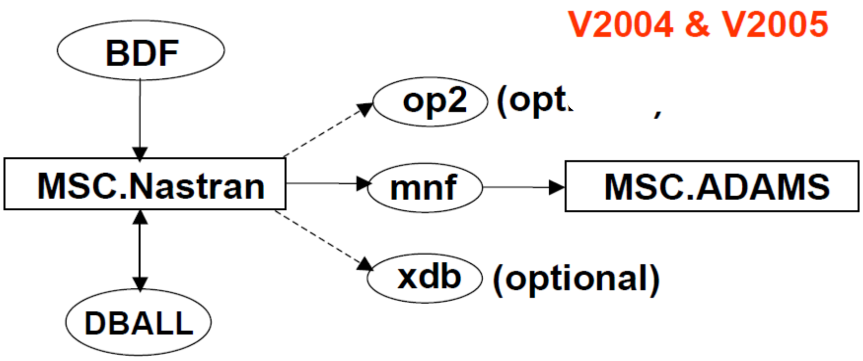

Figure 9.2 : Conversion method of modal neutral file.

You can categorize the modified Craig-Bampton component modes that Adams/Flex uses into two different types:

- Eigenvectors of the component
- Eigenvectors of the boundary (the attachment point DOFs)

These modes are obtained by orthogonalizing the Craig-Bampton modes. Any one of these modes can be enabled or disabled during the dynamic simulation. You should disable a mode if it does not contribute to the response of the flexible component during a simulation.

Preparation of MNF file is done with Msc.Nastran, as metioned in Figure 9.3 below; all of the interface modes, residual vectors, preloads and stress modes are integrated with flexible model.

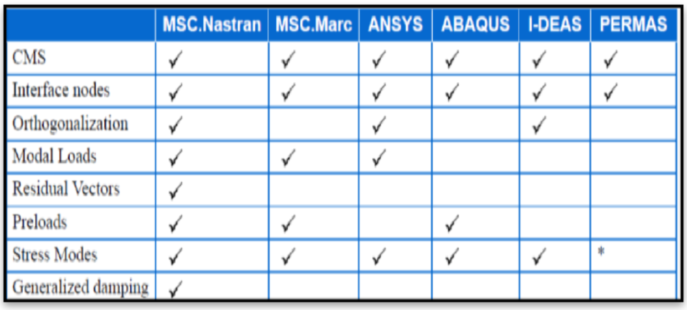

	MSC.Nastran	MSC.Marc	ANSYS	ABAQUS	I-DEAS	PERMAS
CMS	✓	✓	✓	✓	✓	✓
Interface nodes	✓	✓	✓	✓	✓	✓
Orthogonalization	✓		✓		✓	
Modal Loads	✓	✓	✓			
Residual Vectors	✓					
Preloads	✓	✓		✓		
Stress Modes	✓	✓	✓	✓	✓	*
Generalized damping	✓					

Figure 9.3 : Representation of different RBE2 conversion capabilites.

Consider, for example, a FE model in which two separate nodes are completely constrained. These two nodes never move relative to each other during the Adams simulation because none of the mode shapes feature any relative motion between the two nodes. Adams adds six nonlinear rigid body DOF to each flexible body and numerical singularities arise if the rigid body mode shapes are also included. Adams/Flex attempts to disable rigid body modes by default, but Adams/View can fail to detect some rigid body modes because rigid body modes sometimes have nonzero frequencies caused by numerical inaccuracies.

It is easy to replace a rigid body with a flexible body to more realistically model your mechanism. Because it is easy to replace rigid bodies with other flexible bodies, Exchanging a Rigid Body with a Flexible Body, to step through the process of replacing a rigid body with a flexible body. In addition to replacing a rigid body with a flexible body, you can replace an existing flexible body with a new flexible body. This may be useful if you want to modify the design of your flexible component.

For pump shaft, an instrumented hammer test is conducted for the determination of modal response. After several measurements with hammer shock testing, pump shaft’s modal response is interpreted. After construction of meshed pump shaft, critic regions are combined to each other with rigid body elements considering the method of spyder combination. With this DOF limitation, cam lobe, pump shaft endings journal connections are modelled as shown the details in Figure 9.4 below.

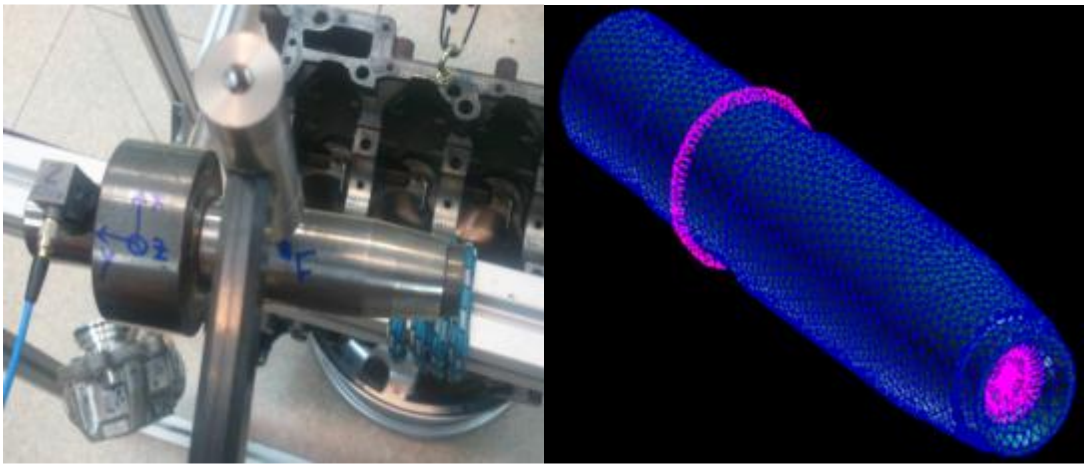

Figure 9.4 : RBE2 points located on pum shaft.

A similar approach is done for rest of the pump sub-components. An instrumented hammer test is conducted for the determination of modal response. After several measurements with hammer shock testing, pump cover modal response is interpreted. After construction of meshed pump cover, critic regions are combined to each other with rigid body elements considering the method of spyder combination. With this DOF limitation, plungers, pump shaft endings journal connections and adapter plate bolt connections are modelled. So, with these dof limited nodes, connections are done via these nodes modelled as shown the details in Figure 9.5 below.

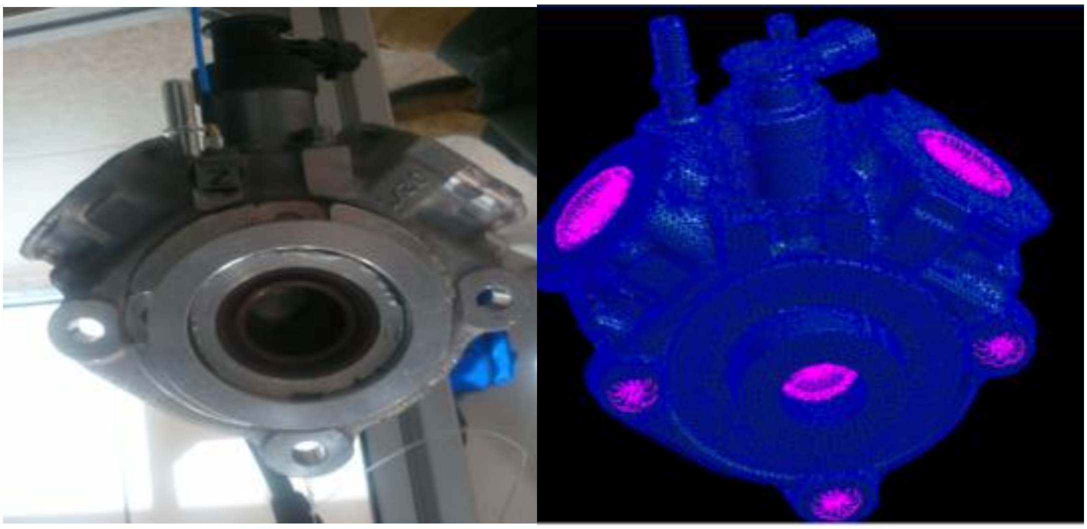

Figure 9.5 : RBE2 points located on pump cover.

Also, the modal configuration needs RBE2 generation which is a rigid connection typically attaching a single node to other multiple nodes. Depending on what DOFs you are transmitting (translations and/or rotations) you are slaving those nodes to the single master as shown with the Figure 9.6. If you consider just translations (to be simple) then the slave nodes will have the same displacements as the master. There will be no relative displacement between the slaves.

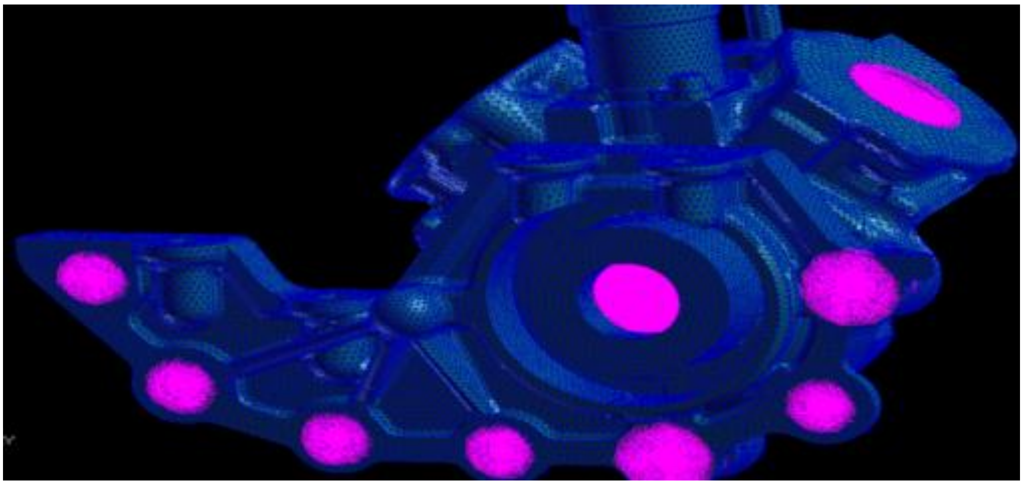

Figure 9.6 : RBE2 points located on system model.

After the construction of high pressure pump model, different modes are activated according to pump response model. Here you can see from the Figure 9.7 below, different modes are considered for each mode.

For the constructed model, similar controls are checked. Under dynamic conditions, pump front and rear journals force response are checked and confirmed.

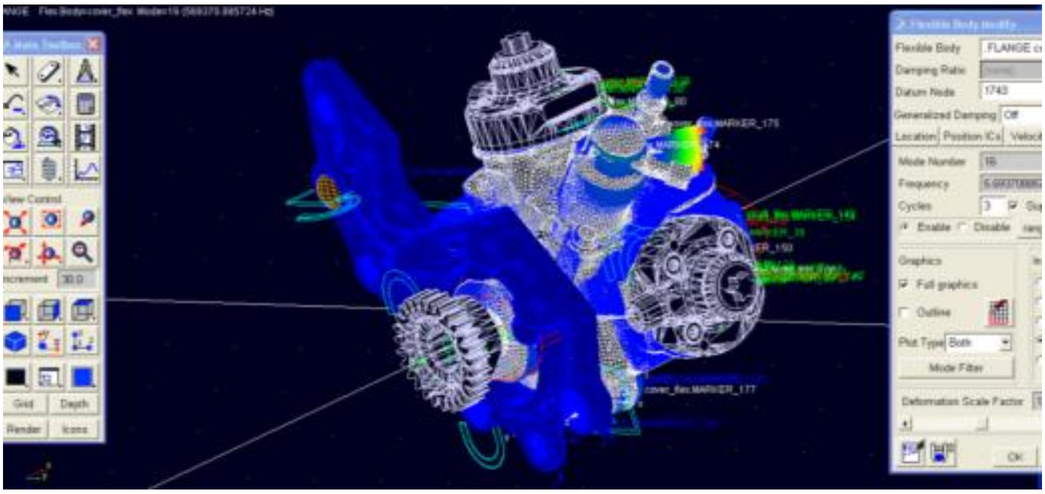
Flexible Body
FLANGE
Damping Ratio
Datum Node
1743
Generalized Damping
Off
Location
Position ICs
Mode Number
16
Frequency
Cycles
3
Enable
Disable
Graphics
Full graphics
Outline
Plot Type
Both
Mode Filter
Deformation Scale Factor
OK
Grid
Depth
Render
Icons
cover_flex.MARKER_177

Figure 9.7 : Different NVH modes including flexible bodies.

Also, plunger force and pump excitation torque including pump dynamic behaviour are checked and confirmed. After the clarification of flexible pump model, different markers are chosen according to real life measurement points. Those points are the locations where accelerometers are installed in Figure 9.8.

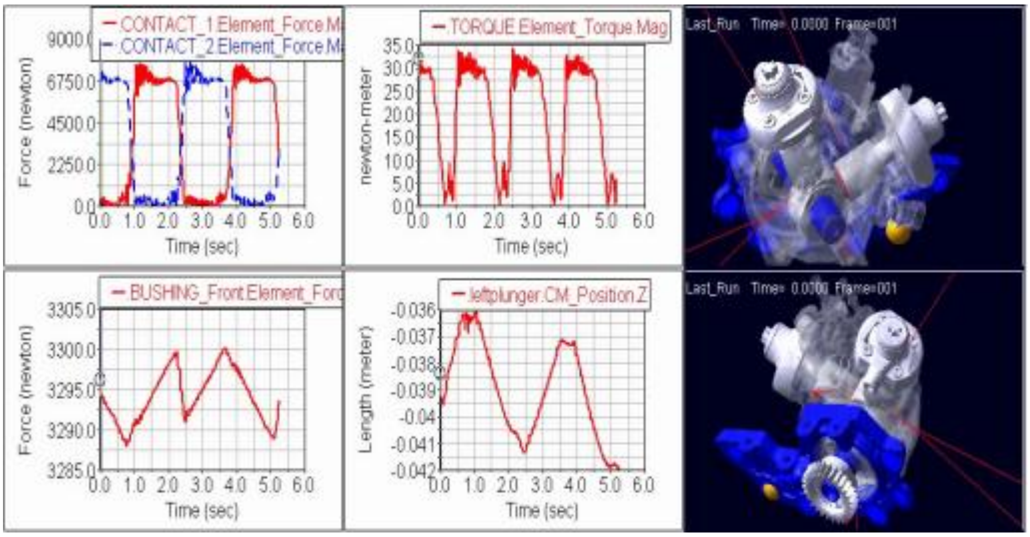

Figure 9.8 : Flexible model initial analysis results.

10. CONCLUSIONS AND RECOMMENDATIONS

With a confirmed flexible model, seevral dynamic measurements are done. Initial testing is almost identical to dyno measurements to have a back to back comparison. The dyno measuremets are done in the dyno measurements section.

Here in the figure below Figure 10.1, on the left hand side the pump model is identical to confirmed with the dyno results, on the right hand side, drive ratio which is the one of the optimization parameters.

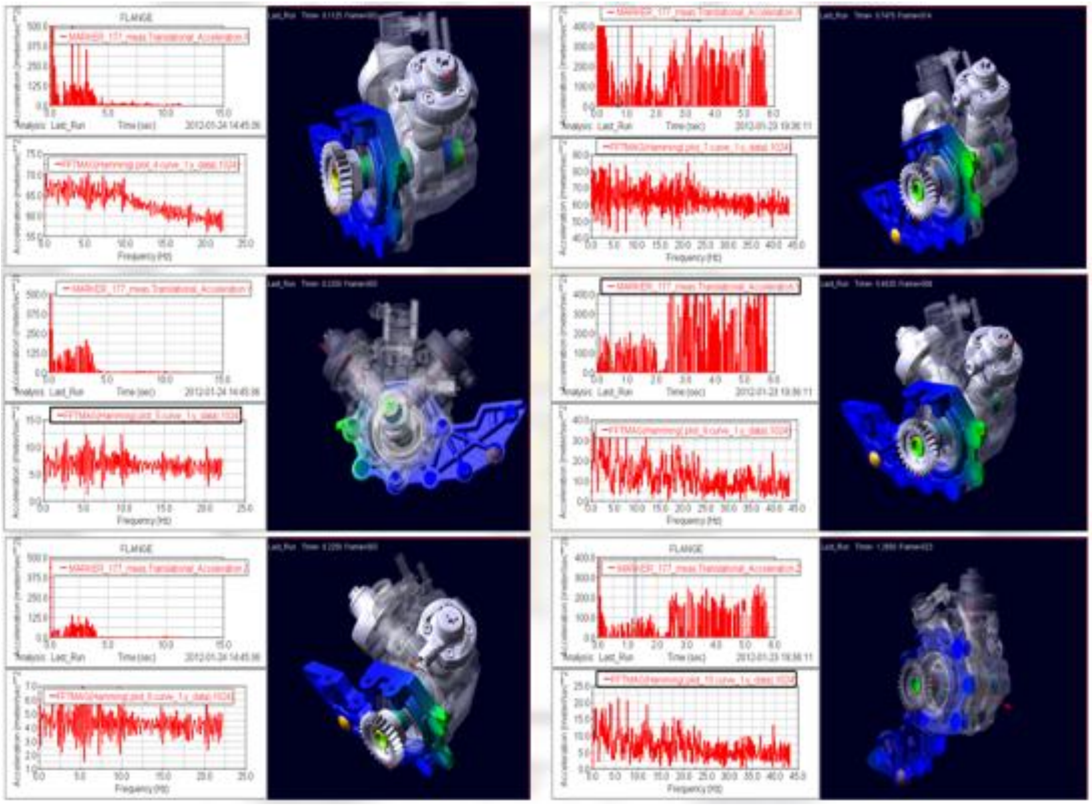

Figure 10.1 : Comparison of NVH response with different drive ratios.

As it is figured out from the analysis results, optimization of the drive ratio can highly result in different NVH responses.

As mentioned, the location of the reference point, the metering unit actuator. This is exaclty similar point of the real life instrumentation location.

As it is figured out from the analysis results in Figure 10.2 again the reference condition is metering unit and another optimization parameter is rail pressure and calibration of the engine. Changing the final rail pressure without any effect on the emissions and fuel consumption, it may highly effect on the NVH response of the model. As it can be figured out from the analysis results, for the critical operating modes, calibration may ba a very effective tool for NVH improvement.

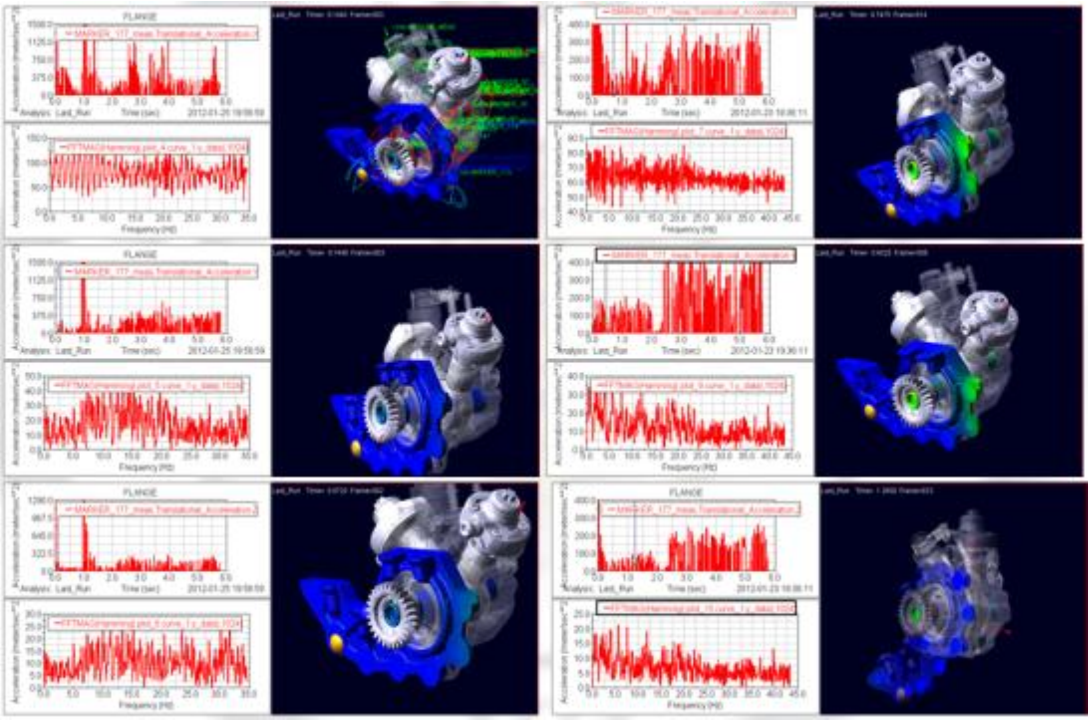

Figure 10.2 : Comparison of NVH response with different final rail pressure.

In this section, all of measurements and analysis are compared to eachother. So far, 1D model construction is explained and results are reviewed. They have already been confirmed with the real world measurements. Accordingly, rigid model is constructed with respect to confirmed results from 1D model. Its results are also reviewed and compared with the 1D model confirmed measurements in deed.

Valvetrain system is also constructed, as listed in below’s figure, all of the results with different gear orientations are reviewed. The details of different orientation of valve train measurements are listed in abbreviations section.

All of these sections shown in figure above is achieved. Vibration measurements are collected from the engine and all of the measurement details are stated in the study. The optimization parameters are also partly tested with the vibrational measurement and valve train confirmation testings details are shown in Figure 10.3.

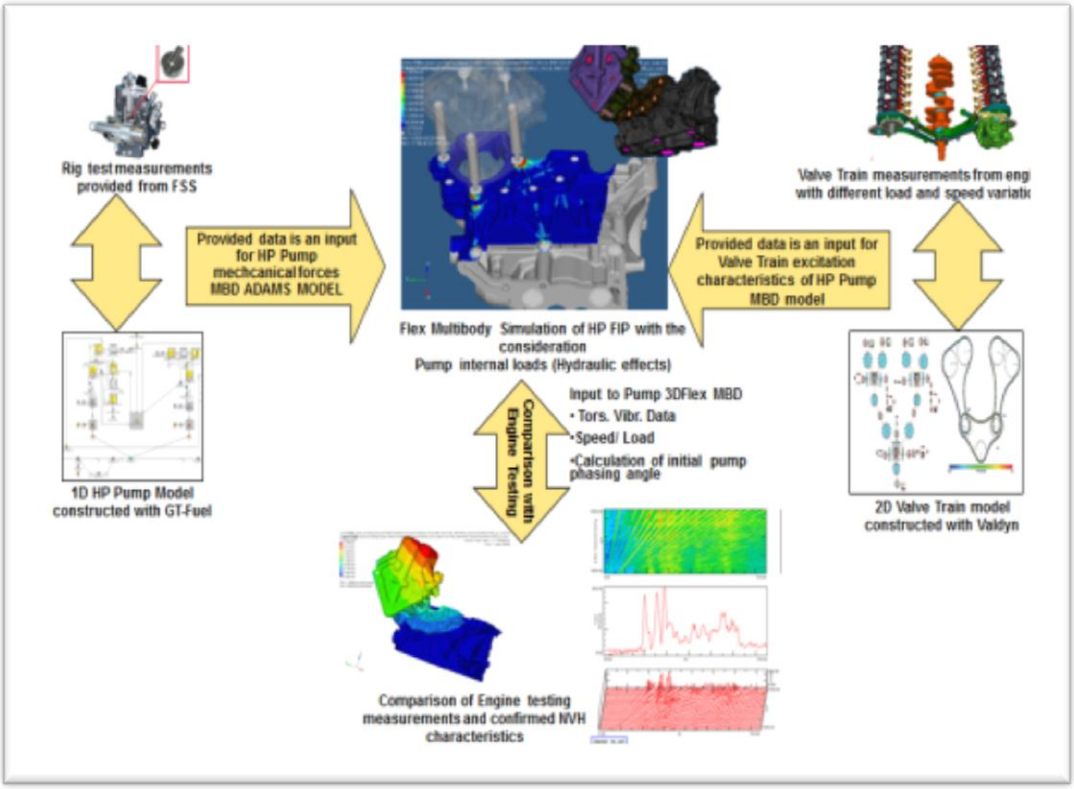
Rig test measurements provided from FSS
Provided data is an input for HP Pump mechcanical forces MBD ADAMS MODEL
Flex Multibody Simulation of HP FIP with the consideration
Pump internal loads (Hydraulic effects)
Provided data is an input for Valve Train excitation characteristics of HP Pump MBD model
Valve Train measurements from engi
with different load and speed variatic
1D HP Pump Model constructed with GT-Fuel
Comparison with Engine Testing
Input to Pump 3DFlex MBD
• Tors. Vibr. Data
•Speed/ Load
•Calculation of initial pump phasing angle
2D Valve Train model constructed with Valdyn
Comparison of Engine testing measurements and confirmed NVH characteristics

Figure 10.3 : Thesis methodology for each phase including analysis outline.

As it can be interpreted from 1D modelling section; even fuel type may have an effect on the behaviour of the high pressure pump. Also, flow rates, inlet pressure and outlet pressure according the metering unit may effect on NVH characteristics.

Another important thing is to have a usefull data from 1D modelling in every engine operating conditions are available to export some data for multi body dynamic alanyses. For instance, ValDyn tool can be integrated with a hdyraulic simulation program. This can also give an idea for preliminary assumption for a minor change possibility.

For the multi body dynamic model, the operating engine speed defined at the high pressure fuel pump and the resistance load defined at the output of high pressure plungers are considered to be the boundary conditions. Both of these mentioned two boundary conditions, especially the engine speed, are very important to the model to reproduce the excessive vibrational characteristics. It has to be emphasized that the engine speed must contain both the frequency and amplitude of the problematic load cases of the engine’s operating conditions which are also reviewed during Valdyn model. By simulating the results of the multi body dynamic model model, it enables possible cases to be analyzed with various kinds of the sub system dynamics such as angular acceleration and velocities of the different load conditions and thus final rail pressure profiles as well as the forces at both cam contact surfaces and high pressure plunger upper surface forces. This also can be seen by the effect coming from valve train. Excitation torque is changing according to required pressue which is recommeded to be found at rail volume.

Typical modal analysis is also performed to the model. It is possible to compare real world measurements and model analysis results.Even the results show partly consistency to eachother, dynamic flex body measurements are much more appreciated from the point of representative effect. With the introduction of flexible model, the items in below are the outcomes of this study;

- By this methodology, FIP NVH characteristics can be optimized with simulation programs and reduce the demand of engine testing necessity.
- If there is no max pump rpm issue and/or fuelling requirement issue with FIP from the point of FIS integrity, pump rpm may be reduced to lower speed profiles.
- Even fuel inlet temperature has minor effect on mechanical output of the FIP, all of the physical properties of working fluid may effect on vibrational response. This response can be tracked with the methodology studied in this thesis.
- MBD simulation programs may give better results from conventional modal analysis results with the consideration of internal reciprocating movement as similar to pumping elements etc.
- Calibration updates on FIP can be also tracked and evaluated by the hydraulic model studied in this thesis.
- Pump Priming is very critical from the point of Valve Train design and durability limits. Also, effect coming from Valve Train should be evaluated during the design and application of the FIP.
- Also, calibration of the sensors on hydraulic system can be another way of the optimization of NVH characteristics.

- Increasing the stroke of the plunger or changing the cam profile of the rotating cam shaft in the FIP may highly result in better NVH characteristics.
- By this methodology, the total cost and timing of the development phase can be reduced and also the flexibility of the factors effecting on NVH can be increased.

REFERENCES

[1]**Soons, Ilona, Prof. Dr. H.Nijrneijer**2004.31, Multibodymodelling of a gear train division DSD section dynamics and control,Technische Universiteit Eindhoven 2004 Thesis Release

[2]**Klarin, Borislav and Jelovic, Mario** 2010: Simulation Methodology for Consideration of Injection System on Engine Noise Contribution, *SAE 2010 release.*

[3**]Speckens, Friedrich-Wilhelm and Buck, Jürgen,**1999:Marked Progress in Both Technique and Handling of Valve Train and Valve Train Drive Calculation on Commercial Platforms, *SAE TECHNICAL PAPER SERIES 1999-01-0560.*

[4]**Challen, Bernard Baranescu, Rodica**1999: Diesel Engine Reference Book Second Edition *ISBN O 7506 2176 1 Library of Congress Cataloguing in Publication Data,* 1999.

[5]**Url-1** <*http://www.boschkraftfahrzeugtechnik.de/en/de/component/component_1_2112.html*>accessed at 20.09.2011.

[6]**Url-2** <*http://www.boschkraftfahrzeugtechnik.de/en/de/component/unitpupm*>accessed at 20.09.2011.

[7]**B. Mahr1 ,**2002: Future and Potential of Diesel Injection Systems, *Conference on Thermo- and Fluid-Dynamic Processes in Diesel Engines* 2002

[8]**O. Bunes, MSc and P.M. Einang, MSc**2009 Comparing the performance of the common rail fuel injection system with the traditional injection system using computer aided modelling and simulation, *International Conference on Marine Science and Technology for Environmental Sustainability,Newcastle, September 2000...*

[9]**Polat, Ö.,**2008: Investigation of Lubrication Effect on Diesel Engine Timing Chain Wear, M. Sc. Thesis, Istanbul Technical University.

[10]**SteinbeisTransferzentrum,** 2008:Electronic Diesel Control STZ Systemtechnik/ Automotive.

[11]**Uysal, U.,** 2010**:** Optimization Of Timing Drive System Design Parameters For Reduced Engıne Power Loss, M. Sc. Thesis, Istanbul Technical University.

[12]**Morse TEC,** 2008: Engine Chain Drive Technology Technical Presentation, Istanbul, Turkey.

[13] **Konyha, Z., Matkovic, K., Gracanin, D., Duras, M., Juric, J., Hauser, H.,** 2007: Interactive Visual Analysis of a Timing Chain Drive Using Segmented Curve View and other Coordinated Views,*IEEE Computer Society*.

[14] **Rodriguez, J., Keribar, R., Fialek, G.,** 2005: A Comprehensive Drive Chain Model Applicable to Valvetrain System, *SAE Technical Paper Series*, 2005-01-1650.

[15] **Valdyn,** 2009: User’s Manual Version 4.3.

[16] **Hiraku, K. Tokuo, K. and Yamada H.** 2005:Development of High Pressure Fuel Pump by using Hydraulic Simulator, *SAE TECHNICAL PAPER SERIES*, 2005

[17] **Gullaksen, J.** 2004: Simulation of Diesel Fuel Injection Dynamics Using MATLAB, *SAE TECHNICAL PAPER SERIES* 2004

[18] **Hydsim Users Guide,** 2009: AVL BOOST VERSION 2010.

[19]G**T-SUITE-Fuel Injection Tutorials and Notes.,** 2010: by Gamma Technologies *www.gtisoft.comSeries,* 2010-1650.

[20]**Idelchik,K -**1986 Handbook of Hydraulic Resistance, Second Edition, *Springer – Verlag, 1986]*

[21]**Wu Xinying, Ouyang Guangyao, Tan Di.,** 2011: The Wear Analysis for Cam Mechanism of Diesel Fuel Injection Pump Based on Multibody Dynamics Theories, *International Conference on Electronic &Mechanical Engineering and Information Technology* 2011

[22]**Ortiz L., Heiserer D.** 2010: Issues Exporting a Multibody Dynamics SystemModel into a Finite Element Analysis Model, *International Conference 2010 SAE International*

[23]**ADAMS/VIEW Notes .,** 2010: Adams Release Notes and Help/Support Book

[24]**Teng, Ho., C. McCandless.** 2005: Performance Analysis of Rail-Pressure Supply Pumps of Common-Rail Fuel Systems for Diesel Engines, *International Conference 2005 SAE International*

[25]**Tan di,Ouyang Guang-yao,WU Xin-ying** 2008: Analysis and Experimental Research on the Abrasion of the Cam Follower of the Electrically Controlled High Pressure Pump *, vehıcle engıne.2008* Chinese Vehcile Technology

[26] **Shu Gequn, Min, L..,** 2009: Research on the Influence of Bench Installation Conditions on Simulation of Engine Main Bearing Load, *International Conference2009 SAE International*

APPENDICES

APPENDIX A.1 : Valve Train Engine Testing Measurements at different loads and ratios

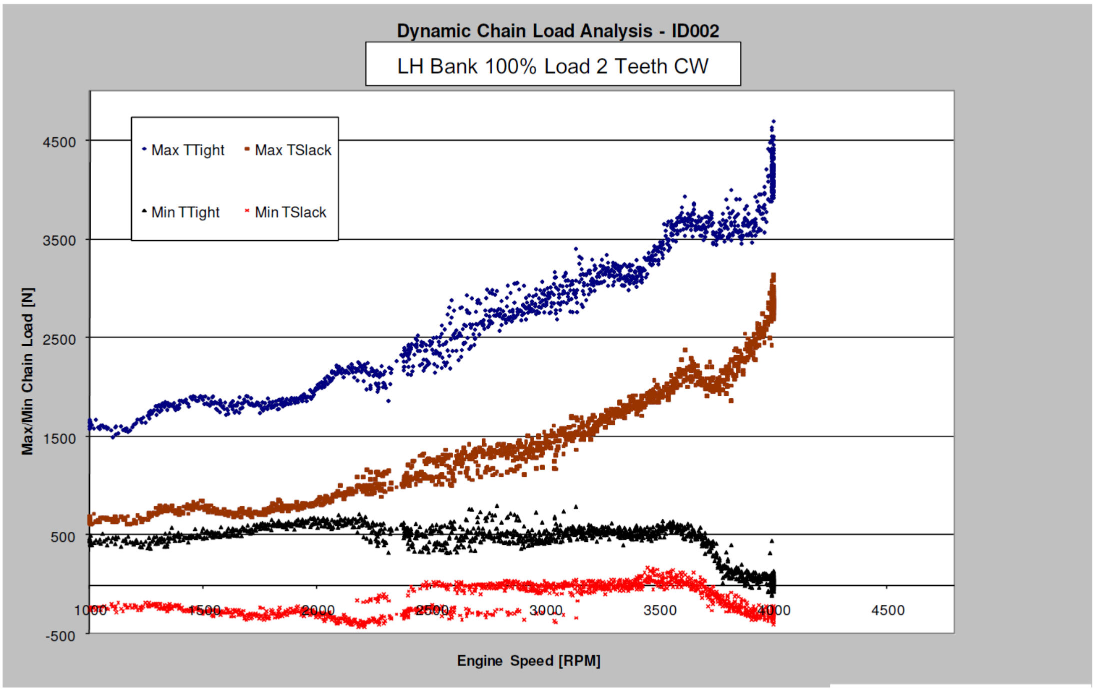

Figure A.1 : 2 Teeth CW valve train measurement.

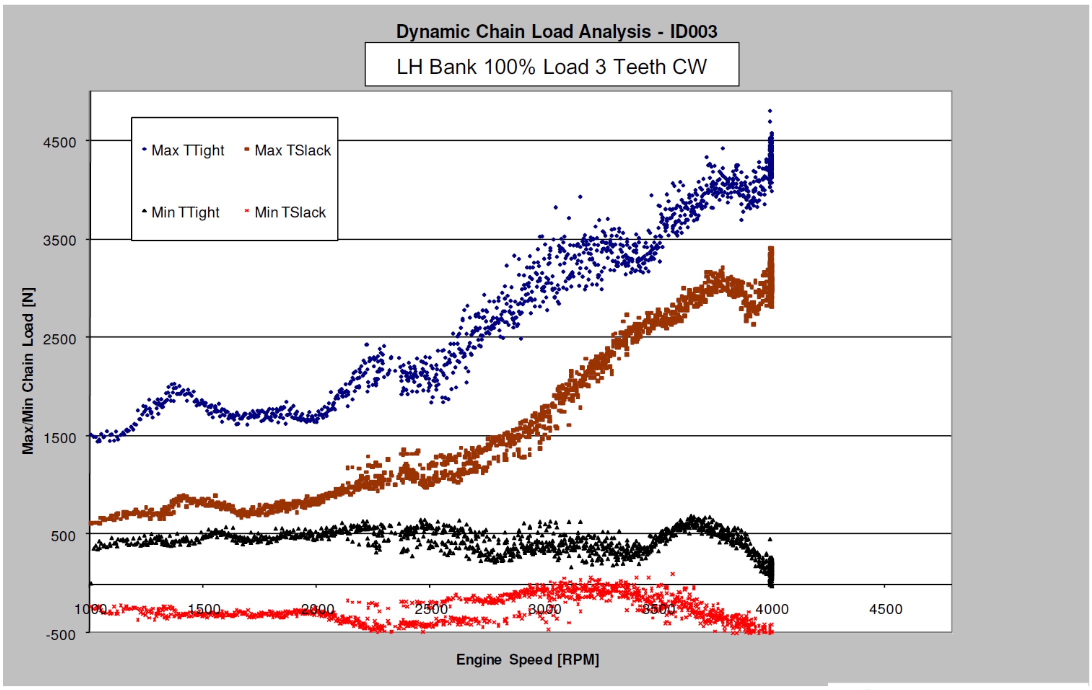

Figure A.2 : 3 Teeth CW valve train measurement.

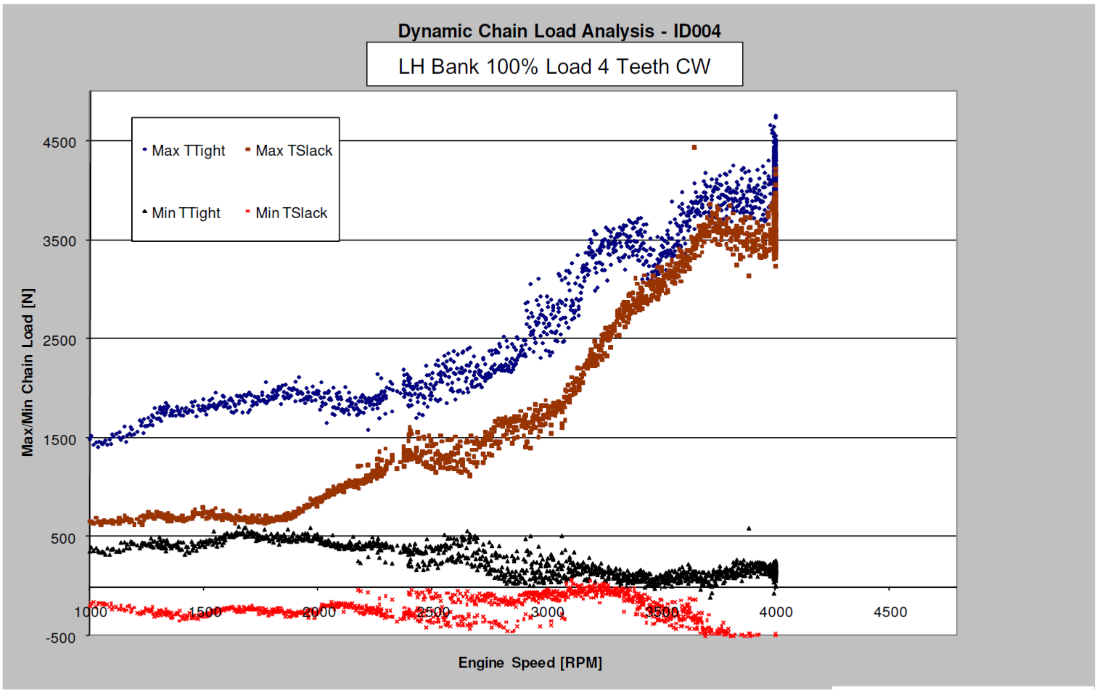

Figure A.3 : 4 Teeth CW valve train measurement.

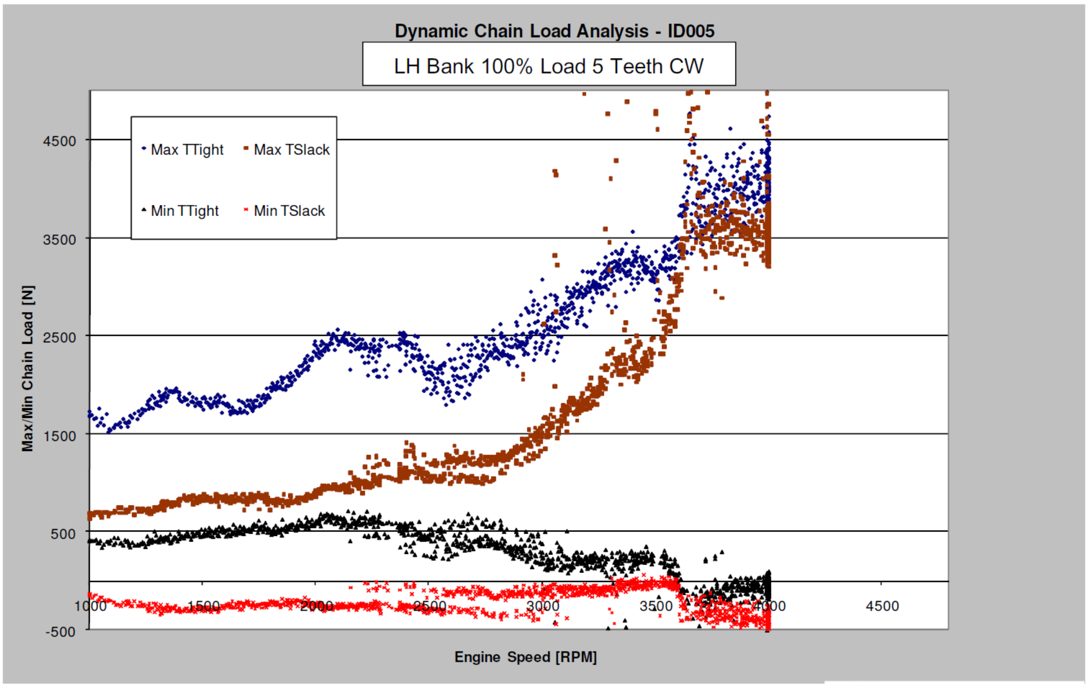

Figure A.4 : 5 Teeth CW valve train measurement.

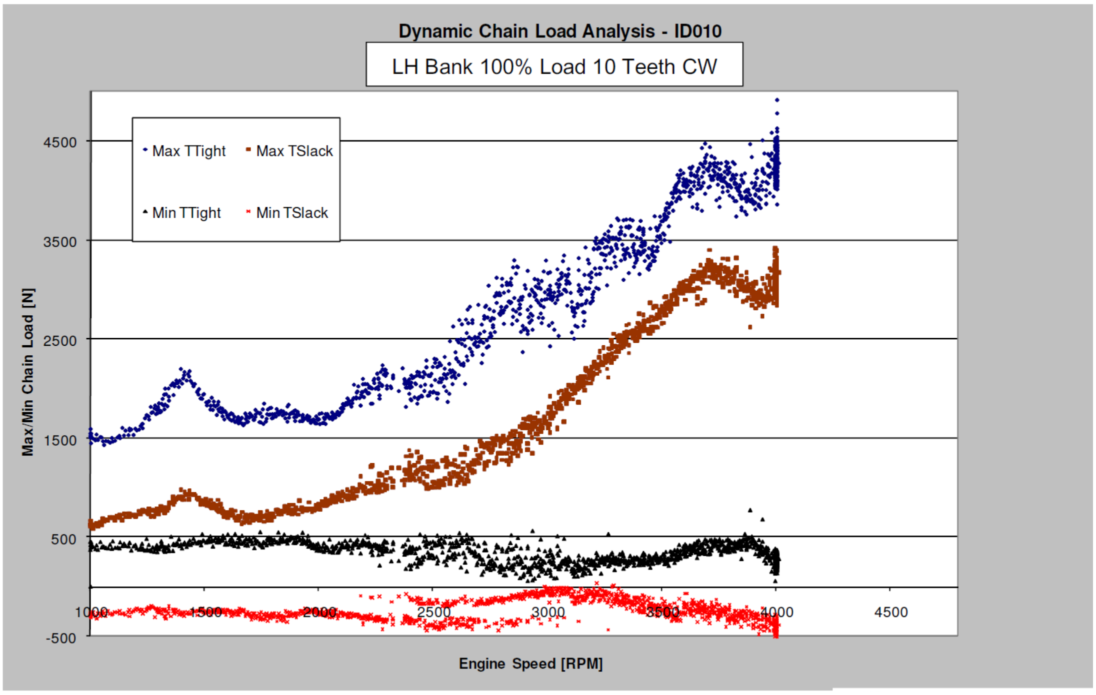

Figure A.5 : 5 Teeth CW valve train measurement.

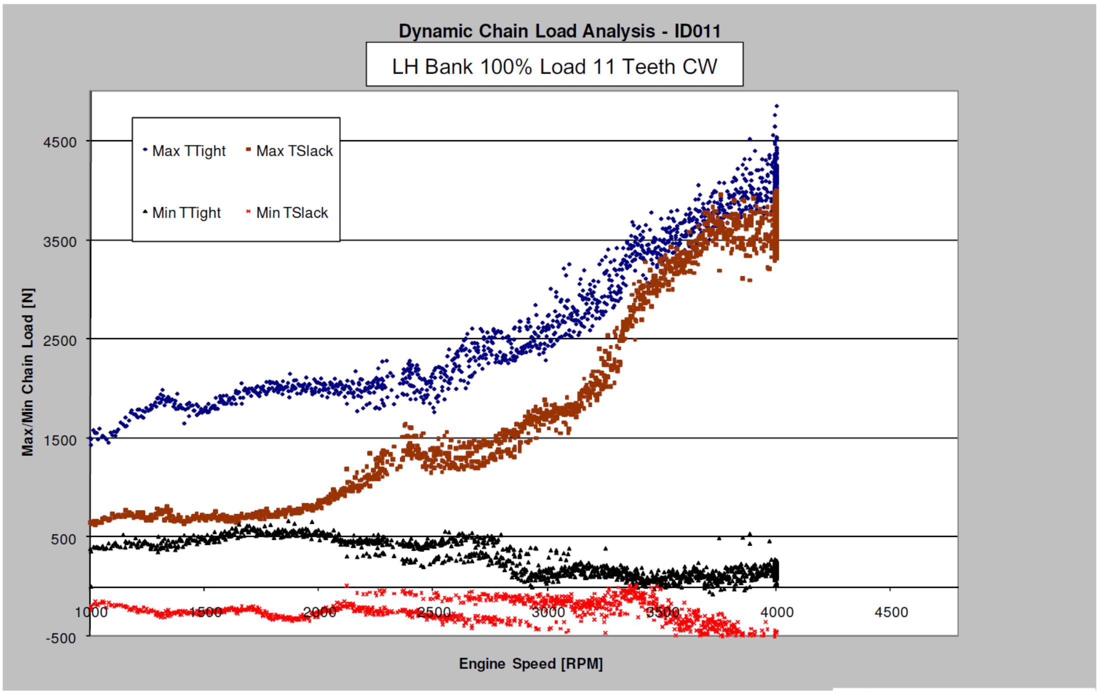

Figure A.6 : 11 Teeth CW valve train measurement.

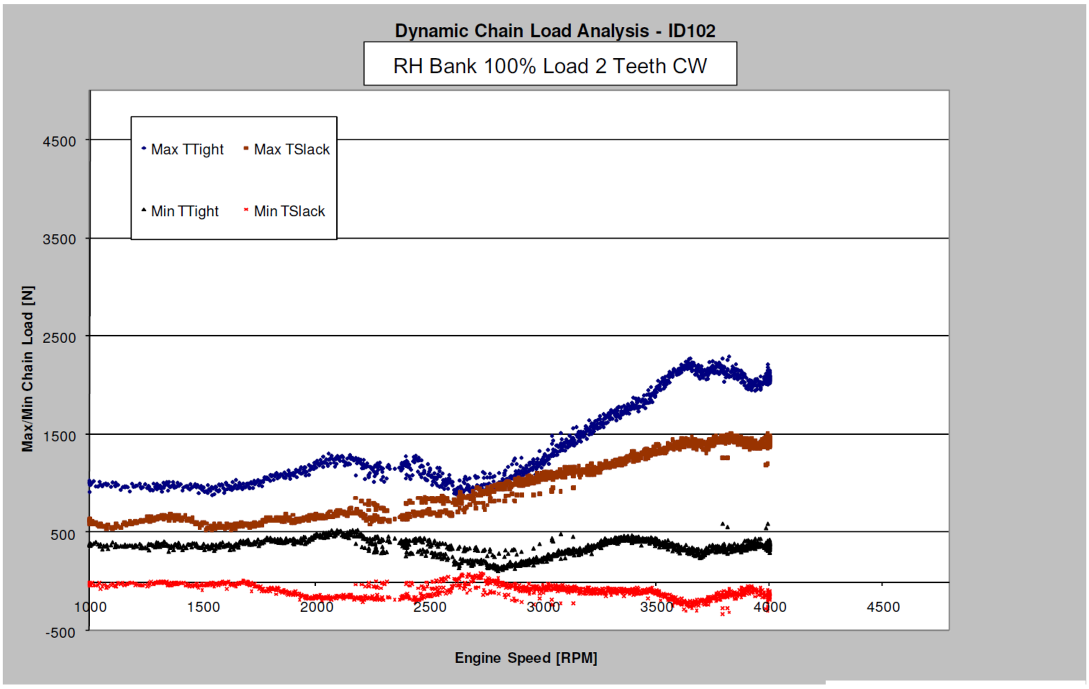

Figure A.7 : 2 Teeth CW valve train measurement.

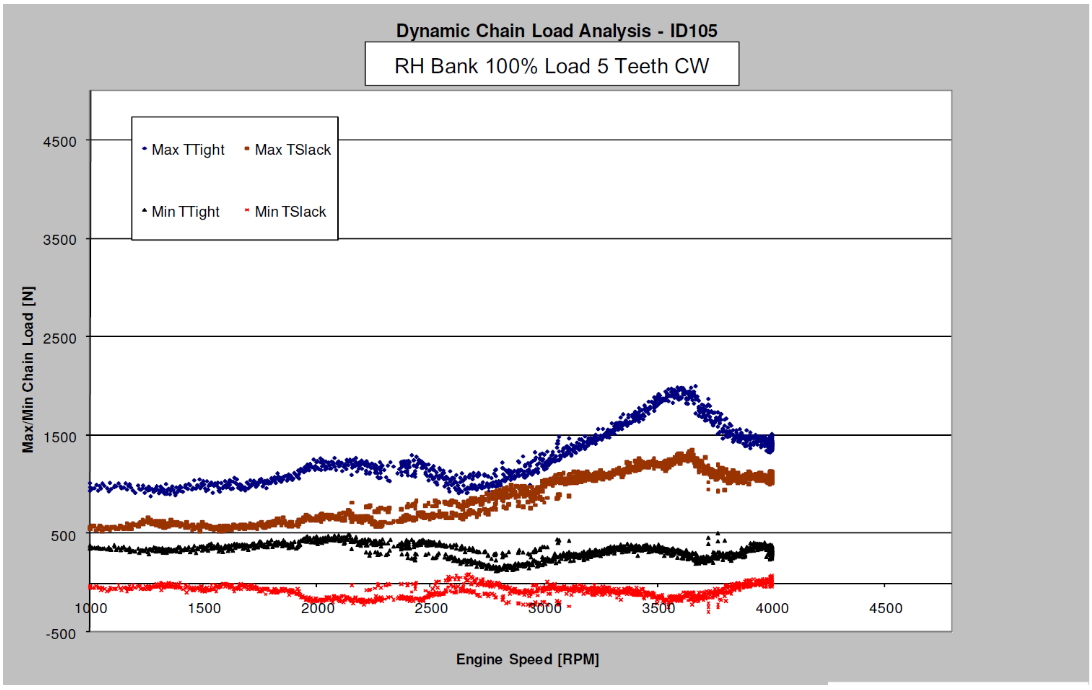

Figure A.8 : 5 Teeth CW valve train measurement.

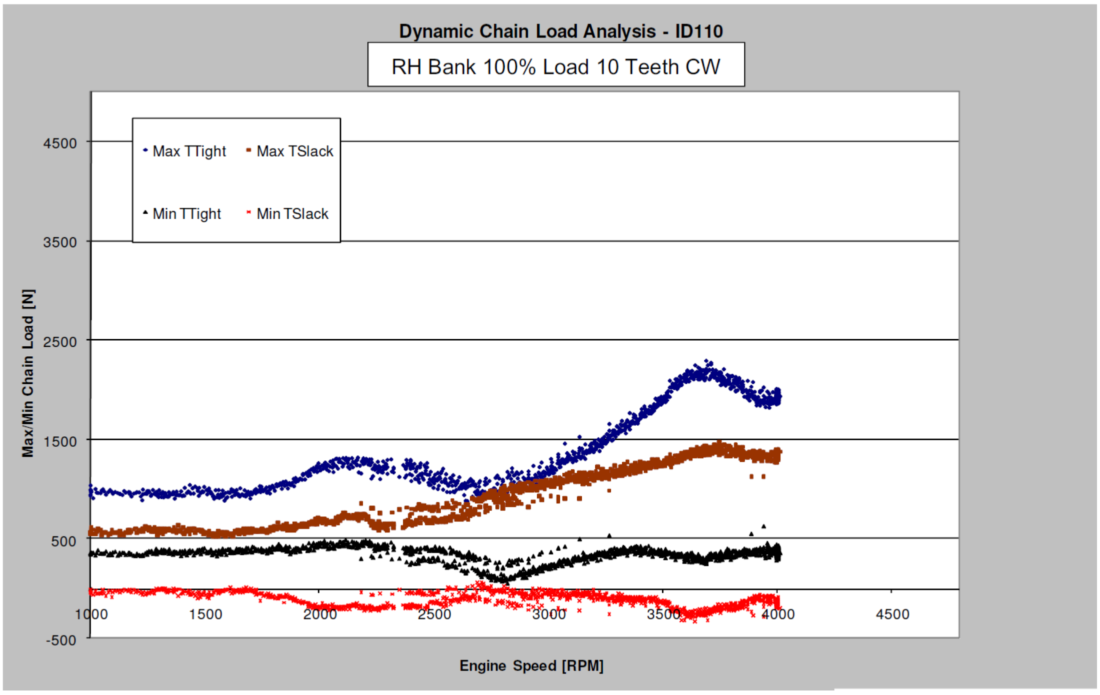

Figure A.9 : 10 Teeth CW valve train measurement.

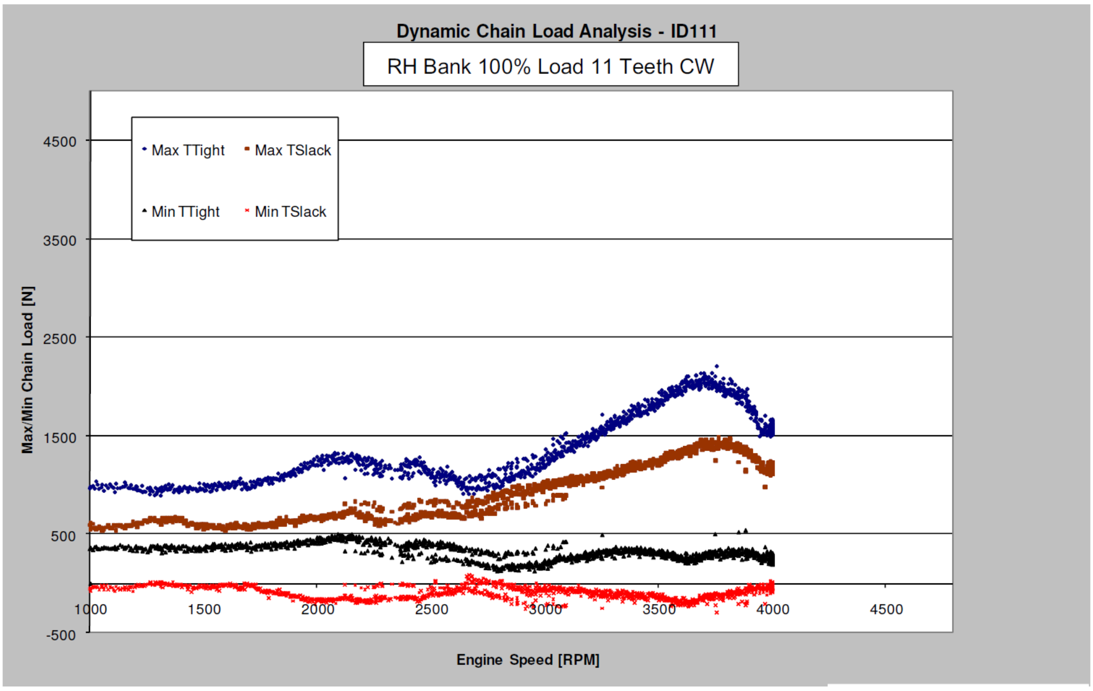

Figure A.10 : 11 Teeth CW valve train measurement.

CURRICULUM VITAE

Name Surname : Yahya SAHIP

Place and Date of Birth : Mersin, 06.08.1985

Address : İcadiye Mah Sübyeci Sok. No:20/2 Üsküdar/
İSTANBUL

E-Mail : yahya_sahip@hotmail.com

B.Sc. : Yildiz Technical University